Secondary processes in the pegmatites of the Larvik Plutonic Complex, Norway

Karoline Haakenrud Aasberg

Master Thesis in Geosciences

Study programme: Mineralogy, petrology and geochemistry

60 Credits

Natural History Museum

Department of Geosciences

Faculty of Mathematics and Natural Sciences

University of Oslo

02/06/2022

Supervisors: Henrik Friis (Natural History Museum, University of Oslo)

Tom Andersen (Department of Geosciences, University of Oslo)

This work is published digitally through DUO – Digitale Utgivelser ved UiO

http://www.duo.uio.no

It is also catalogued in BIBSYS (http://www.bibsys.no/english)

Acknowledgments

First, I would like to thank my supervisors Henrik Friis and Tom Andersen for your sincere interest in my project and for providing excellent comments and feedback the past year. It has been very much appreciated. Also, a special thanks to Henrik for spending a whole day with me in the LPC, going to all the sampling localities and sharing all your knowledge of the area, plutonic rocks and pegmatites.

Thanks to Muriel Marie Laure Erambert for taking such an interest in my project and providing excellent help and guidance using the microprobe at the Department of Geosciences. I would also like to thank Nélia Castro for going through all the necessary training and introductions for the PXRD and SEM-EDS at the Natural History Museum Salahalldin Akhavan for preparing my thin sections and Siri Simonsen for helping me with the SEM-EDS at the Department of Geosciences.

Lastly, I would like to acknowledge the other master students at the Natural History Museum for always being helpful and ready for coffee, lunch and ice cream breaks. My family, boyfriend and friends for always being so positive and supportive. A special thanks to my boyfriend Magnus for helping me collecting all my samples in the LPC even though you do not have the slightest interest in rocks.

Abstract

The Langesundsfjord area is located in the western part of the Larvik Plutonic Complex (LPC) in the SE corner of the Permian Oslo Rift. This part of the complex consists mainly of undersaturated, miaskitic larvikite and mildly agpaitic nepheline syenites with accompanying Langesundsfjord nepheline syenite pegmatites. The mineral assemblage of these pegmatites consisting of primary mafic minerals such as black amphibole, annite and aegirine-augite, the feldspathoids sodalite, nepheline and cancrinite and the feldspars albite and microcline among rare HFSE and REE-minerals such as eudialyte-and wöhlerite group Minerals. A later hydrothermal stage of the pegmatite formation caused a suite of secondary minerals to form at the expense of the primary feldspathoids. A later widespread zeolitization of both primary and secondary phases are abundant in the LPC pegmatites often found as the porous alteration product *spreustein*. The hydrothermal process behind the secondary minerals, zeolitization and s*preustein* with interstitial Al-hydroxides has not been studied since Brøgger reported voluminous masses from the LPC in the late 1880s.

Optical microscopy and SEM-EDS were used for mineral identification and to investigate textural relationships. EMPA was conducted to look at the element mobility between primary and secondary phases subjected to the magmatic fluids, to determine the mineral paragenesis and the overall evolution of the system. A crystallization sequence was proposed where secondary and later zeolite group minerals form in response to hydrothermal processes initiated by an immiscibility separating a saline brine from the Na-rich pegmatitic melt. The secondary minerals formed as a result of the saline brine reacting with the primary feldspathoids. The progressive increase in H_2O-and decrease in Cl^- content of the fluid initiated the crystallization of zeolites. A closed system has been proposed as the source of the secondary suite of minerals with the following zeolitization. The latest forming phases, *spreustein*, Al-hydroxides and calcite could be the result of later percolation of external meteoric waters reacting with the zeolites.

Glossary

LPC	Larvik Plutonic Complex
RS 1-10	Ring sections 1-10 in the LPC
REE	Rare Earth Elements (Lanthanides)
HFSE	High Field Strength Elements
EGM	Eudialyte Group Minerals
SEM	Scanning Electron Microscope
EDS	Energy-dispersive X-ray spectrometry
EDX	Energy dispersive X-ray detector
PXRD	Powder X-Ray diffraction analysis
EMP(A)	Electron microprobe (analysis)
PPL	Plane polarized light in optical microscopy
XPL	Cross polarized light in optical microscopy
TVEx	Samples from the Vevja quarry in Tvedalen
SA1-x	Samples from the Saga 1 quarry
SAGx	Samples from the Sagåsen quarry
ØSTx	Samples from the Østskogen quarry
EPXx	Samples as epoxy mounts

Table of selected minerals relevant in the text

Mineral name	Abbreviation	Chemical formula	Primary/secondary
Aegirine – Augite	Aeg - Aug	$(Na,Ca)(Fe^{2+}, Fe^{3+})Si_2O_6)$	Primary & secondary
Albite	Ab	$NaAlSi_3O_8$	Primary & secondary
Analcime	Anl	$NaAlSi_2O_6 \cdot H_2O$	Primary
Annite	Ann	$KFe^{2+}{}_3(AlSi_3O_{10})(OH)_2$	Primary & secondary
Black amphibole	Amp	$[Na][Na_2][Fe^{2+}{}_4Fe^{3+}]Si_8O_{22}(OH)_2$	Primary
Böhmite / Diaspor	Bhm / Dsp	$AlO(OH)$	Primary
Calcite	Cal	$CaCO_3$	Primary & secondary
Cancrinite	Ccn	$Na_6Ca_2(Al_6Si_6O_{24})(CO_3,SO_4)_2 \cdot 2H_2O$	Primary & secondary
Fluorite	Flr	CaF_2	Primary
Microcline	Mcc	$KAlSi_3O_8$	Primary & secondary
Natrolite	Ntr	$Na_{16}Al_{16}Si_{24}O_{80} \cdot 16H_2O$	Primary
Nepheline	Nph	$Na_3KAl_4Si_4O_{16}$	Primary
Sodalite	Sdl	$Na_8Si_6Al_6O_{24}Cl_2$	Primary & secondary
Thomsonite - Ca	Thm-Ca	$Na_4Ca_8Al_{20}Si_{20}O_{80} \cdot 24H_2O$	Primary

Table of Contents

Appendix

1. Introduction

1.1 Regional geology

1.1.1 The Precambrian

In Precambrian times the future site of the Oslo Rift was part of the Southwest Scandinavian Domain, the youngest of three domains making up the current Baltic Shield. The domain was formed during the Gothian orogeny from 1.75-1.5 Ga as a product of subduction to the present west of the Baltic Shield, the basement of this supracrustal formation is still unknown (Gaál & Gorbatschev, 1987). The newly formed crust was later reworked by metamorphism and granitic intrusions from 1.5-1.4 Ga during the Hallandian orogeny followed by a period of rifting from 1.35-1.25 Ga (Starmer, 1985; Gaál & Gorbatschev, 1987). During the early period of the Sveconorwegian-Grenvillian orogeny, 1.25-0.9 Ga the area was subjected to isoclinal folding linked to the early-kinematics of the Sveconorwegian high-grade metamorphism and emplacement of granitic intrusions. The Baltic Shield was concurrently affected by subduction along a continent-ocean boundary through to the end of the Sveconorwegian-Grenvillian orogeny (Gorbatschev, 1980; Falkum, 1985; Starmer, 1985; Verschure, 1985; Demaiffe and Michot, 1985; Gaál & Gorbatschev, 1987).

1.1.2 The Permian Oslo Rift

Located in the northernmost part of the Rotliegendes basin system we find the Permian Oslo rift, extending from the Sorgenfrei –Tornquist Fault Zone in the south up to Lake Mjøsa in the north (Fig.1) (Neumann et. al., 2004). During the Carboniferous and Cretaceous, Northern Europe was subjected to a continuous series of events in response to the final amalgamation of the supercontinent Pangea (Torsvik et al., 1998). The purely extensional Oslo Rift was active from ~305-261±6 Ma (Corfu & Dahlgren, 2008; Larsen et. al, 2008; Olsen, 2018) and linked to the dextral transtensional tectonics related to the final stages of the Varsican orogeny as it advanced northwards into continental Europe (Torsvik et al., 1998).

Rifts are known to follow precursor zones of weakness within basement rock and the Oslo rift may not be an exception. The complex Precambrian history of the Oslo Region has seemingly controlled the position and path of the rift through pre-existing lithospheric structures (Brøgger, 1886; Swensson, 1990; Pascal et al., 2004; Ebbing et al., 2005). A substantial difference in the lithospheric thickness of two Precambrian domains at depth underneath the rift zone may have initiated and sustained the highly volcanic nature of the Oslo rift. With the magma building up at the lithosphere-asthenosphere boundary, strain was localized, deformation enhanced and the lithosphere weakened initiating the formation of the graben segments (Pascal et al., 2004). The rift is divided into four segments; the northern Rendalen Graben and the *classical* Oslo Graben which consist of the southern offshore Skagerrak Graben, the Vestfold Graben and the Akershus Graben. All segments add up to a total length of ~500 km (Larsen et al., 2008)

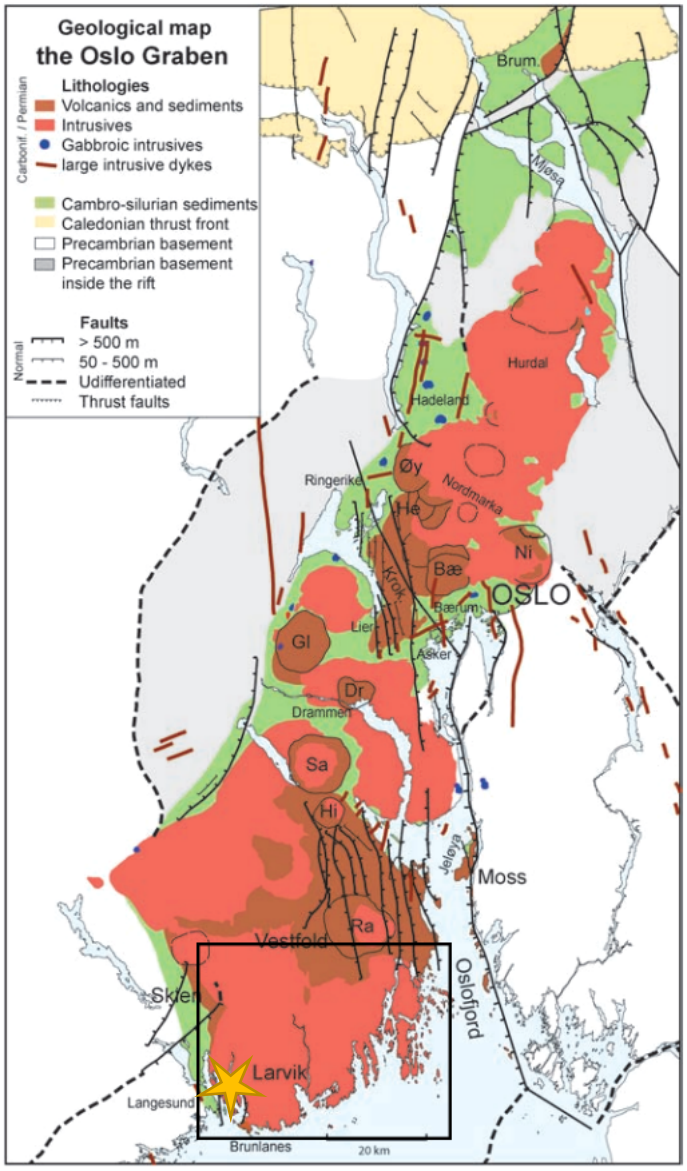

Figure 1: A geological map of the Oslo Graben, the black box outlines the LPC and the yellow star highlights the study area, Langesundsfjorden. Modified from Larsen et al., (2008)

The earliest alkaline mafic volcanism in the Oslo Rift occurred 300.4 ± 0.7 to 298.9 ± 0.7 Ma between the Skagerrak and the Vestfold grabens (Corfu & Dahlgren, 2008), similar volcanism named the B1 basalt is also found at the eastern flanks of the Vestfold graben and between the Vestfold and Akershus grabens (Neumann et al., 2002, 2004). This early alkaline mafic volcanism

was followed by eruption of vast amounts of rhomb porphyry lavas, with later emplacement of its plutonic equivalent, over-to undersaturated larvikites and nepheline syenites (Appendix II) (Larsen et al., 2008). The intermediate intrusive larvikites and rhomb porphyry lavas are slightly silica over-to undersaturated in the LPC, with the remaining rocks from the Oslo Region are strongly silica oversaturated (Neumann, 1980). Recent U-Pb ages measured by Corfu & Larsen (2020) from the Krokskogen area indicate that this magmatism spanned for most of the active rifting period. The next stages of rifting included the formation of central volcanoes and calderas, erosion and clastic fill sedimentation of the grabens and emplacement of syenitic to granitic batholiths north of the LPC (Larsen et al., 2008). Today's exposed surface is estimated to be 1-3 km below the original Permian surface, due to uplift and extensive erosion of volcanic rocks the underlying intrusive rocks and pegmatites and its structures are now exposed on the surface (Neumann et al., 1992).

1.2 The Larvik Plutonic Complex

The Larvik Plutonic Complex (LPC), located in the southwest corner of the Oslo Rift are the oldest intrusions in the terrestrial part of the rift zone (Neumann 1980). The LPC consists of 10 semi-circular, *ring sections* (RS) of intermediate, hypersolvus monzonitic rocks with compositions ranging from silica over-to undersaturated (Fig. 2) (Neumann 1980). U-Pb ages of the monzonites show a shift in igneous activity from 299 Ma in the east to 289 Ma in the western part of the complex. The oldest rocks are slightly oversaturated and becomes progressively more undersaturated towards the western younger end (Rämö et al., 2022). The oldest ring sections, RS-1 and RS-2 consists of quartz bearing larvikite and tønsbergite (Appendix II) both vastly intruded by quartz syenite pegmatites (Raade et al., 1978; Neumann, 1980**)**. The larvikites found in RS-3 and RS-5 do not contain quartz or nepheline, whilst the ones found in RS-4 and RS-6 through to RS-8 are nepheline bearing larvikites, some nepheline syenites are also found intruded here (Barth, 1944; Raade, 1973; Oftedahl & Petersen, 1978; Rämö et al., 2022). The most undersaturated rocks in the complex, the nepheline syenites, both lardalites and the younger foyaite dominates in RS-9 and RS-10 (Appendix II) (Dahlgren, 2010). The western end of the LPC consists of two related magmatic systems, an undersaturated monzonite (296-289

Ma) and a nepheline syenite (~296-288 Ma). According to U-Pb dating, the time of emplacement coincide with the Oslo rift attaining its full width (Rämö et al., 2022). Numerous nepheline syenite pegmatites dykes cut the western part of the plutonic complex (Brøgger, 1890; Dahlgren, 2010).

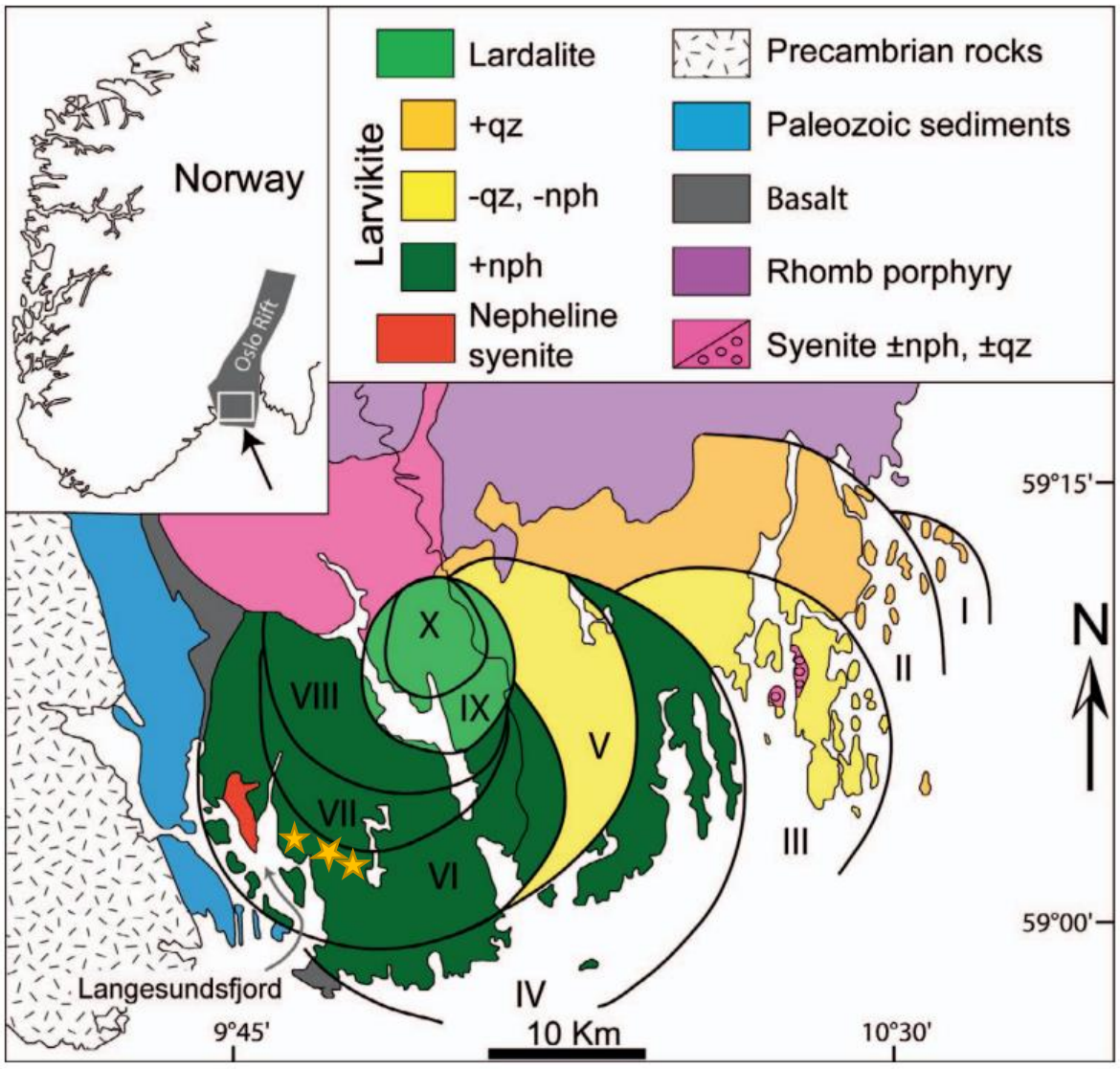

Figure 2: A simplified geological map of the Larvik Plutonic Complex and its ring sections, the yellow stars highlight the sampling localities. From left to right; Saga 1/Sagåsen, Østskogen and the Vevja quarry. Modified from Petersen, (1978); Dahlgren, (2010).

The rocks from the LPC have a uniform enrichment in incompatible elements such as Rb, Hf, Ta, Th and U as well as very low but uniform initial ratios of Th/U and $^{87}Sr/^{86}Sr$. Reflecting a relatively homogeneous and enriched mantle source containing only small degrees of crustal contamination (Finstad, 1972; Raade, 1973, 1978; Weigand, 1975**;** Sundvoll, 1978a, b; Neumann, 1980). Crystal fractionation in a periodically refilled magma chamber, partial re-melting of previously crystallized

alkaline gabbro and mixing between magmas would likely all occur in the crust during rifting. All these processes can obscure the initial ratios and result in enrichment of incompatible elements. With this in mind, the magmas from the Oslo rift may therefore come from a depleted mantle source based on Sm-Nd and Rb-Sr isotope data (Neumann, 1980). Neumann (1980) proposed a polybaric crystallization model for the LPC where fractionation of alkali-to transitional basalts occurred in a series of magma chambers at the crust-mantle boundary. Each RS represents at least one batch of intermediate magma which underwent fractionation in *situ* (Neumann, 1976, 1980). A shallow emplacement at ≤0.5GPa (Neumann et al. 1988; Andersen & Seiersten, 1994) coupled with fractionation of slightly undersaturated or oversaturated melt yielded more strongly oversaturated or undersaturated melts. Forming larvikite, lardalite or foyaite (Appendix II) depending on the silica activity in the magma during ascent (Neumann, 1980).

Analysis of fluid inclusions entrained in apatite from larvikites in the LPC by Andersen & Seiersten, (1994) gave an emplacement depth between 0.5-0.8GPa. A new crystallization model was proposed by Rämö et al. (2022) where the complex was fed by a mantle-derived polybaric low-to mid-crustal melt column in response to the opening of the rift. This model allows for independent pressure-controlled liquid lines of decent paths for low pressure larvikite and high pressure lardalite and foyaite. All sourced from a mildly alkaline basalt melt with final equilibration at ~0.5GPa. The polybaric fractionation column was tapped at different levels, delivering undersaturated monzonite larvikite and nepheline syenite melts from shallow and deep parts of the system accordingly (Rämö et al., 2022).
Brøgger (1890) and Groome (2017), both suggesting the nepheline syenite pluton and associated pegmatites were indeed intruded into the overlaying larvikite pluton when it was still hot (Fig. 3). This fits the proposed melt column as the source of both the low pressure larvikite and high pressure nepheline syenite melts. This is further elaborated in the section *“1.3 alkaline pegmatites”.* Whether or not larvikite and lardalite/foyaite originated from a uniform parent magma remains an open question (Petersen, 1978; Neumann, 1980**;** Dahlgren et al. 1996; Rämö et al., 2022).

1.3 Alkaline pegmatites in the LPC

1.3.1 Pegmatites

Pegmatites are defined as rocks consisting of interlocking crystals with large crystal sizes often >2.5 cm crystallized from a melt. They form during the final stages of crystallization from a fluid rich residue melt and can host a variety of rare minerals (Jahns, 1953). Most pegmatites have a granitic composition and consist of quartz, feldspar and mica, known as granitic pegmatites. Pegmatites are often found to have the same composition as their source pluton. Other varieties are gabbro pegmatites, syenite pegmatites and nepheline syenite pegmatites, but any other plutonic rock name combined with pegmatite is possible (London & Kontak, 2012). Pegmatites can be the source of valuable economic minerals rich in lithium and beryllium. Gemstones are also found in pegmatites classified as miarolitic (London & Kontak, 2012).

In intrusive igneous rocks large crystal size is indicative of a slow cooling rate, giving the minerals sufficient time to grow. This does not explain the large crystal size observed in pegmatites. In pegmatites the initial magma contains significant amount of dissolved volatiles like water, chlorine, fluorine and CO_2. As the magma crystallizes the residue melt becomes increasingly more enriched in these volatiles. Eventually there is an overabundance of volatiles, and an immiscibility occurs, where a volatile rich fluid separates from the melt (Thomas et al., 2000). The fluid consists of superheated water extremely rich in dissolved ions as the ions partition into the fluid rather than the melt. The low viscosity and abundance of dissolved ions in the fluid allows it to move freely and rapidly form large crystals at high temperature. The fluid is often found in smaller pockets along the margins of the batholiths, in fractures at the margins or intruded into neighbouring rocks (Da Mommio, 2022). The high temperature and low viscosity makes it possible for the pegmatitic melt to travel and crystallize far distances from its source pluton. This is vastly observed in the LPC where nepheline syenite pegmatites are found intruded into larvikite in close proximity or greater distances away from the parent nepheline syenite pluton (Fig. 3), (Dahlgren, 2010).

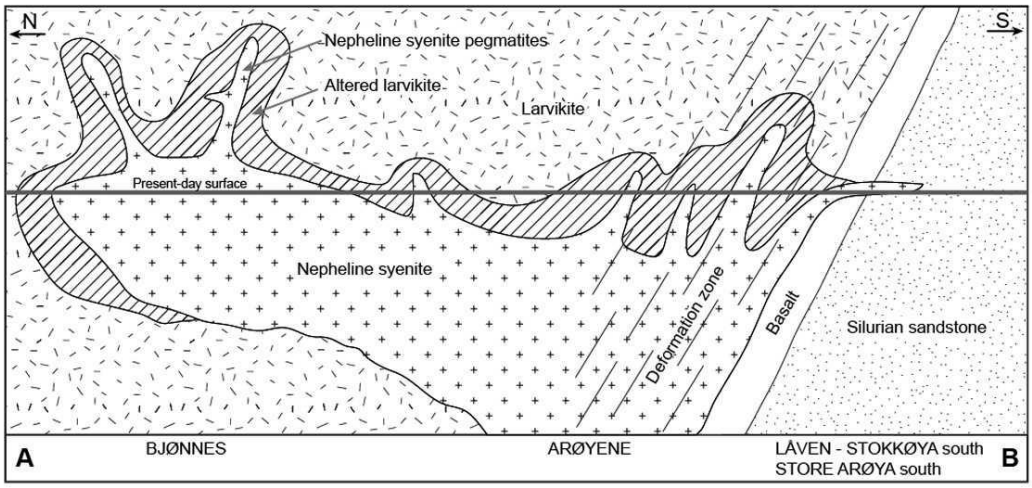

Figure 3: Show the possible nepheline syenite pluton underneath the larvikite in the LPC, nepheline syenite pegmatites have intruded into the host larvikite. From Dahlgren, (2010).

1.3.2 Alkaline pegmatites

Large crystallizing intrusions of feldspathoid syenites are known to form pegmatites made up of minerals such as sodalite, nepheline, alkali feldspar, aegirine and sodic amphibole. A suite of rare minerals enriched in water and incompatible elements, REE, Sr, Ba, Zr, Nb, Li, Be and Th are also common (Brøgger, 1890; Larsen, 1996, 2010). To distinguish these pegmatites from the common granitic pegmatites often referred to as just *pegmatites* the term alkaline pegmatites are used (London & Kontak, 2012). These pegmatites reflect the bulk composition of their host rock. In the LPC, nepheline syenite pegmatites are found widely intruded into larvikite and nepheline syenites and are found to have a composition ranging from transitional to agpaitic (Sunde et. al., 2019). The term agpaitic was introduced by Ussing in 1912 for nepheline syenites with an alkalinity index (AI) (Na + K)/Al ≥ 1.2, today we use the term to describe peralkaline nepheline syenites with complex Na-Ca-Ti-Zr-silicate minerals such as the eudialyte (EGM), wöhlerite and rinkite (Le Maitre, 2003). Pegmatites sourced from crystallizing larvikite plutons are also abundant in the LPC, having a miaskitic composition. The term miaskitic is used where the elements titanium and zirconium are incorporated into simple minerals such as zircon, titanite and ilmenite (Le Maitre, 2003).To change the liquidus assemblage of nepheline syenite magma from miaskitic to agpaitic multiple processes could be involved including an increase in peralkalinity pushing towards crystallization of EGM, increase in water activity causing saturation with an aqueous fluid phase or an

increase in fluorine (HF) activity, stabilizing liquidus assemblages with wöhlerite, hiortdahlite, låvenite and fluorite (Andersen et al. 2010).

1.3.3 The Langesundsfjord nepheline syenite pegmatites

The Langesundsfjord nepheline syenite pegmatites are midly agpaitic, contain volatile-bearing Zr-silicates like eudialyte-and wöhlerite group minerals found intruded into nepheline bearing larvikites in RS-6 (Andersen et al., 2010, Larsen et al. 2010). These pegmatites are usually zoned, not particulary coarse grained and often observed as irregular veins ranging in size from 10 centimeters up to more than 10s of meters (Dahlgren, 2010). The most abundant minerals in the Langesundfjord nepheline syenite pegmatites are brown nepheline and microcline. The emplacement and crystallization of the host larvikite pluton occurred at shallow-crustal depth (2-3 km) reaching its solidus at 850-860℃. This defined the maximum pressure and temperature at which pegmatite emplacement could have occurred in the LPC (Neumann, 1976, 1980).

The main rock-forming minerals including the Zr-silicates formed first as part of the magmatic stages of pegmatite formation and are characterized by their euhedral to subhedral shapes and relatively large crystal sizes, increasing towards the core. These primary rock-forming minerals include the anhydrous nepheline, microcline, aegirine-augite sodalite, cancrinite and albite and the hydrous minerals black amphibole and annite. All growing in the direction perpendicular to the host-rock interface (Dahlgren, 2010). The pegmatite forming melts utilised fractures already present in the host larvikites where both brittle and ductile shear-zones already existed (Groom, 2017). This indicate as pointed out by Brøgger (1890) that the pegmatites and nepheline syenites must have intruded into the larvikite when it was still hot (Fig. 3). The alkalinity of these pegmatites is proven to increase in the later stages due to the crystallization of sacchariodal albite, fibrous aegirine and zeolites (Brøgger, 1890; Khomyakov, 1995; Larsen, 2010, Sunde et al., 2019). These secondary phases are part of the later hydrothermal stages of pegmatite formation, initiated by an immiscibility of a saline brine from the Na-rich melt. This separation occurred in response to the residue melt becoming increasingly enriched in fluids as the anhydrous primary minerals continued to crystallize. The secondary minerals are

mainly sodalite, cancrinite and zeolites forming at the expense of the primary minerals Sunde et al. 2019).

1.4 Zeolites in the LPC

The complex zeolite framework is built by corner sharing of SiO_4 and AlO_4 tetrahedron results in open channels and voids occupied by the exchangeable Na^+ in the crystal lattice (Armbruster & Gunter, 2001). Zeolites are defined as hydrated aluminosilicate minerals capable of dehydration and rehydration and are often used as cation exchangers and molecular sieves (Dyer & Faghihian 1998). The zeolite structure and chemical properties permit minerals such as analcime to have wide utilization in a number of fields, such as catalysts in petroleum industry, fertilizers in agriculture, adsorbents in wastewater treatment, and membranes in surfactants and gas separation (Chen et al., 2017). Zeolites form under low pressures and temperatures in the presence of fluids and widely observed to form in the late stages of pegmatite formation (Larsen et al., 2010). Sodic zeolites like analcime and natrolite are often associated with peralkaline and alkaline complexes and found to replace primary feldspathoids during the hydrothermal stages of pegmatite formation. The most common zeolites observed in the LPC are natrolite and analcime, in a few locations thomsonite-Ca is also found in smaller amounts (Larsen et al., 2010). Extensive zeolitization and alteration of the primary minerals such as nepheline, sodalite, cancrinite and microcline as well as crystallization of low-temperature hydroxides and hydrous silicates do characterize the hydrothermal stage of pegmatite formation (Andersen et al., 2010). The alteration product observed as a result of this zeolitization is commonly referred to as *spreustein* in the LPC area (Brøgger, 1890), this alteration product is elaborated further in sections *1.4.1* and *1.4.2.*

1.4.1 Spreustein in the literature

Edgar (1965) examined a total of 16 samples named “hydronephelite”, “ranite” or “gieseckite”, from the Ontario area in Canada and the Langesundsfjord in the LPC. All these terms are readily used to describe observed low temperature, hydrothermal alteration products of nepheline since the early nineteenth century. In 1813, Allan described “gieseckite” for the first time in samples from Greenland, the material

occurred in compact feldspar and was labelled a hydrous pseudomorph after nepheline. This was later also described from Diana, Lewis County in New York. The term “ranite” was first used by Paijkull (1874) for a material from Låven in the Langesundfjord. Brøgger (1890) pointed out that the composition of ranite was similar to *spreustein,* which is one of many names given to a hydrothermal alteration product mainly containing natrolite from the rocks in the LPC.

The name "hydronephelite" was first used by Clarke (1886) for material from Litchfield, Maine interpreted to be an alteration product of sodalite. Walker and Parsons (1926) described "hydronephelite" as a white-pink alteration of cancrinite in nepheline syenites from the French River area in Ontario whilst Tilley and Harwood (1931) described fibrous "hydronephelite" from titan-augite rocks at Scawt Hill in Northern Ireland. Thugutt (1932) suggested that "hydronephelite" was a mixture of natrolite and gibbsite and that it could be distinguished from natrolite by its lower birefringence. From an analysis of optically homogeneous "hydronephelite" from Hawaii, Dunham (1933) suggested it could be a solid solution of natrolite and diaspore as the analysis showed considerably higher Al_2O_3 than required to form natrolite. Moyd (1949), described nepheline-bearing rocks of South-Eastern Ontario and reported individual nepheline crystals showing up to three zonally arranged alteration products, opaque white cancrinite, fine-grained pink material "hydronephelite" and fine-grained green material "gieseckite" where the last two formed by low-temperature hydrothermal activity.

Oftedahl (1952) suggested that "hydronephelite" consisted of mixtures of natrolite and a pseudo-hexagonal mineral he called “true hydronephelite." The pseudo-hexagonal mineral is later found to be fully pseudomorphed nepheline (Dahlgren, 2010). Gieseckite is now a term used for pseudomorphs of fine-grained muscovite after an unknown mineral and it is generally recognized that "hydronephelite" and “ranite" are not true mineral species but intimate mixtures of natrolite, other zeolites, micas and Al-hydroxides (Edgar, 1965). “Hydronephelite” is still today day used as another named for the German *spreustein*. Numerous writers have reported "hydronephelites" as a low temperature alteration product of nepheline, but the physical appearance and the chemical compositions do vary considerably. Colours such as white, pink, red and green has been mentioned as alteration products of

sodalite, nepheline and cancrinite (Edgar, 1965). The process forming the observed *spreustein* ”hydronephelite” is still an unanswered question.

1.4.2 Spreustein in the LPC

Spreustein is found in pegmatites all across the LPC and occur as dense, finely fibrous masses up to kilograms in weight. The main mineral found in s*preustein* is natrolite with smaller amounts of interstitial analcime, annite, calcite and abundant Al-hydroxides. The colour can be everything from white, pink, orange, red or brown and are found to be everything from fine to coarse grained (Larsen et al., 2010). Natrolite is a volume-to-volume hydrothermal alteration product of nepheline, but also found replacing primary and secondary sodalite, primary cancrinite and occasionally feldspars such as microcline and albite (Larsen et al., 2010). Unaltered nepheline and sodalite are often observed in the central core of minerals otherwise rimmed by *spreustein*. It is also abundantly found as fracture fillings (Larsen et al., 2010). Well-defined *spreustein* pseudomorphs after nepheline and sodalite are common in the LPC. Vugs in *spreustein* can host well-developed natrolite and thomsonite-Ca crystals as well as Al-hydroxides such as böhmite and purple diaspore often together with platy calcite (Larsen et al., 2010). Zeolitization is a well-known phenomenon linked to alkaline complexes all over the world (Marks & Markl, 2017), but the alteration product *spreustein* is fairly unheard of in the modern literature. Edgar published the last research article mentioning *spreustein* and “hydronephelite” in 1965.

The main scope of this study is to determine the processes causing the crystallization of the secondary minerals found in the LPC pegmatites, the later zeolitization and the further alteration into *spreustein* with abundant Al-hydroxides. The complex eudialyte and wöhlerite group minerals abundantly found in these pegmatites are not part of the scope and left out in this study. The aim is to propose a mineral paragenesis for the whole system and determine the source and composition of the fluids responsible for the formation all the secondary phases including *spreustein* widely observed in the Langesundsfjord nepheline syenite pegmatites.

2. Methodology

A total of 37 pegmatite samples were collected through field work from three different localities in the LPC, 26 samples from Saga 1, three from the Sagåsen and three from the Østskogen quarry. A fourth locality, the Vevja quarry in the Tvedalen area, was added to the study when five samples were found in the rock collection at NHM. The samples were chosen based on the degree of alteration into zeolites and the presence of *spreustein*. Samples where zeolitization of nepheline and/or sodalite had occurred were favoured as well as rocks with a mineral assemblage including blue secondary sodalite and cancrinite. Most samples were chosen for thin section making, but some were collected due to their well-developed zeolite crystals in vugs in spreustein. All samples were cleaned after collection and a diamond saw was used to reduce the size of large samples into thin section blocks. A total of 22 thin sections blocks was sent to the Department of Geosciences, University of Oslo.

Unfortunately, nine of the prepared thin sections fragmented during preparation when the epoxy was applied (Fig. 4), the samples all had varying amounts of zeolites present. An explanation is that absorption of some component of the epoxy used during preparation of the sections caused the zeolites to expand and caused the fragmentation. In total 13 of the 22 planned thin sections were made, 30 µm thick and polished until uncovered. The remaining 9 broken thin section blocks was cut with a diamond saw, grinded to size and mounted in epoxy, these epoxy mounts were later grinded down and polished at NHM using a Struers LaboPol-30. A total of 12 epoxy mounts were made to replacement the 9 broken thin sections, to make sure all the interesting parts of the samples where included. An overview of all the selected samples and the conducted analysis are presented in Table 1. A map of the study area is provided showing the sampling localities (Fig. 5).

2.1.1 Mineral formulae and abbreviations

Ideal mineral formulae used within this text, for identification and calculation purposes follow the Official IMA–CNMNC List of Mineral Names (Miyawaki et. al, 2022). Mineral abbreviations used in figures throughout this text are in accordance with Warr (2021). All relevant minerals, their abbreviations and ideal formulae can be found in the *Glossary.* A recalculation was done of all referenced reactions in the *4.*

Discussion section using the old chemical formula of nepheline to accommodate the new formula including the K^+ component and to obtain consistency throughout. This is relevant for reactions (2), (4), (6), (7), (11) and (12).

Figure 4: An example of one of the fragmented thin sections from thin section preparation.

2.1.2 Optical microscopy

Optical microscopy was used for mineral identification and observation of relationships between minerals phases in thin section. Both plane polarized light (PPL) and cross-polarized light (XPL) were used. Optical microscopy in the form of reflected light was used to verify the quality of polishing of the epoxy mounts and to distinguish between hematite and magnetite based on crystal shape.

2.1.3 Scanning electron microscope (SEM)

Energy-dispersive X-ray spectrometry (EDS) in a SEM was done in the Geo Laboratory at the Natural History Museum (NHM) and the Department of Geosciences at the University of Oslo. The instrument used at NHM was a Hitachi S–3600N scanning electron microscope (SEM) equipped with a Bruker XFlash® 5030 energy dispersive X-ray detector (EDX), running on Quantax 400 (Esprit 1.9). Uncoated samples were analysed in variable pressure (VP) mode at 15Pa and with the acceleration voltage set to 15kV. The instrument used at the Department of Geosciences was a Hitachi SU5000 SEM equipped with a Dual Bruker Quantax XFlash 30 EDS system running on Espirit 2.2. A Carbon Coater Cressington 208C was used to apply carbon films on the selected epoxy mounts. High Vacuum (HV) mode (<1Pa) was used with an acceleration voltage of 15kV. EDS was used for

mineral identification and to familiarize with the epoxy samples and their mineral phase relations through semi-quantitative elemental analysis and hyperspectral mapping. Backscatter electron (BSE) imaging was conducted using SEM to identify, locate minerals of interest and familiarise with their phase relations in preparation for the electron microprobe analysis.

2.1.4 Powder X-ray diffraction (PXRD)

Powder X-ray Diffraction (PXRD) was done at the Geo Laboratory at NHM for qualitative mineral identification. Pre-treatments of the powder samples included separation of the minerals of interest and grinding the material down to a very fine powder with ethanol using an agate mortar. Ethanol helped with the transportation of the sample from the mortar to the sample holder and kept it in place on the sample holder until fully dry. The instrument used was a Siemens D5005 Powder X-ray diffractometer (PXRD) with Bragg-Brentano geometry, a scintillation counter, and a Cu X-ray source. The software Bruker's EVA was used for phase identification. The software identifies the mineral phase by comparing the observed results with the Crystallography Open Database (COD) and the most recent PDF-4+2020 RDB database from the International Centre of Diffraction Data (ICDD). Multiple mineral phases could be identified in each powder sample. The PXRD was used to make sure that mineral identification had been done correctly in samples where minerals had a sufficient large size. A shorter run of 46 minutes was used initially, but if the shorter run failed to identity the mineral or revealed the sample to contain multiple phases a longer 3 hour program was used.

2.1.5 Electron microprobe analysis (EMPA)

Electron microprobe analysis was conducted at the Department of Geosciences, using a Cameca SX100 instrument fitted with five wavelength dispersive (WDS) spectrometers and a Bruker XFlash SDD EDS detector. The Calibration standards and X-ray lines used were wollastonite (Si Kα, Ca Kα), albite (Na Kα), orthoclase (K Kα), pyrophanite (Ti Kα, Mn Kα), $BaSO_4$ (S Kα), synthetic alforsite (Cl Kα), Al_2O_3 (Al Kα), MgO (Mg Kα) and Fe metal (Fe Kα). Matrix effects and elemental overlaps were corrected with the Cameca PAP procedure implemented in the Cameca software

(Pouchou and Pichoir, 1984). An accelerating voltage of 15kV was used for all analyses. A counting time of 10 seconds were used for all chosen elements except for Ca which had a 20 second count. The start counting time was used to prevent element migration due to burning of the minerals. Sodium and K were analysed first as they are most susceptible to dissipation.

The selected minerals were analysed using different “programs” with varying elements of interest, beam currents-and diameters settings to obtain the best possible result for each data point. Most analysis was conducted using the “sodalite program” measuring weight% oxides of Na, Si, Ca, Fe, Al, Mn, Mg, S, Cl and K, the program used a beam current of 10 nA and a beam diameter of 10 µm. Minerals analysed using this program included sodalite, nepheline, albite, microcline, analcime and natrolite. The “cancrinite program” measured weight% oxides of Na, Si, Ca, Fe, Al, Mn, Mg, S and Ti, with a beam current of 6 nA and a beam diameter of 10 µm to limit the burning of the cancrinite minerals and prevent element migration. Biotite was analysed using a program set up for Na, Si, Ca, Fe, Al, Mg, Ti, K and Cr with a beam current of 10 nA and a beam diameter of 10 µm.

Backscattered electron imaging and printed scans of thin sections and the epoxy mounts were used to locate areas of interest in the selected samples. Light imaging was used to locate areas/minerals of interest in the thin sections. The selected epoxy mounts and thin sections were coated with a thin carbon film. The crystal structure of zeolites and the porous nature of *spreustein* made it very difficult to obtain good EMPA of the latter, as a result only lager crystals of individual zeolites found within fairly unaltered host minerals were analysed. Each area of interest was analysed with 3-4 analytical points in close proximity of each other to avoid anomalous data and increase the precision of the analysis. Unfortunately, a lot of the thin sections were unfit for the EMPA due an uneven surface. Zeolites and strongly hydrothermally altered minerals such as the ones in question has shown to make thin section making very difficult, most EMPA is therefore only conducted on epoxy mounts. All relevant data points are presented in the results, with a calculated two standard deviation shown in brackets. The full list of EMP analysis points is attached in Appendix III, all analysis points having an orange colour has been excluded from the results due to their totals being too low, high or inconsistent with the other points.

Table 1: Analysis conducted on the chosen samples

Samples	Location	Analysis			
		Optical	EDS	PXRD	EMPA
SA1 - 2	Saga 1	✓		✓	
SA1-3A	Saga 1	✓			✓
SA1-3B	Saga 1	✓			
SA1-3C	Saga 1	✓			
SA1-9	Saga 1	✓			
SA1-13B	Saga 1	✓			
SA1-18	Saga 1	✓			
SA1-19	Saga 1	✓		✓	
SA1-22	Saga 1	✓		✓	
SA1-24	Saga 1	✓		✓	
SA1-25A	Saga 1	✓		✓	
SA 1-25B	Saga 1	✓		✓	
SAG3	Sagåsen	✓			
TVE2	Vevja			✓	
ØST2	Østskogen	✓			
EPX1	Vevja		✓		✓
EPX2	Saga 1		✓	✓	✓
EPX3	Vevja		✓		
EPX5	Saga 1		✓		✓
EPX7	Saga 1		✓	✓	
EPX8	Saga 1		✓	✓	
EPX9	Saga 1		✓	✓	✓
EPX10	Østskogen		✓		✓
EPX11	Vevja		✓	✓	
EPX12	Vevja		✓	✓	✓

** EDS – Energy-dispersive X-ray spectrometry

** PXRD – Powder x-ray diffraction

** EMPA – Electron microprobe analysis

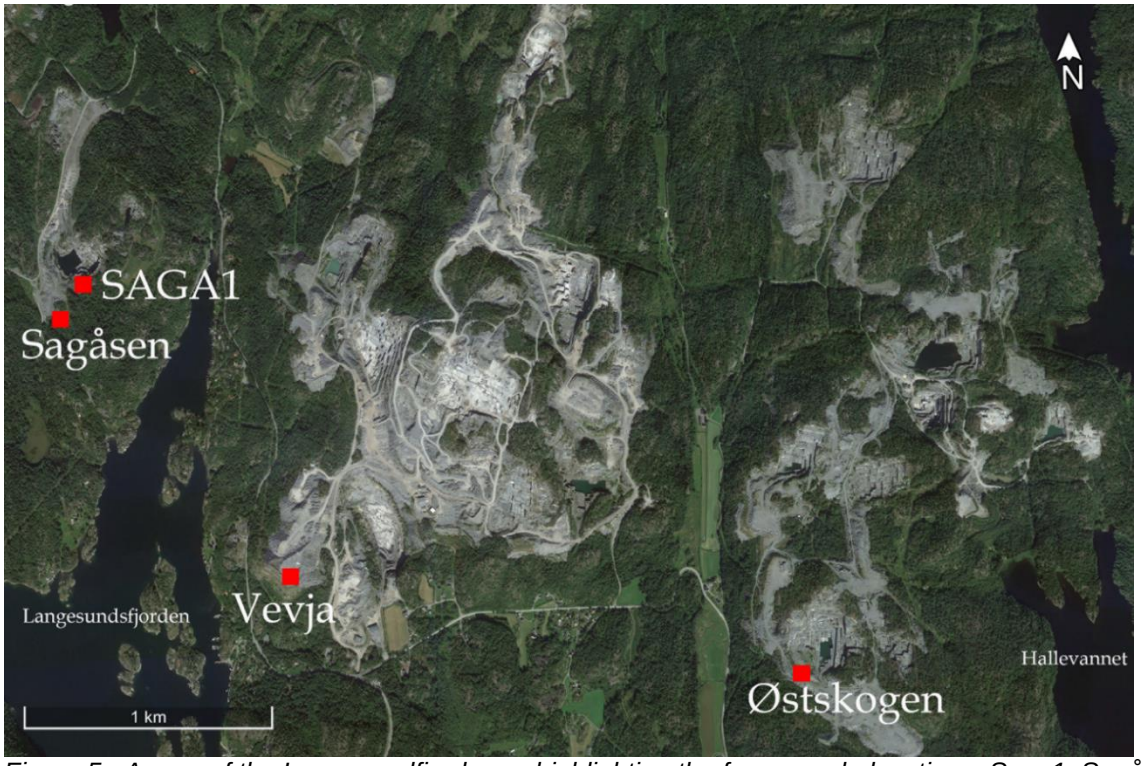

Figure 5: A map of the Langesundfjord area highlighting the four sample locations; Saga1, Sagåsen, Vevja and Østskogen quarries. Image from Google Earth (05/01/2022).

3. Results

Quantitative analyses were obtained by EMPA of selected samples containing minerals such as primary and secondary sodalite, nepheline, cancrinite, annite and calcite as well as zeolites; analcime, natrolite and thomsonite-Ca. The relationship between phases is presented based on textural relationships observed in SEM-BSE images, optical microscopy and from hand samples. Transects across phase boundaries as well as through single phases were run to examine the element mobility throughout the areas of interest. The findings are presented in tables with complementing graphs and figures to best explain the findings from the selected samples.

3.1 Nepheline

Nepheline is one of the main minerals found in the LPC pegmatites and crystallize as euhedral to subhedral crystals late in the magmatic stages of pegmatite formation. Some nepheline crystals are found to exhibit a good hexagonal shape. The mineral is easily recognised by its greasy lustre, brown colour and often large size up to

decimetres. During the hydrothermal stages nepheline has been observed altered into zeolites and further into *spreustein.* Nepheline is found replaced by both analcime and natrolite, as rims, fracture fill and as interstitial pods and veins (Fig. 6). A transition into a grey variety of nepheline rich in secondary annite is abundantly observed in close proximity to its alteration products such as zeolites, cancrinite and secondary blue sodalite (Fig. 7). Secondary microcline, sodalite, analcime and natrolite are found as inclusions in grey nepheline. EMPA was conducted on multiple samples of brown, transitional and grey nepheline and are presented in Table 2. The results show very consistent inter-grain compositions for the grey, brown and transitional nephelines, but clear differences between them. The composition of grey nepheline is very close to the ideal formula for nepheline.

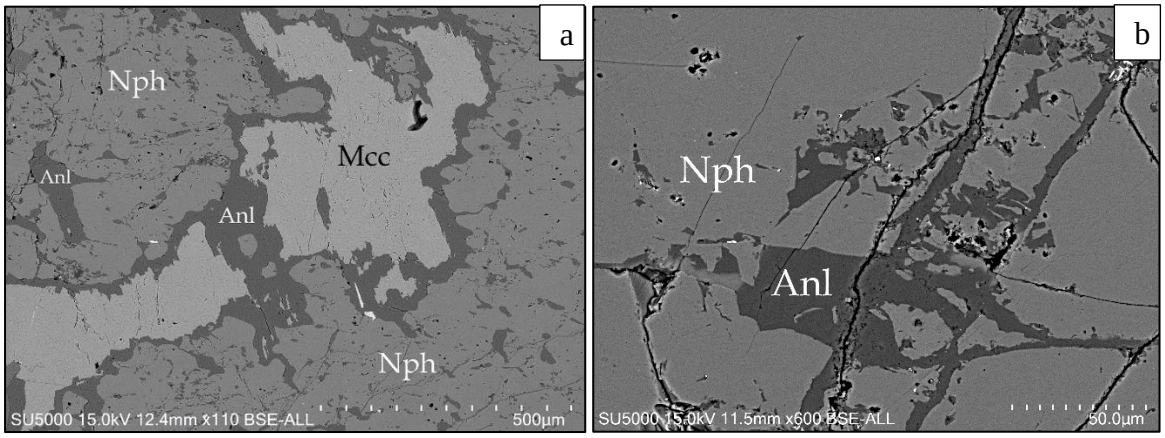

Figure 6: a) Grey, secondary nepheline with interstitial microcline rimmed by analcime, small analcime pods and veins are also abundantly present. b) Brown nepheline exhibiting replacement of analcime in fractures. Anl=analcime, Mcc=microcline, Nph=nepheline

Chemical transects with EMPA were performed across the boundary between brown and grey nepheline. These results show prominent changes as nepheline transitions from brown to grey (Table 2). A silica excess was found in all the nepheline samples, but the highest silica content was found in brown nepheline decreasing as it transitioned into grey. This seems to correlate with an increase in Al^{3+} content moving from brown into grey nepheline, substituting $Si^{4+} \rightarrow Al^{3+}$ as the transition proceed (Fig. 8a). K^+ content increase when transitioning from brown to grey, Na^+ is consistent through the transition only decreasing by a small amount when transitioning into grey. There no obvious substitution occurring between Na^+ and K^+ as evident from Figure 8c. This means there will be vacancies at the site occupied by K^+ in brown nepheline. Fe^{3+} are only present in transitional and brown nepheline, but

totals are low and the uncertainty high in transitional nepheline. Brown (1970) has demonstrated that there is an inverse relationship between Fe^{3+} and Al^{3+}, Al^{3+} is decreasing when Fe^{3+} is increasing and vice versa, which correlates well with observations from the analysed samples (Fig. 8b).

Table 2: Representative compositions (weight% oxides) of nepheline

Sample	EPX10	EPX9	EPX9	EPX9	EPX12	EPX12	EPX12	EXP5
Analysis no	5 / 4	83 / 3	32 / 2	31 / 2	46 / 2	69 / 2	72 / 2	80 / 4
Br/G/Bo	G	G	Bo	Br	G	Bo	Br	Br
n	7	3	1	4	7	2	9	9
Na_2O	16.2(2)	16.40(9)	16.64	16.6(3)	16.4(2)	16.64(5)	16.7(3)	16.5(2)
SiO_2	42.0(9)	42.1(2)	43.46	45.2(2)	42.3(5)	43.1(3)	45.1(8)	44.8(3)
K_2O	7.1(6)	7.4(2)	6.57	5.4(1)	7.3(3)	6.7(3)	5.5(3)	5.5(1)
CaO	0.01(3)	-	0.00	-	0.01(2)	0.00(7)	0.001(9)	0.01(2)
Fe_2O_3	0.1(1)	0.04(6)	0.14	0.64(8)	0.08(8)	0.22(2)	0.6(1)	0.5(1)
Al_2O_3	33.4(7)	33.9(6)	32.89	31.6(4)	33.7(4)	33.0(8)	31.7(4)	31.3(5)
MgO	0.01(1)	0.01(2)	0.01	-	0.01(2)	0.01(2)	0.01(3)	0.01(1)
MnO	0.01(2)	0.01(1)	0.00	0.01(1)	0.01(2)	0.01(2)	0.01(3)	0.01(3)
Cl	0.01(1)	0.005(7)	0.02	0.009(9)	0.01(2)	0.0093(0)	0.01(1)	0.002(9)
S	0.01(2)	0.01(2)	0.03	0.01(2)	0.01(2)	0.02(5)	0.01(1)	0.01(2)
$-O=Cl_2$	-	-	0.01	-	-	-	-	-
Total	99.01	100.00	99.78	99.69	99.96	99.91	99.77	98.90
Formula based on 16 O per formula unit								
Si^{4+}	4.11	4.08	4.19	4.32	4.10	4.17	4.31	4.33
Al^{3+}	3.85	3.88	3.74	3.56	3.86	3.76	3.58	3.56
Fe^{3+}	<0.01	<0.01	0.01	0.03	<0.01	0.01	0.02	0.02
Ca^{2+}	<0.01	-	-	-	<0.01	-	<0.01	<0.01
Na^{+}	3.08	3.08	3.11	3.08	3.09	3.11	3.10	3.09
K^{+}	0.89	0.92	0.81	0.66	0.90	0.83	0.68	0.68
Mn^{2+}	<0.01	-	-	-	<0.01	<0.01	<0.01	-
Mg^{2+}	-	-	-	-	<0.01	<0.01	<0.01	<0.01
SO_4^{2-}	-	<0.01	<0.01	<0.01	-	<0.01	<0.01	<0.01
Cl^{-}	<0.01	<0.01	<0.01	<0.01	<0.01	<0.01	<0.01	<0.01

*Type: B=brown G=grey Bo=boundary

The optical properties of brown and grey nepheline are the same in thin section both PPL and XPL, the only way to differentiate them is by the presence of small interstitial annite crystal abundantly found within the grey nepheline. In BSE imagining grey nepheline and blue sodalite are indistinguishable, only EDS analysis or EMPA can determine the differences. Brown nepheline is easily distinguished from sodalite in BSE by its darker grey colour. Grey nepheline has abundant inclusions of analcime, microcline and sodalite often found rimmed by analcime within nepheline.

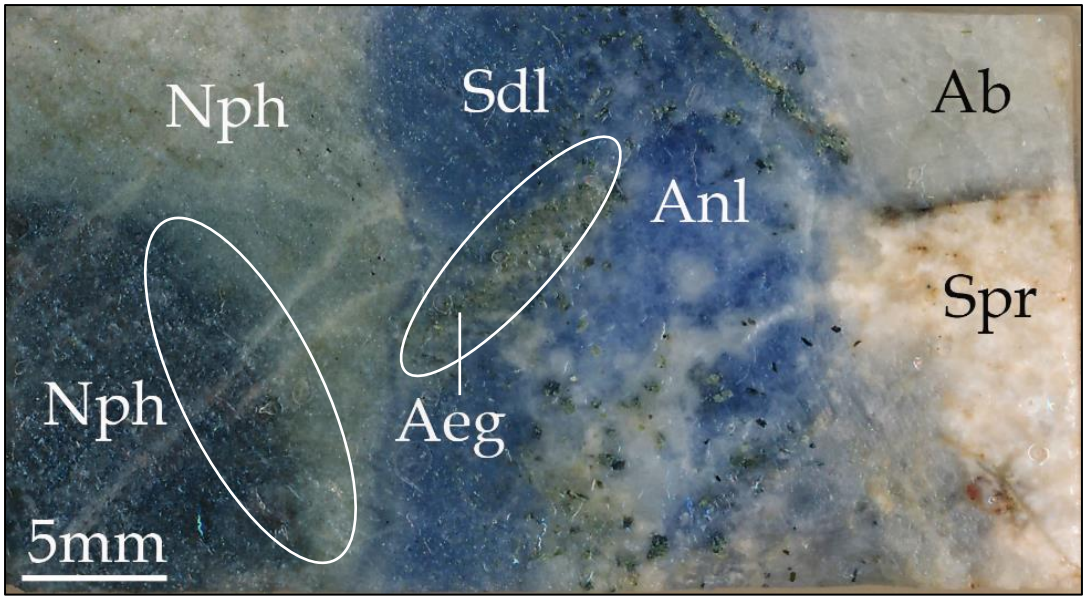

Figure 7: Exhibits the sharp transition from brown to grey nepheline in sample Epx 12. Ab=albite, Aeg= aegirine. Anl=analcime, Nph=nepheline

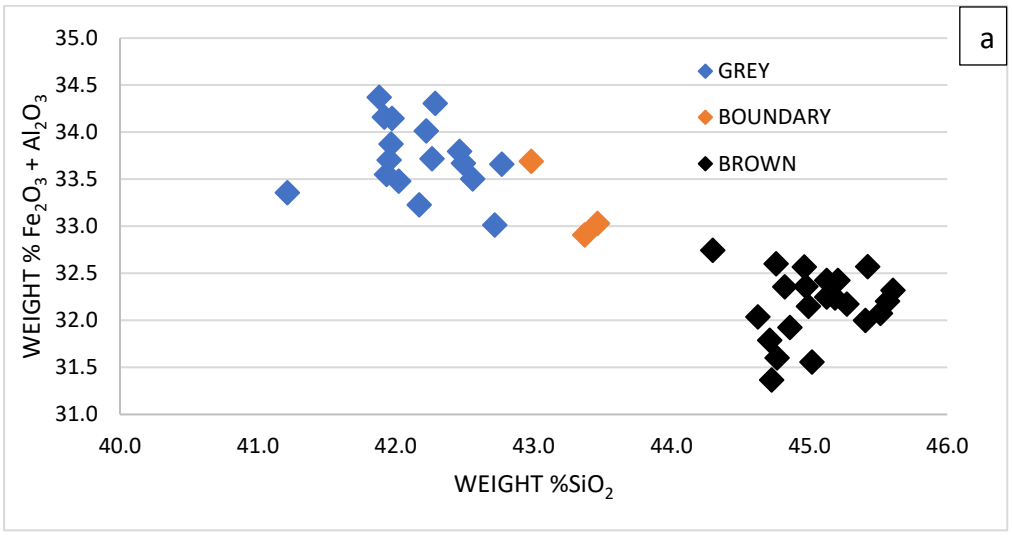

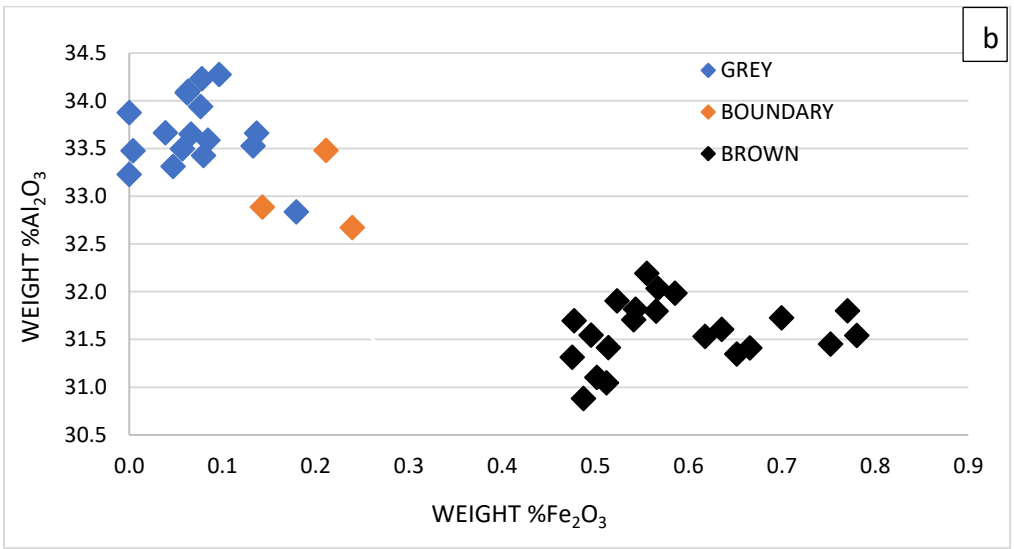

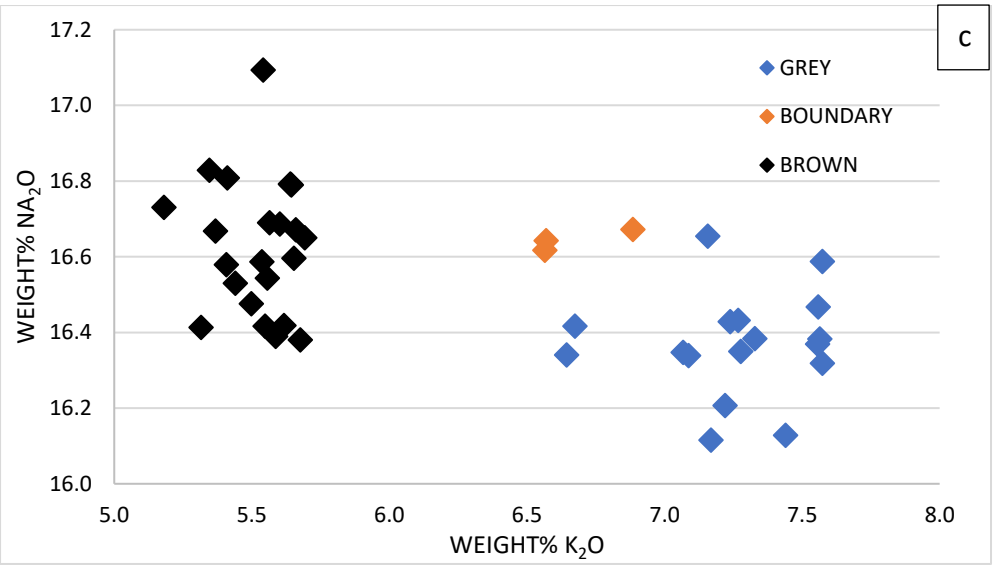

Figure 8: show the substitutional relationships between elements in brown, transitional and grey nepheline. a) Show the correlation between (Al_2O_3 + Fe_2O_3)↔SiO_2. b) Show the substitutional relationship between Fe_2O_3↔Al_2O_3. c) Show the substitutional relationship between Na_2O↔K_2O.

3.1.1 Red abrupt reaction rim

Another interesting and abundantly observed feature is red abrupt reaction rims at the boundaries between brown nepheline and red *spreustein* also found filling cracks at the boundary between albite, nepheline and *spreustein* (Fig. 9). This has also been observed as very thin veins following cracks and small depressions in larger brown nepheline crystals. The brown nepheline does not exhibit any compositional changes in contact with the abrupt reaction rim, the texture of the red material is non-crystalline and does not show any birefringence colours in XPL (Fig. 10b). Figure 11 shows the chemical variations of Na_2O, SiO_2, CaO, Al_2O_3, K_2O and Fe_2O_3 graphically as we move from brown nepheline, through the reaction rim and into red natrolite (Fig. 9). The EMPA results of the red reaction rim gave low totals due to its porous texture, but it does give an indication of the elements present. An interestingly high content of CaO and a slightly higher content of Fe_2O_3 compared to what found in the brown nepheline is noteworthy. Nepheline in the samples do not incorporate any CaO, whilst a little component of CaO and Fe_2O_3 has been incorporated into the neighbouring natrolite.

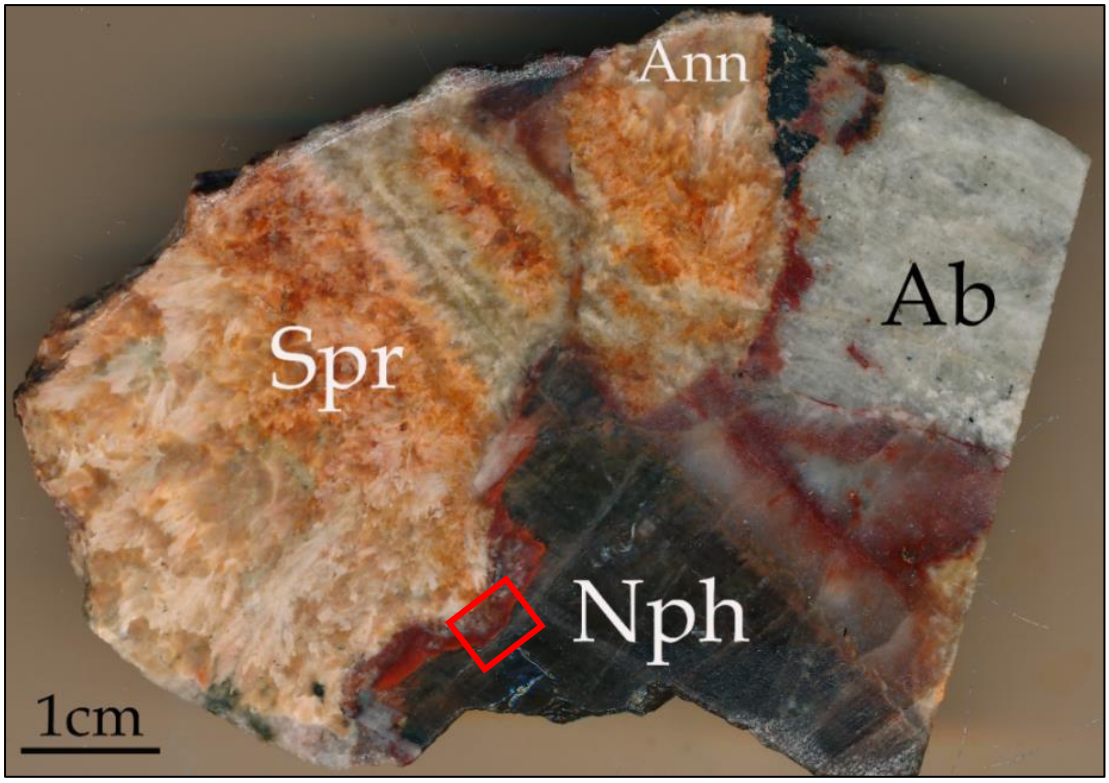

Figure 9: Sample SA1-3 show a red abrupt reaction rim in between brown nepheline and spreustein, the red substance is filling fractures between albite crystals and larger cracks in spreustein. The red highlighted box show the location of Figure 10. Ab=albite, Ann=annite, Nph=nepheline, Spr=spreustein

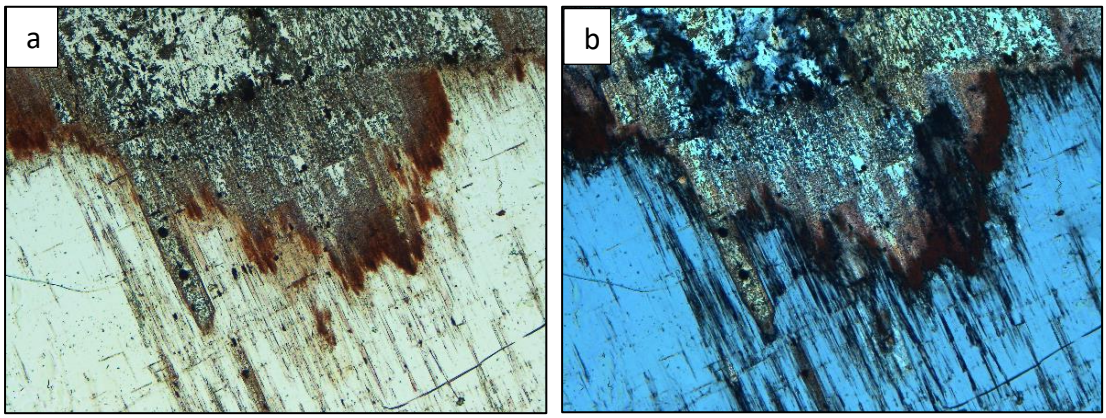

Figure 10: Show how the red reaction rim must have reacted with the nepheline and crystallized. The same red material is found crystallizing in fractures between albite crystals in Figure 9. a) PPL b) XPL. Field of view is 2 mm.

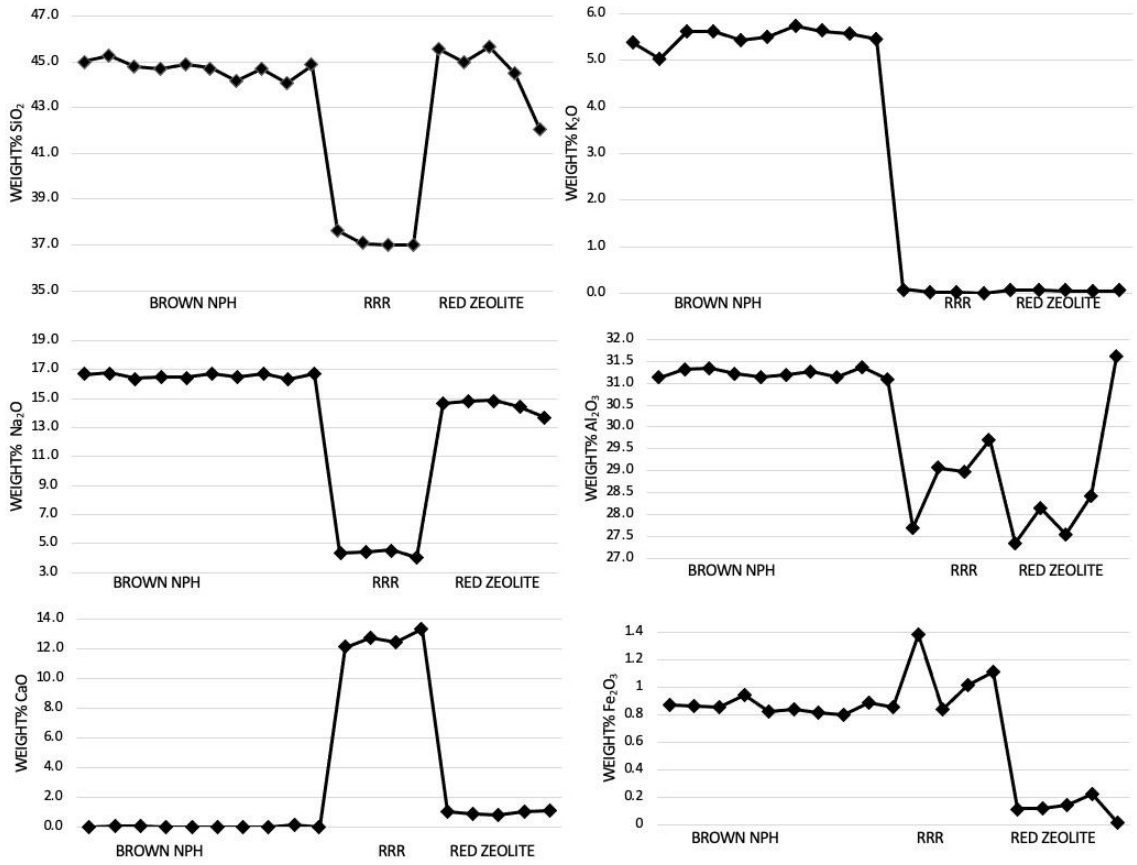

Figure 11: Show transects through brown nepheline, a red abrupt reaction rim into red zeolites. The points are given in weight% oxides. Transect follows the direction and path of the red arrow in Figure 9. RRR= red abrupt reaction rim

3.2 Sodalite

Sodalite is very abundant and found in most of the collected samples as primary green sodalite or secondary blue sodalite. Primary sodalite crystallize in the magmatic stage of pegmatite formation before nepheline whilst the secondary sodalite forms later during the hydrothermal stages. Both primary and secondary sodalite are abundantly observed altered into zeolites and *spreustein* (Fig. 12). Primary sodalite exhibits a greenish grey colour and has a greasy lustre, resembling nepheline. The crystals are euhedral to subhedral and vary in size from centimetres to decimetres. The second generation of sodalite has a distinct blue colour, a dull lustre and is easily distinguished from its first generation equivalent. The secondary sodalite is always found together with brown or grey nepheline. Replacement of nepheline by sodalite is commonly observed, some samples even exhibits the hexagonal shape characteristic of nepheline from the Vevja quarry.

The most prominent difference between primary and secondary sodalite is evident in SEM-BSE imaging, primary minerals exhibits large euhedral to anhedral crystals, with abundant fractures. Zeolites, mainly natrolite is found as rims, filling fractures or as pesudomorphs in the form of porous *spreustein* (Fig.13b). The secondary sodalite occur in two ways, either as larger euhedral to anhedral crystals like the primary sodalite or as larger aggregates of small rounded sodalite embedded in analcime (Fig. 13c). In a sample from the Vevja quarry rounded sodalite and cancrinite was found embedded in analcime (Fig. 13d). Sodalite with interstital analcime has a lighter blue colour, the more analcime the lighter the blue colour (Fig. 13a). The cause of the different textures is unclear, samples exhibiting aggregates of small rounded sodalite with analcime are found from both the Saga 1 and the Vevja quarry.

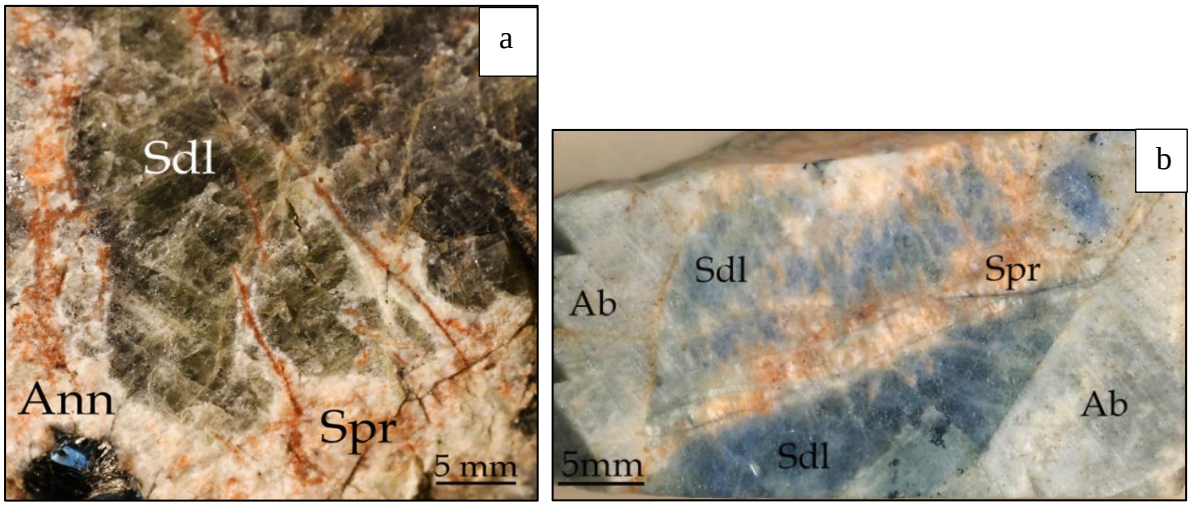

Figure 12 a) Primary green sodalite show extensive alteration into spreustein both as a rim around the mineral as well as fracture filling. b) Exhibits secondary blue sodalite with a sharp boundary to albite, spreustein is filling fractures in the mineral. Fractures are going through albite as well, but albite is unaffected. Ab=albite, Ann=annite, Sdl = sodalite, Spr=spreustein.

The EMPA results (Table 3) show that primary sodalite has incorporated a minor amount of Fe^{3+} and SO_4^{2-}. There is no evidence for a substitutional relationship between Si^{4+} and Al^{3+}. The EMPA results of both primary and secondary sodalite are very similar to the ideal chemical formula. The excess Na^{+} present in all the samples can reflect its growth environment. The sample EPX1 has a large aggregate of smaller rounded sodalite with cancrinite fully embedded in analcime (Fig. 13d). Secondary sodalite in sample EXP5 exhibit the same rounded aggregates of smaller sodalite crystals only without the presence of cancrinite (Fig. 13c). This sample do

also have a very dark blue colour close to the boundary with brown nepheline where no interstitial analcime in present. The amount of interstitial analcime increases with distance from the brown nepheline (Fig. 13a). Secondary sodalite in sample EPX12, has the larger euhedral to anhedral sodalite crystals with abundant fractures at the boundary to grey nepheline. The composition of this sample varies from the two others in that it contains some K^+ also observed in primary sodalite from Sample EPX10.

Table 3: Representative compositions (weight% oxides) of sodalite

Sample	EPX10	EPX1	EPX12	EXP5
Analysis no	12 / 4	12 / 1	53 / 2	60 / 4
Type*	P	S	S	S
n	10	43	2	20
Na_2O	25.6(2)	25.4(3)	25.9(1)	25.5(3)
SiO_2	36.9(4)	36.9(3)	36.9(4)	36.9(5)
Cl	7.3(1)	7.3(2)	7.19(3)	7.3(3)
K_2O	0.05(5)	0.02(3)	0.03(1)	0.02(2)
CaO	0.01(2)	0.02(4)	0.01(2)	0.0(1)
Fe_2O_3	0.2(2)	0.037(6)	0.08(6)	0.0(1)
Al_2O_3	30.9(5)	30.99(6)	30.7(1)	30.8(4)
MgO	0.01(2)	0.01(3)	0.01(2)	0.01(2)
MnO	0.02(5)	0.01(3)	-	0.01(2)
SO_4^{2-}	0.08(8)	0.03(6)	0.1(1)	0.01(3)
$-O=Cl_2$	1.61	1.65	1.62	1.65
Total	99.73	99.13	99.28	99.04
	Formula based on 26 anions (O,Cl)			
Si^{4+}	5.99	6.01	6.01	6.02
Al^{3+}	5.92	5.95	5.90	5.92
Fe^{3+}	0.01	<0.01	<0.01	<0.01
Na^+	8.07	8.02	8.18	8.07
Ca^{2+}	<0.01	-	-	0.01
K^+	0.01	<0.01	0.01	<0.01
Mn^{2+}	<0.01	<0.01	-	<0.01
Mg^{2+}	<0.01	<0.01	<0.01	<0.01
SO_4^{2-}	0.01	<0.01	<0.01	<0.01
Cl^-	2.02	2.02	1.99	2.02

*Type: P=Primary S = Secondary

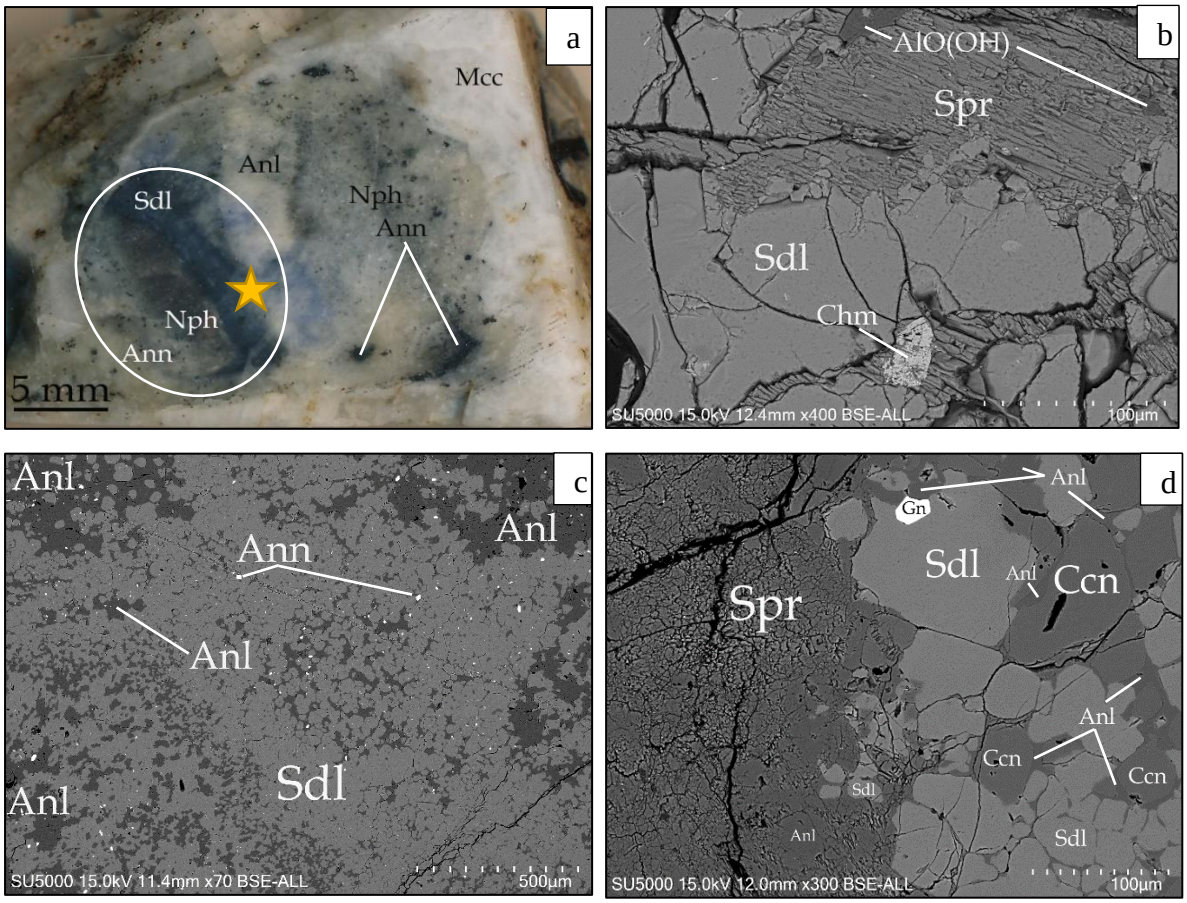

Figure 13 a) Sample EPX5 exhibiting brown nepheline transitioning into grey nepeline with interstital annite. A sharp boundary betweem brown nepheline and dark blue sodalite, transitioning into a light blue as interstital analcime content increase. The yellow star show the location of Fig. 13c. b) Primary sodalite, exhibiting the euhedral to anhedral shape with abundant fractures, some sprustein with abundant Al-hydroxides and some chamosite replacing sodalite. c) Sample EPX5, exhibiting aggregate of small rounded secondary sodalite with interstital analcime, abundant annite found within sodalite and analcime. d) Sample TVE1, show rounded secondary sodalite with cancrinite and analcime, all phases are being replaced by spreustein. Ab=albite, Anl=analcime, Ann=annite, Ccn=cancrinite, Chm=chamosite. Gn=galena, Mcc=microcline, Nph=nephline, Spr=spreustein, Sdl=sodalite

3.3 Cancrinite

Primary cancrinite crystallize during the magmatic stage of pegmatite formation, have a euhedral to subhedral shape, large size (1-7cm) and often rich in annite and aegirine crystals (<1-2 mm) (Appendix I, 1A). Primary cancrinite is frequently observed between individual feldspar crystals. Primary cancrinite can be altered into pink natrolite and/or *spreustein* as a result of hydrothermal alteration. Cancrinite has been observed transitioning into a crème white colour at the boundary with s*preustein* (Fig. 14). Alteration of primary cancrinite into a pink to greyish intergrowth of thomsonite-Ca and calcite was found in one sample from the Vevja quarry, in this sample brown nepheline were in contact with cancrinite (Appendix I, 8B).

A second generation of cancrinite forms later during the hydrothermal stages in the presence of nepheline. These do often exhibit a pale-yellow colour with abundant clusters of annite and aegirine crystals filling the cracks. Secondary cancrinite has been observed with natrolite or analcime filling internal fractures. In a sample from the Vevja quarry rounded cancrinite and sodalite was embedded in an analcime matrix, where the neighbouring mineral was later replaced by *spreustein* (Fig. 13d).

Cancrinite group is hexagonal and trigonal framework aluminosilicate with a zeolite-type structure which exhibits wide channels and cages which is occupied by large cations such as K^+, Na^+, Ca^{2+} as well as some anions CO_3^{2-}, SO_4^{2-}, Cl^-, OH^- and H_2O molecules (Rastsvetaeva et al., 2007). From the EMPA results (Table 4) it is evident that the extra framework cations are mainly Na^+ which has very high values (6.82 – 7.23) apfu and subordinately by Ca^{2+} which has very low values compared to the ideal formula ranging from (0.49-0-89) apfu, the ideal formula would have a 6:2 relationship between Na^+ and Ca^{2+}. The excess in Na^+ and subordinate Ca^{2+}-deficiency can indicate a substitution happening between $Ca^{2+} \rightarrow Na^+$. To obtain the charge balance in the formula a substitution of $Ca^{2+} \rightarrow 2Na$ would occur, this agrees with the high number of excess Na^+ in the analysed samples. Another possibility is a coupled substitution between ($Na^+ + Si^{4+} \rightarrow Ca^{2+} + Al^{3+}$) which also obtain the charge balance of the formula. This is rather unlikely to occur according to Figure 15 which show no correlation between this coupled substitutions. The anhydrous totals of weight% oxides obtained from the analysed cancrinite correlates well with the totals obtained by Sirbescu & Jenkins, (1999) who ran experiments on cancrinite to determine its stability in the system Na_2O-CaO-Al_2O_3-SiO_2-CO_2-H_2O.

The formula was calculated on the basis of (Si+Al) = 12 apfu whilst the volatile content, CO_3^{2-} was calculated stoichiometrically on the basis of the charge balance and the accepted value of H_2O equals 2 molecules pfu in accordance with Dumanska-Slovik et al., (2016). Cancrinite is a good indicator of the Ca^{2+} and CO_3^{2-} in the system at the time of crystallization.

Table 4: Representative compositions (weight% oxides) of cancrinite

Sample	EPX1	EPX1	EPX2	EPX9	EPX9
Analysis no.	1 / 3	8 / 3	20 / 3	54 / 3	10 / 2
n	9	4	3	4	4
Na_2O	21.2(1)	21.2(3)	20.9(2)	21.4(4)	21.7(4)
SiO_2	37.2(7)	36.1(5)	37.7(6)	37.3(4)	38.1(4)
CaO	3.3(2)	3.3(3)	3.50(5)	3.3(1)	2.7(3)
FeO	0.03(5)	0.04(2)	0.05(2	0.01(3)	0.02(4)
Al_2O_3	26.9(4)	27.2(5)	26.7(1)	27.1(3)	27.8(5)
MnO	0.04(5)	0.07(5)	0.03(5)	0.03(2)	0.01(4)
SO_4^{2-}	0.15(4)	0.15(9)	0.004(9)	0.01(4)	0.01(3)
MgO	0.000(3)	0.000(1)	-	-	-
Total	89.01	88.28	89.09	89.23	90.43
	Number of ions on the basis of Si + Al = 12 apfu				
Si^{4+}	6.48	6.36	6.48	6.47	6.45
Al^{3+}	5.52	5.64	5.52	5.53	5.55
Na^{+}	7.14	7.25	6.99	7.19	7.12
Ca^{2+}	0.62	0.63	0.69	0.61	0.49
Mn^{2+}	0.01	0.01	0.01	0.01	<0.01
Fe^{2+}	0.01	0.01	0.01	<0.01	<0.01
CO_3^{2-} *	1.06	1.06	1.06	1.06	1.05
SO_4^{2-}	0.02	0.03	-	-	-

*Type: Calculated value

Spreustein formed from cancrinite is dominated by pink natrolite, but zeolites precipitated in fractures within cancrinite is always analcime. The presence of analcime within cancrinite is not evident in hand sample, only by SEM-BSE imaging (Fig. 16). Cancrinite changes its colour from yellow to crème white at the boundary with pink *spreustein* (Fig.14). The white cancrinite has low content of Ca^{2+}, CO_3^{2-}, SO_4^{2-} and Fe^{2+} as evident from Analysis no. 54 / 3 and 10 / 2 in Table 4. It is often observed in the presence of brown nepheline which in turn also do transitioning into *spreustein* with a high Ca-content. This confirms the presence of Ca^{2+} available in the system.

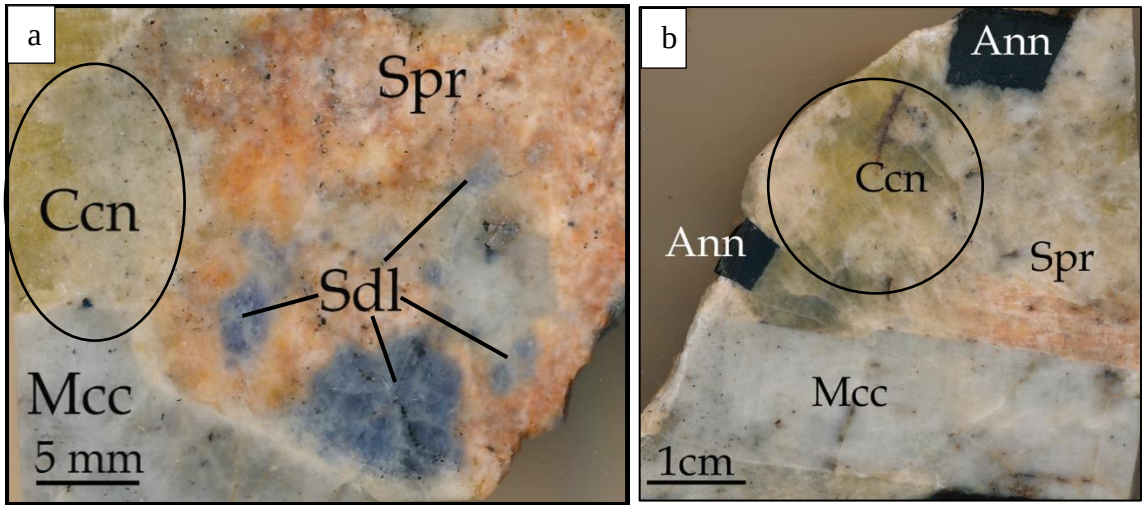

Figure 14: a) Cancrinite transitioning into crème white colours variety with interstitial annite in the presence of spreustein replacing both secondary sodalite and cancrinite. b) The same colour change is present as the transition into spreustein proceeds, this sample also contains secondary sodalite and interstitial annite. Ann=annite, Ccn=cancrinite, Mcc=microcline, Sdl=sodalite, Spr=spreustein

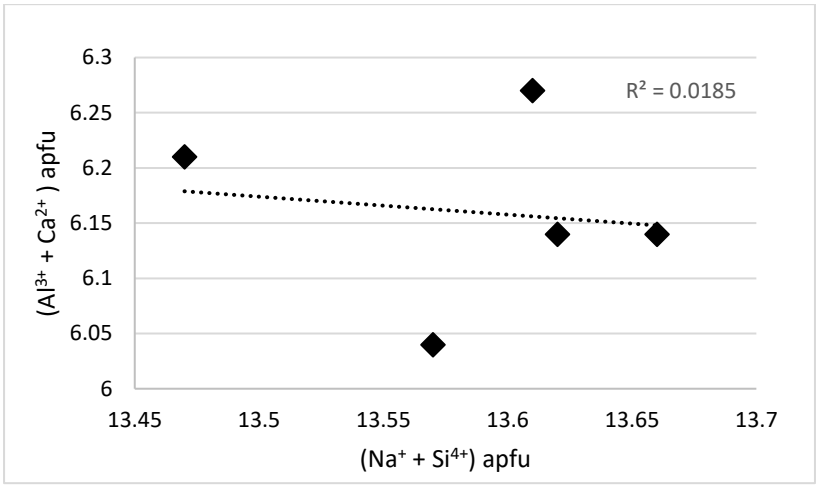

Figure 15: Show the possible coupled substitution (Al^{3+}+Ca^{2+} →Na^{+}+Si^{4+}) in cancrinite which do not show any correlation.

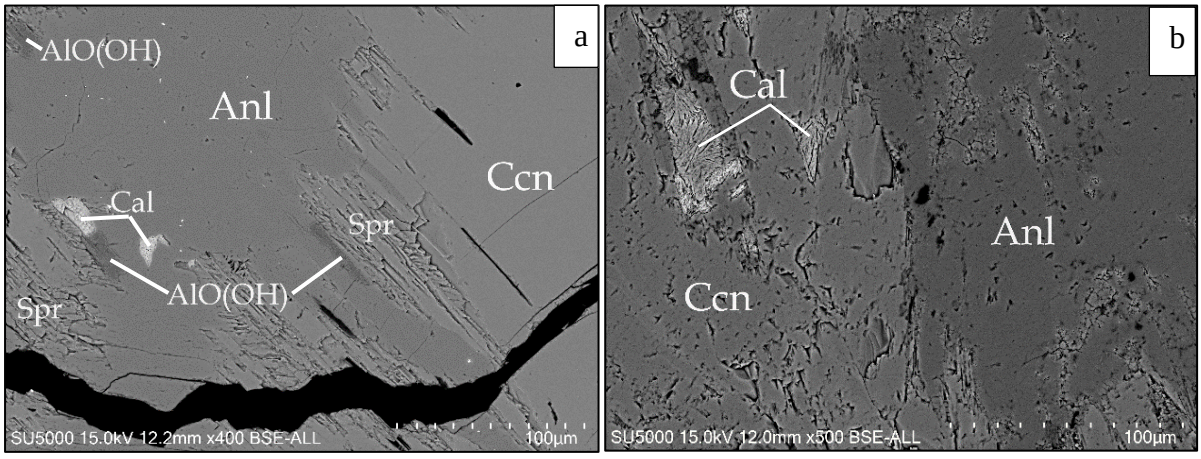

Figure 16: a) A vein of analcime going through cancrinite, some spreustein has started do develop along the boundaries. Enclosed Al-hydroxides and pods of calcite are found within analcime. b) Cancrinite being replaced by analcime, some calcite is also present. AlO(OH)=Al-hydroxides, Anl=analcime, Cal=calcite, Ccn=cancrinite, Spr=spreustein

3.4 Aegirine – Augite

Primary aegirine-augite is one of the first minerals to crystallize in the magmatic stages, whilst the second-generation of aegirine crystallizes during the later hydrothermal stages. Primary large aegirine-augite crystals are found in between feldspar, nepheline and *spreustein,* having euhedral to subhedral shapes and large sizes from centimetres to decimetres. A second generation of small elongated green aegirine crystals, a few even observed having an acicular crystal habit were found embedded in analcime in a sample from the Saga 1 quarry. Elongated secondary aegirine is widely found filling cracks in cancrinite and secondary sodalite. A fibrous, dense and dull green aegirine crystals as an intergrowth with annite crystals (<1-1mm) were found as a rim or complete pseudomorphs of black amphiboles in the presence of sacchariodal albite in a sample from Saga 1.

3.5 Analcime

Analcime is an abundant zeolite forming as replacement of feldspathoids during the hydrothermal stages of pegmatite formation. Analcime is widely found as an interstitial phase in secondary sodalite and *spreustein* or as pods and veins in primary and secondary sodalite, nepheline and cancrinite. Analcime is also found as a rim around microcline, especially within grey nepheline (Fig. 6a). Analcime has also been observed as a matrix hosting rounded secondary sodalite with or without rounded cancrinite. Large aggregates of white analcime are found to host secondary annite, thomsonite-Ca, calcite, natrolite and Al-hydroxides and are abundantly found within *spreustein* (Fig. 17).

EMPA data of analcime (Table 5) from the samples have nearly stoichiometric composition with Si/Al ranging from 1.9-2.05 apfu only some minor incorporation of K^+ into the Na^+ site in the structure. Due to the high water content in the analcime crystal structure and the porous nature of the mineral, EMPA totals was a bit low in some of the data points. Overall, the results are consistent even though analcime does crystallize because of alteration of multiple and very diverse minerals. The main change between analcime and the other main zeolite, natrolite, is that analcime always has a white colour, whereas natrolite can incorporate cations into the structure and change its colour accordingly.

Table 5: Representative composition (weight% oxides) of analcime

Sample	Analcime			
	EPX2	EXP1	EXP5	EXP10
Analysis no	24 / 3	51 / 3	69 / 4	38 / 4
n	11	3	5	6
Na_2O	13.7(1)	13.69(1)	13.7(4)	13.79(4)
SiO_2	54.6(6)	54.1(2)	53.8(7)	52.8(7)
Cl	0.004(1)	0.003(5)	0.01(2)	0.01(1)
K_2O	0.06(3)	0.07(3)	0.1(1)	0.26(1)
CaO	0.01(2)	0.02(1)	0.01(2)	0.01(1)
FeO	0.0118(2)	0.001(3)	0.02(3)	0.01(3)
Al_2O_3	22.6(6)	22.49(1)	22.8(5)	23.48(6)
MgO	0.002(1)	0.01(1)	0.01(2)	0.001(6)
MnO	0.008(2)	0.02(4)	0.018(2)	0.01(3)
SO_3	0.008(2)	0.01(3)	0.018(1)	0.02(3)
Total	91.18	90.46	90.73	90.48
	Formula based on 4 cations			
Si^{4+}	2.02	2.02	2.00	1.97
Al^{3+}	0.99	0.99	1.00	1.03
Na^{+}	0.99	0.99	0.99	1.00
K^{+}	<0.01	<0.01	0.01	0.01
Cl^{-}	<0.01	<0.01	<0.01	<0.01
Si/Al	2.05	2.04	2.00	1.91

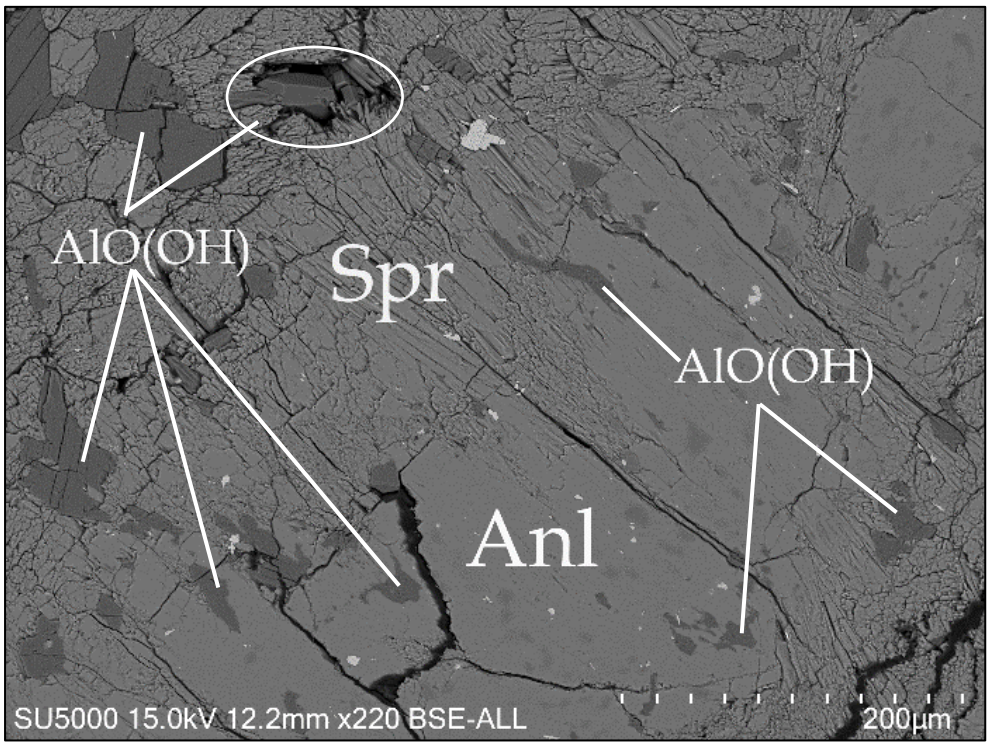

Figure 17: BSE image of analcime and spreustein with abundant Al-hydroxide as an interstitial phase in spreustein and fully enclosed in analcime. Small annite is also present in light grey colour. Spreustein and analcime is easy distinguishable due to their different textural properties. AlO(OH)=Al-hydroxides, Anl=analcime, Spr=spreustein.

3.6 Natrolite

Natrolite is always present in the LPC pegmatites where extensive hydrothermal alteration has occurred and linked to the late hydrothermal stages of pegmatite formation. Natrolite is also the main mineral in the alteration product *spreustein*. Natrolite is the most abundant zeolite found in the samples and appears in a wide range of colours. Everything from colourless, white to dark red and brown is observed, the darker colours are commonly found as *spreustein*. White to pink natrolite is associated with hydrothermal alteration of cancrinite (Fig. 14) and sodalite (Fig. 12) and orange/red to darker brown colours of natrolite when forming at the expense of brown nepheline (Fig. 9). The observations indicate that the chemical composition of natrolite varies, depending on the parent mineral (Table 6). The colourless to white natrolite are the ones closest to the ideal formula, ion exchange is not evident in these samples. In pink to red natrolite Ca^{2+} and minor amounts of K^{+}, Mg^{2+}, Mn^{2+} and Fe^{3+} have been found incorporated into the natrolite structure. The general formula for zeolites allows for large variations in chemical composition, the only constraint being Lowenstein's rule saying that Si>Al (Passaglia & Sheppard, 2001). It is evident from the analysis that natrolite does incorporate cations into its structure during replacement, which cations are being incorporated is highly dependent on the mineral being replaced. Natrolite found together with analcime does exhibit the lowest amounts of incorporated ions.

Table 6: Representative composition (weight% oxides) of natrolite

Sample	Natrolite								
	EXP2	EPX9	EPX 9	EPX 9	EPX2	EPX1	EPX9	EPX10	EPX10
Analysis no	72 / 1	19 / 2	65 / 3	23 / 2	30 / 3	45 / 3	58 / 3	16 / 4	18 / 4
n	1	4	3	2	10	4	4	2	3
Na_2O	14.58	14.7(3)	14.8(2)	13.70(3)	15.6(2)	15.2(4)	15.29(3)	14.3(6)	15.2(6)
SiO_2	45.62	45.18(9)	45.05(2)	42.05(2)	47.7(4)	46.3(4)	46.4(9)	44.2(5)	45.3(4)
Cl	-	0.011(9)	0.01(1)	0.008(1)	0.01(1)	0.002(7)	0.01(1)	0.0005(9)	0.01(2)
K_2O	0.04	0.06(2)	0.06(6)	0.059(5)	0.035(2)	0.08(4)	0.10(2)	0.4(2)	0.8(4)
CaO	1.12	0.9(1)	1.016(7)	1.105(6)	0.03(5)	0.4(5)	0.6(3)	1.36(1)	0.3(2)
Fe_2O_3	-	0.15(9)	0.03(7)	0.05(6)	0.01(3)	0.02(3)	0.002(7)	0.2(4)	0.04(2)
Al_2O_3	26.68	27.8(8)	27.1(4)	31.61(1)	25.89(5)	25.9(7)	26.4(3)	28.3(9)	27.5(5)
MgO	0.02	0.006(2)	-	0.002(4)	0.01(1)	0.000(1)	0.01(1)	0.01(1)	0.01(2)
MnO	0.03	0.04(4)	0.027(3)	0.003(7)	0.01(2)	0.01(1)	0.01(2)	0.01(3)	0.01(2)
SO_4^{2-}	-	0.01(2)	-	0.01(2)	0.01(2)	0.004(9)	0.01(1)	0.01(2)	0.02(3)
Total	88.08	88.99	88.12	88.61	89.34	88.07	88.99	89.11	89.38
	Anhydrous formula unit composition based on 80 oxygens								
Si^{4+}	23.73	23.29	23.46	21.76	24.39	24.08	23.91	22.87	23.39
Al^{3+}	16.36	16.92	16.65	19.28	15.61	15.91	16.07	17.28	16.72
Na^{+}	14.70	14.70	14.96	13.75	15.49	15.35	15.28	14.43	15.28
Ca^{2+}	0.62	0.52	0.57	0.61	0.02	0.25	0.37	0.76	0.16
K^{+}	0.02	0.04	0.04	0.04	0.02	0.05	0.07	0.32	0.53
Mn^{2+}	0.01	0.02	0.01	<0.01	<0.01	<0.01	<0.01	0.01	<0.01
Fe^{3+}	-	0.03	0.01	0.02	<0.01	<0.01	<0.01	0.06	0.01
Mg^{2+}	0.02	<0.01	-	-	0.01	-	0.01	0.01	0.01
SO_4^{2-}	-	0.01	-	-	0.00	<0.01	<0.01	0.01	0.01
Cl^{-}	-	0.01	<0.01	0.01	0.01	<0.01	0.01	-	0.01
Si / (Al + Si)	0.59	0.58	0.58	0.53	0.61	0.60	0.60	0.57	0.58

3.7 Thomsonite-Ca

Thomsonite-Ca is another zeolite forming in the LPC pegmatites during the late hydrothermal stages of pegmatite formation. Well-developed colourless and pink crystals of thomsonite-Ca has been observed in vugs in *spreustein* in one of the collected samples from Saga 1 quarry (Appendix I, 7C). Some other inclusions of thomsonite-Ca within analcime have been observed in close proximity to cancrinite. An intimate intergrowth of thomsonite-Ca and calcite was also found replacing cancrinite in a sample from Vevja quarry (Appendix I, 8B), this sample has a transitional boundary between cancrinite and brown nepheline. Thomsonite-Ca from the samples differs from the ideal formula having a slight Ca-deficiency. The following substitution, $Ca^{2+} \rightarrow 2Na^{+}$ can explain the Ca-deficiency as well as the excess Na^{+} in the structural formula of thomsonite-Ca in the samples (Table 7).

Table 7: Representative composition (weight% oxides) of Thomsonite-Ca and calcite

Sample	Tmh-Ca			Calcite
	EPX2	EPX2	EPX2	EPX2
Analysis no	71 / 1	74 / 1	75 / 1	76 / 1
Na_2O	4.66	6.14	4.06	0.06
SiO_2	37.83	39.04	37.59	0.13
Cl	-	-	-	0.04
K_2O	-	0.01	0.02	-
CaO	12.06	10.58	13.15	50.09
Fe_2O_3	0.06	0.04	0.01	0.03
Al_2O_3	28.64	28.50	28.93	0.04
MnO	-	-	0.02	0.76
SO_3^-	-	-	-	0.02
O=Cl	-	-	-	0.01
CO_2*	-	-	-	40.16
Total	83.26	84.31	83.78	91.32
Anhydrous formula unit composition based on 80 oxygens				*1 cation*
Si^{4+}	21.05	21.42	20.83	-
Al^{3+}	18.77	18.43	18.89	-
Na^{+}	5.03	6.53	4.36	<0.01
Ca^{2+}	7.19	6.22	7.81	0.99
K^{+}	<0.01	0.01	0.01	-
Mn^{2+}	-	-	0.01	0.01
Fe^{3+}	0.01	0.01	<0.01	-

CO_2 calculated from ideal formula*

3.8 Calcite

Calcite is considered a widespread mineral and is one of the latest minerals to crystalize in the hydrothermal stages of pegmatite formation. Calcite exhibits a white to pinkish colour and observed as veins, small individual pods and well-developed flaky crystals together with Al-hydroxides within larger zeolites or in vugs in *spreustein*. Calcite was found as inclusions in thomsonite-Ca in a few of the collected samples, mainly within larger clusters of analcime (Fig. 18a). Calcite is also present in samples as late veins cutting through *spreustein* and the red abrupt reaction rim found as a boundary layer between brown nepheline and red *spreustein*. Calcite is also commonly observed together with Al-hydroxides within analcime and *spreustein* (Fig. 18b). An interesting sample (TVE2) from the Vevja quarry contains brown nepheline, cancrinite, calcite and thomsonite-Ca (Appendix I).

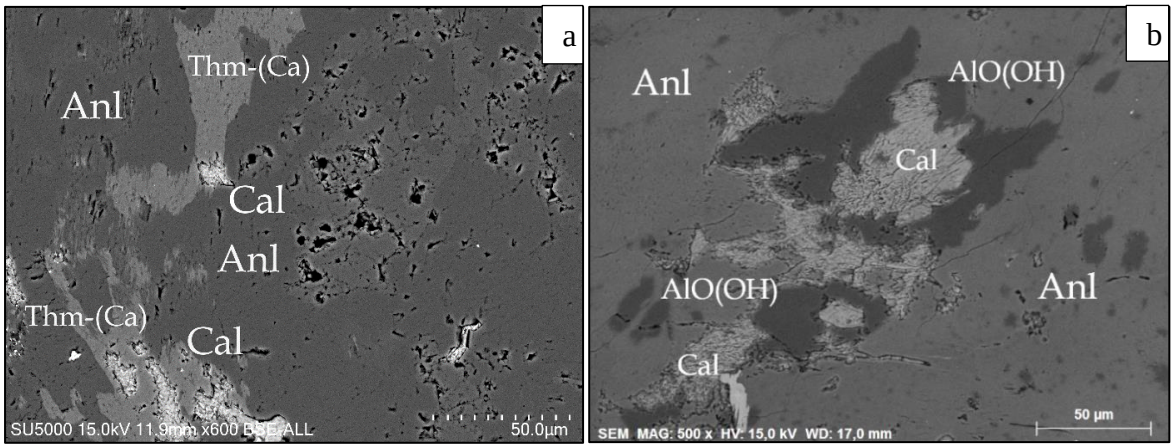

Figure 18; a) Thomsonite-Ca interstitial with calcite within larger masses of analcime from sample EPX2. b) Calcite with/without Al-hydroxides as an interstitial phase in analcime from sample EPX9. AlO(OH)=Al-hydroxides, Anl=analcime, Cal=calcite, Thm-Ca=thomsonite-Ca.

3.9 Annite

Most primary annite crystallize early in the magmatic stages of pegmatite formation. Secondary smaller annite crystals (<1–2mm) form during the later hydrothermal stages. Annite is a very common mineral in the LPC, the primary minerals are well-developed pseudohexagonal prisms and are found embedded in feldspar. Primary annite have large sizes from centimetres to decimetres. Secondary smaller annite crystals are abundantly found interstitial in grey nepheline, secondary sodalite, cancrinite, analcime, microcline, albite and *spreustein.* Annite coronas are also commonly observed around larger magnetite crystals in the samples, or as inclusions in smaller magnetite crystals within nepheline or in *spreustein.*

EMPA show consistent compositions of the primary and secondary annite, but there are prominent differences between the two generations. The primary annite was found to have a higher Mg^{2+} and Ti^{4+} content than the secondary which in turn has a higher Fe^{2+} and slightly higher Al^{3+} content (Table 8). The following substitutions $Mg^{2+} \rightarrow Fe^{2+}$ and $(Ti^{4+} + Si^{4+}) \rightarrow Al^{3+}$ (Fig. 19) explains the difference between primary and secondary annite and the increase seen in Fe^{2+} and Al^{3+} content in the second generation. Secondary annite in the samples have a composition very close to ideal formula of annite. Some Ca^{2+} and Na^{+} was detected in the secondary annite, this is often seen as substitution for K^{+} in the formula. Magnetite is abundantly observed with annite in SEM-BSE. Larger crystals of magnetite are also found with annite coronas in hand samples together with nepheline and microcline.

Table 8: Representative composition (weight% oxides) of annite

Sample	Annite			
	EPX 9	EPX 9	EPX9	EPX9
Analysis no	79 / 3	71 / 3	82 / 3	86 / 3
Type*	P	S	S	S
n	3	6	1	2
Na_2O	0.09(2)	0.07(4)	0.11	0.06(6)
SiO_2	35.4(8)	32.3(9)	30.53	32.7(7)
CaO	-	0.012(4)	2.91	-
FeO	32.5(5)	37.5(9)	35.75	37.7(6)
Al_2O_3	10.5(1)	12.9(8)	12.10	12.1(2)
MnO	0.61(7)	0.58(3)	0.72	0.93(6)
MgO	3.08(2)	0.4(4)	0.46	0.6(2)
TiO_2	2.7(5)	0.2(3)	0.31	0.25(6)
K_2O	9.3(1)	8.8(4)	8.55	8.97(2)
Cr_2O_3	0.021(8)	0.003(1)	-	0.001(2)
Total	94.27	92.98	91.44	93.50
	Formula based on 8 cations			
Si^{4+}	3.01	2.87	2.85	2.91
Al^{3+}	1.05	0.68	0.67	0.63
Na^{+}	0.02	0.01	0.01	0.01
Ca^{2+}	-	-	0.15	-
K^{+}	1.01	0.50	0.51	0.51
Ti^{4+}	0.18	0.01	0.01	0.01
Mn^{2+}	0.04	0.02	0.03	0.04
Fe^{2+}	2.31	1.39	1.40	1.40
Mg^{2+}	0.39	0.03	0.03	0.04
Cr^{3+}	0.01	-	-	-

**Type: P=Primary S=secondary*

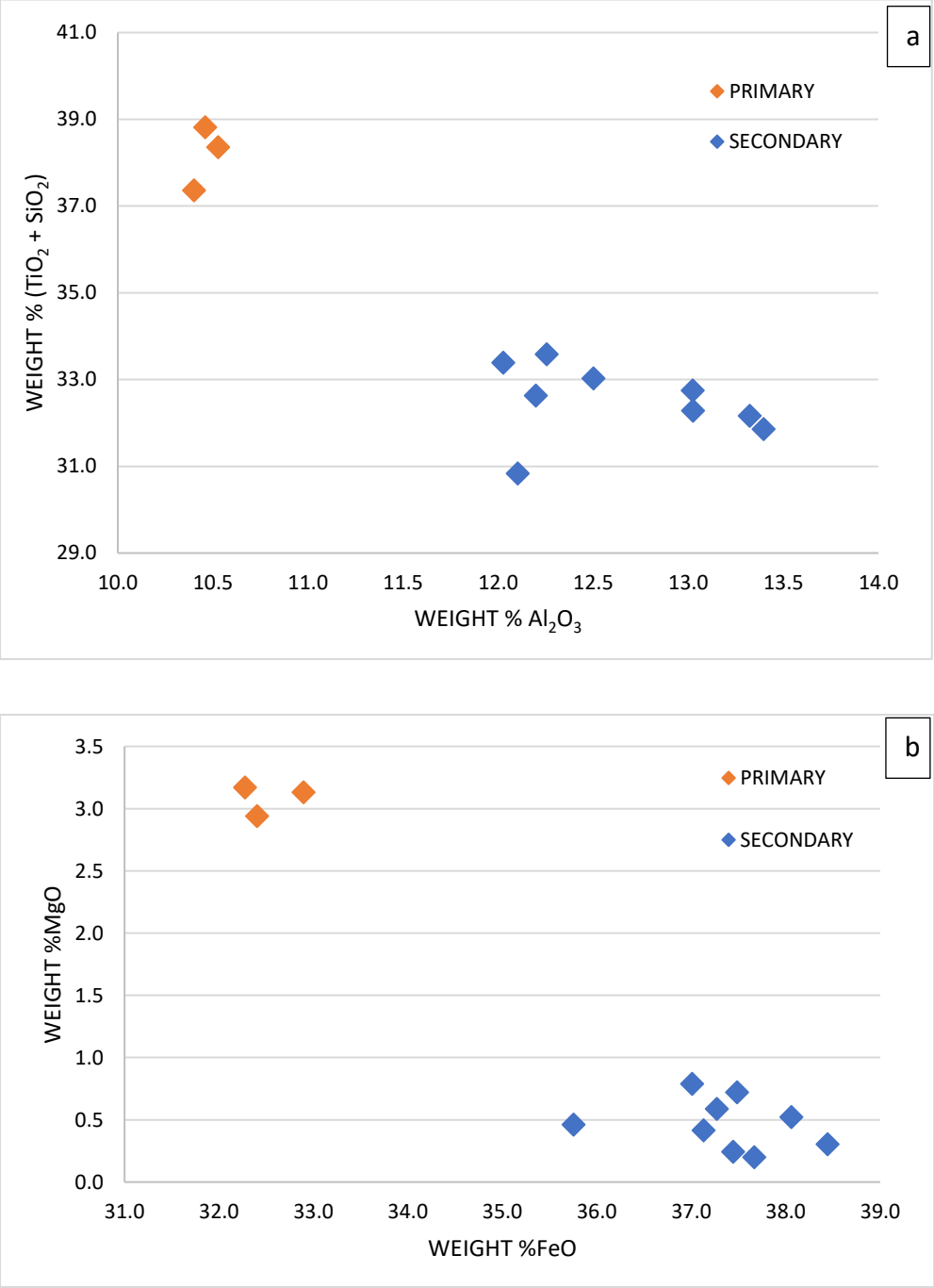

Figure 19: a) Show the substitutional relationship found between (TiO_2+SiO_2)↔Al_2O_3 in primary and secondary annite. b) Show the substitutional relationship between MgO↔FeO in primary and secondary annite.

3.10 Microcline and albite

Microcline crystallizes as one of the latest minerals in the magmatic stage of pegmatite formation together with albite. The crystals are pale grey to grey in colour and can be anything from centimetres to decimetres in size. During the hydrothermal stages some microcline crystals have been observed altered into *spreustein.*

Microcline is often found rimmed by analcime fully embedded in grey nepheline with or without albite and secondary sodalite present (Fig. 6a). Hydrothermally altered microcline are abundantly found to be rich in small (<1-1mm) annite crystals. The extensive hydrothermal alteration responsible for zeolitization of felspathoids does not have any effect on the chemical composition of microcline, even in contact with zeolites it has a composition very close to the ideal formula

Table 9: Representative composition (weight% oxides) of microcline and albite

Sample	Microcline			Albite	
	EPX10	EPX10	EPX 12	EPX 9	EPX9
Analysis no	1 / 4	43 / 4	57 / 2	3 / 2	62 / 3
n	2	8	1	6	2
Na2O	0.51(1)	0.6(4)	0.29	11.8(2)	11.7(1)
SiO2	64.668(9)	64.5(5)	64.67	68.9(3)	67.9(5)
Cl	0.005(8)	0.01(2)	-	0.01(1)	0.004(8)
K2O	16.42(8)	16.21	16.96	0.12(2)	0.1(2)
CaO	-	-	-	0.01(2)	0.01(1)
FeO	0.10(1)	0.04(6)	0.03	0.26(9)	0.29(5)
Al2O3	17.8(1)	17.8(3)	17.97	18.8(1)	18.7(5)
MgO	0.01(1)	0.01(2)	-	0.003(9)	0.02(3)
MnO	0.005(2)	0.01(2)	0.01	0.01(2)	-
SO3	0.001(2)	0.01(3)	0.02	0.01(2)	-
Total	99.36	99.76	99.95	100.11	98.95
	Formula based on 8 oxygens				
Si^{4+}	3.00	3.01	3.00	3.01	3.00
Al^{3+}	0.97	0.98	0.98	0.97	0.98
Na^{+}	0.05	0.06	0.03	1.01	1.01
Ca^{2+}	<0.01	-	-	0.01	0.01
K^{+}	1.01	0.96	1.00	<0.01	-
Fe^{3+}	<0.01	<0.01	<0.01	0.01	0.01
Mn^{2+}	<0.01	-	-	<0.01	<0.01

Albite crystallize as one of the latest minerals in the magmatic stage of pegmatite formation. Albite has a white to greyish colour and are observed in a wide range of sizes, from millimetres to centimetres. Albite is found interstitial with grey nepheline and sodalite together with zeolites in samples from the Saga 1 and Vevja quarry. A white fine grained saccharidal albite *sugar albite* of hydrothermal origin together with zeolites and fibrous aegirine was found in one sample from Saga 1. Albite is usually found with microcline, sodalite and cancrinite, natrolite has also been observed to replace albite in the presence of nepheline. Incorporation of Fe^{3+} is also

found to occur in albite (Table 9). This is a product of the $Al^{3+} \rightarrow Fe^{3+}$ substitution widely observed to occur in the system.

3.11 Al-hydroxides

Al-hydroxides, such as diaspore and böhmite are some of the last minerals to form during the hydrothermal stages of pegmatite formation. Diaspore and böhmite are dimorphs and abundantly found in vugs in *spreustein,* as well as inclusions fully enclosed in analcime. They are observed as intergrowths with calcite, as smaller inclusions in larger natrolite-and analcime crystals and are also abundantly found in-between analcime and cancrinite. Well-developed *sugar like* brown böhmite crystals is found in one of the collected samples together with white natrolite crystals, flaky white calcite and well-developed colourless and pink thomsonite-Ca crystals in *spreustein*. Analcime as with natrolite has a typical porous crystal habit typical of zeolites and abundantly found to host Al-hydroxides as an enclosed phase in close proximity to *spreustein*. Al-hydroxides have different textural relationships with analcime and *spreustein,* evident from SEM-BSE images (Fig. 17). Al-hydroxides and analcime looks to have a dissolution-precipitation relationships, whilst Al-hydroxides are observed to settle in voids and cracks in *spreustein.*

EMPA results of the Al-hydroxides did produce very low total values of weight% oxides, only a small quantity of larger well-developed crystals of purple diaspore and brown böhmite are found within cavities in *spreustein* and can be easily distinguished from each other. Unfortunately, this is not the case for most of the Al-hydroxides found within analcime and *spreustein*. The grain sizes are too small to identify through optical microscopy and the grains are not large enough to be detected for XRD analysis. These uncertainties make it impossible to distinguish between böhmite/diaspore in the samples. The term Al-hydroxides is therefore used in this study.

4. Discussion

According to the textures and relationships between minerals observed in hand samples, thin sections and epoxy mounts the primary minerals in the selected samples are aegirine-augite, black amphibole, sodalite, nepheline, cancrinite, microcline and albite. The starting composition of the pegmatite melt in the LPC had a silica undersaturated bulk composition with sufficiently high content of NaCl to form the primary sodalite (Barker, 1976). The first minerals to form were the mafics, further sodalite, nepheline and cancrinite and lastly feldspars microcline and albite. The distinctive primary and secondary HFSE-and REE-minerals found in the LPC pegmatites are not within the scope of this study and therefore left out.

The secondary minerals of the LPC pegmatites are found to form during the later hydrothermal stages of pegmatite formation and formed at the expense of the primary minerals (Dahlgren, 2010). The magmatic fluid responsible for the crystallization of the secondary minerals had a starting composition of a saline brine (Sunde et al., 2019). The secondary minerals of interest include secondary blue sodalite, cancrinite, microcline, albite, annite and calcite as well as zeolite group minerals such as natrolite, analcime and thomsonite-Ca. These minerals are typically seen in the LPC pegmatites, similar findings and crystallization sequences are in agreement with previous studies from the area by Larsen et al. (2010) and Sunde et al. (2019). The widespread zeolitization has been reported from multiple alkaline complexes in the world (Marks & Markle, 2017), but the alteration phase *spreustein* with its interstitial Al-hydroxides are fairly scarce in the literature. The secondary process behind the latest phases formed in the LPC pegmatites including the widely observed phenomenon spreustein with Al-hydroxides has been unknown ever since Brøgger first mentioned it in the late 1880s.

4.1 The hydrothermal stages of pegmatite formation

Groome (2017) did a detailed study of the Bjønnes nepheline syenite intrusion and its surroundings including the Sagåsen quarry. He frequently observed eudialyte breaking down to form secondary aegirine and zircon according to the unbalanced reaction (1), both minerals abundantly observed in collected samples of the LPC pegmatites. The breakdown of eudialyte could have occurred in response to the

increasingly fluid rich residue melt resulting from the crystallization of the mainly anhydrous minerals assemblage in the magmatic stages of pegmatite formation.

Reaction (1)

$$\mathrm{Na_{15}Ca_6Fe_3^{2+}SiZr_3Si_{25}O_{73}(O,OH,H_2O)_3(Cl,OH)_2\ (Eud) + 12F^-}$$
$$\mathrm{\rightarrow 3NaFe^{3+}Si_2O_6\ (Aeg)\ + 3ZrSiO_4\ (Zr) + 6CaF_2\ (Fl) + 12Na^+ + 17Si^{4+}}$$
$$\mathrm{+ 43O^- + 2Cl^-}$$

This reaction may mark the beginning of the hydrothermal processes caused by the increasing amounts of fluids in the residue melt, penetrating through fractures and cleavage planes resulting in alteration of EGM. In hydrothermal environments such as the one in question fluids rich in F^-, H_2O and CO_3^{2-} causes Zr, Nb and REE's to become more soluble and therefore also easily mobilised (Piilonen et al., 2013, Groome, 2017). This is a good explanation for the observed suite of REE and Nb minerals found as small interstitial phases throughout the samples. Nielsen (1979) described reaction (2) of nepheline in the presence of $Na_2Si_2O_5$ *Nds* and Cl, both products are released from the reaction (1).

Reaction (2)

$$\mathrm{Na_3KAl_4Si_4O_{16}\ (Nph) + Na_2Si_2O_5\ (Nds) + 3\ HCl\ + 8\ SiO_2}$$
$$\mathrm{\rightarrow 3\ NaAlSi_3O_8\ (Ab) + KAlSi_3O_8(Mcc) + NaCl}$$

Reaction (2) results in an enrichment in NaCl in the magmatic fluid and a secondary albite crystallizing at the expense of nepheline. Pods of albite and microcline within nepheline are abundantly observed in BSE images. The incorporation of more NaCl and H_2O into the residue melt can have been part of the reason for the observed immiscibility between the saline brine and the Na-rich residue melt.

The NaCl fluids evolve when Si-undersaturated magma is cooling (Kilinc & Burnham, 1972), NaCl readily partition into the aqueous phase and would be removed from the silicate melt (Sharp et al., 1989). Crystallization of albite from an albite-rich, NaCl-H2O bearing liquid leads to an increasing concentration of NaCl and H_2O in the liquid seen in Reaction (2) until a H_2O-NaCl rich fluid (or vapor) develops (Van Groos

& Wyllie, 1969). Binsted (1981) in his studies of the system Ab-Ne-NaCl-H_2O recognized the presence of a NaCl-enriched hydrous fluid phase in equilibrium with a silicate melt. With the additional components of SiO_2 and Al_2O_3 in this phase, the potential for subsequent sodalite crystallization appears possible by crystallize from the NaCl-rich liquid or by reaction of pre-existing phases with such a liquid (Woolley & Platt, 1988). The increase in NaCl content of the fluids as a product of reaction (2) increase the solubility of H_2O remarkably. Burnham and Jahns (1962) have shown that the presence of 0.3 percent NaCl causes an increase in the H_2O solubility comparable with an increase in pressure from 1 to 3kbars (Woolley & Platt, 1988).

4.2 Nepheline

4.2.1 Fe-rich nepheline

According to the ideal formula of nepheline no Fe^{3+} should be incorporated and the colour should be grey to whitish. From the results (Table 2) it is evident that brown nepheline has a higher content of Fe^{3+} than the grey equivalent. Therefore, it seems likely that the amount of Fe^{3+} is affecting the colour of nepheline. The incorporation of Fe^{3+} into the nepheline structure has been studied by Onuma et al. (1972), they argue that the composition of nepheline reflects the bulk composition of the starting material in the Na_2O-Fe_2O_3-Al_2O_3-SiO_2 system. They further suggested that Fe-nepheline crystallize when the parent melt or fluids have a sufficient content of alkalis, especially Na_2O and available Fe_2O_3. By calculating the formula for both brown and grey nepheline from the samples, it is evident that there are some vacant positions in the structure of brown nepheline. A higher silica content in brown nepheline is in agreement with Onuma et al. (1972).

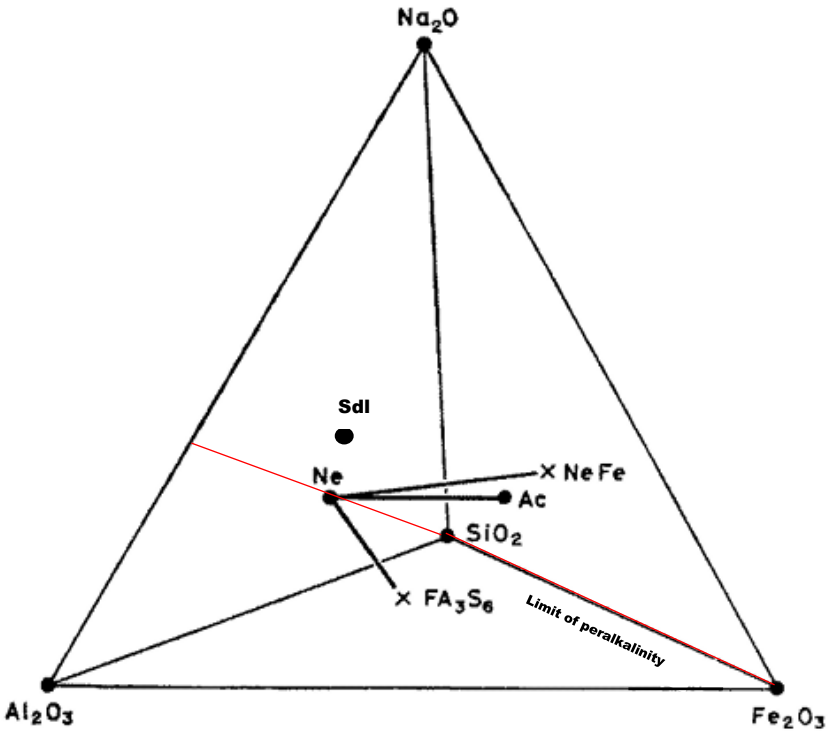

Figure 20: Quaternary plot of the system: Na_2O-Fe_2O_3-Al_2O_3-SiO_2. The red line show the limit of peralkalinity in the system. Ne= nepheline, xNe Fe = nepheline series, ac = acmite series. Modified from Onuma and Yoshikawa (1972).

Further studies by Onuma and Yoshikawa (1972) suggest that Fe^{3+} can be incorporated into the nepheline structure in either one of two ways in the system Na_2O-Fe_2O_3-Al_2O_3-SiO_2. A $Fe^{3+} \rightarrow Al^{3+}$ substitution observed in iron-bearing nepheline gives the "Fe-nepheline" series, and the coupled substitutions ($Na^+ \rightarrow \square$) and (Fe^{3+}, $Al^{3+} \rightarrow Si^{4+}$) gives the "Nepheline-acmite" series (Fig. 20). By this definition the results indicate this being the Fe-nepheline series, operating in the part of the system poor in Al_2O_3 and enriched in Si^{4+}. Onuma and Yoshikawa (1972) show that the iron content of natural nepheline is not influenced by the total iron in the melt, only the ferric iron and alkali composition. A nepheline crystallizing from a magma with high total iron content, but with a low ferric-ferrous ratio will thus have a low iron content. Fe^{3+} incorporation into the nepheline structure is therefore highly dependent on the oxygen fugacity and the bulk composition of the parent melt. The nepheline from the LPC pegmatites do follow the "Fe-nepheline" series according to the observed substitution, even though the values of Fe^{3+} are low. Meaning that most of the Fe^{3+} in the system was already taken up by other primary phases which crystallized before nepheline, such as black amphiboles, aegirine and magnetite.

4.2.2 Red abrupt reaction rim

A red abrupt reaction rim is commonly observed between brown nepheline and *spreustein* (Fig. 9). Unfortunately, the nature of the rim was porous something that made the EMPA results inconsistent and prone to low totals. The high content of Ca^{2+} and some Fe^{3+} is the reason for its bright red colour, the same colour is present in natrolite with the same composition. The Fe^{3+} found in the rim can possibly have come from brown nepheline as it releases Fe^{3+} when transitioning into grey nepheline. It is though interesting how it is found to crystallize within the boundaries between albite crystals in close proximity to *spreustein* and brown nepheline. Its origin is most likely a fluid which was in equilibrium with *spreustein*, the textural relationship with nepheline indicates that the red material crystallized when it reacted with nepheline and/or albite (Fig. 10).

4.3 Sodalite

After the crystallization of primary sodalite, another generation of sodalite grew, with a very similar composition (Table 3). The presence of Fe^{3+} in primary sodalite is a possible explanation for the darker green colour compared to the secondary bright blue sodalite. The colour of the two generations makes them easily distinguishable. Secondary sodalite is commonly observed together with nepheline, cancrinite, microcline, albite, natrolite and analcime, the first four frequently observed forming inclusions within each other. From SEM-BSE imaging there is evidence of analcime and secondary sodalite (+microcline) forming concurrently within nepheline (Fig. 21), but secondary sodalite is also commonly observed to crystallize first, later being replaced by analcime (Fig. 22). Secondary sodalite is always in contact with nepheline, this is widely observed in hand sample and in BSE images, albite is only found using BSE imaging within nepheline often together with natrolite (Fig. 23).

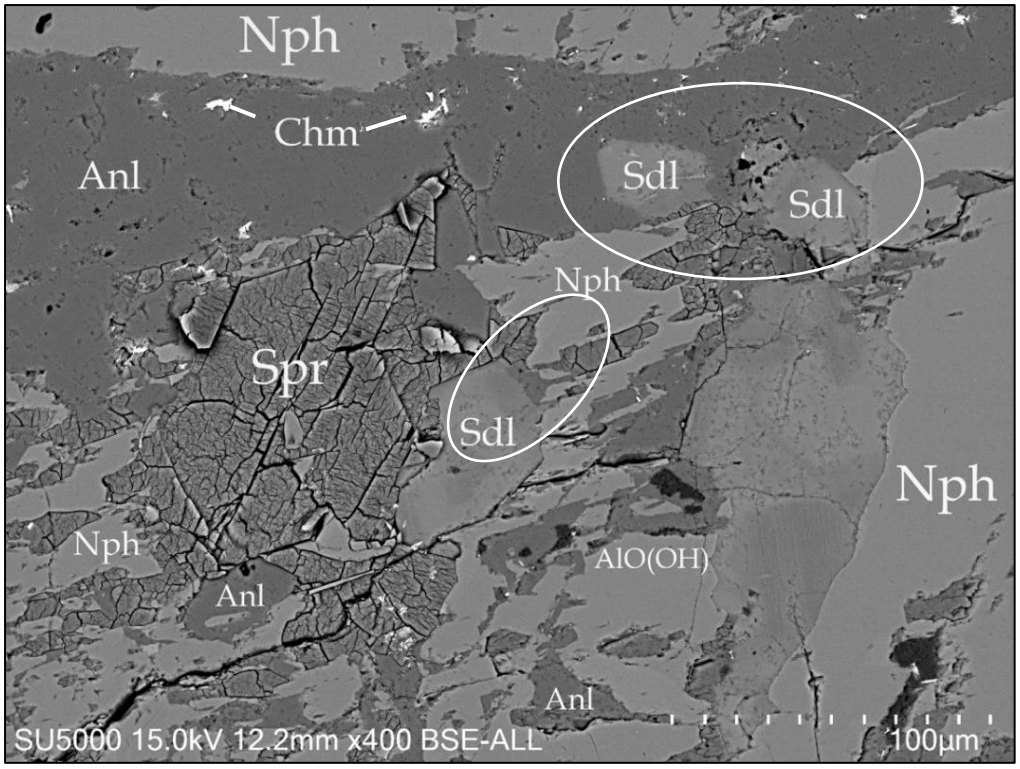

Figure 21: Show the relationship between nepheline, secondary sodalite and analcime within grey nepheline in sample EPX10. Sodalite forming as pods in contact with nepheline and analcime. Spreustein is also present replacing nepheline. AlO(OH)= Al-hydroxides, Anl=analcime, Chm=chamosite, Nph=nepheline, Sdl=secondary sodalite.

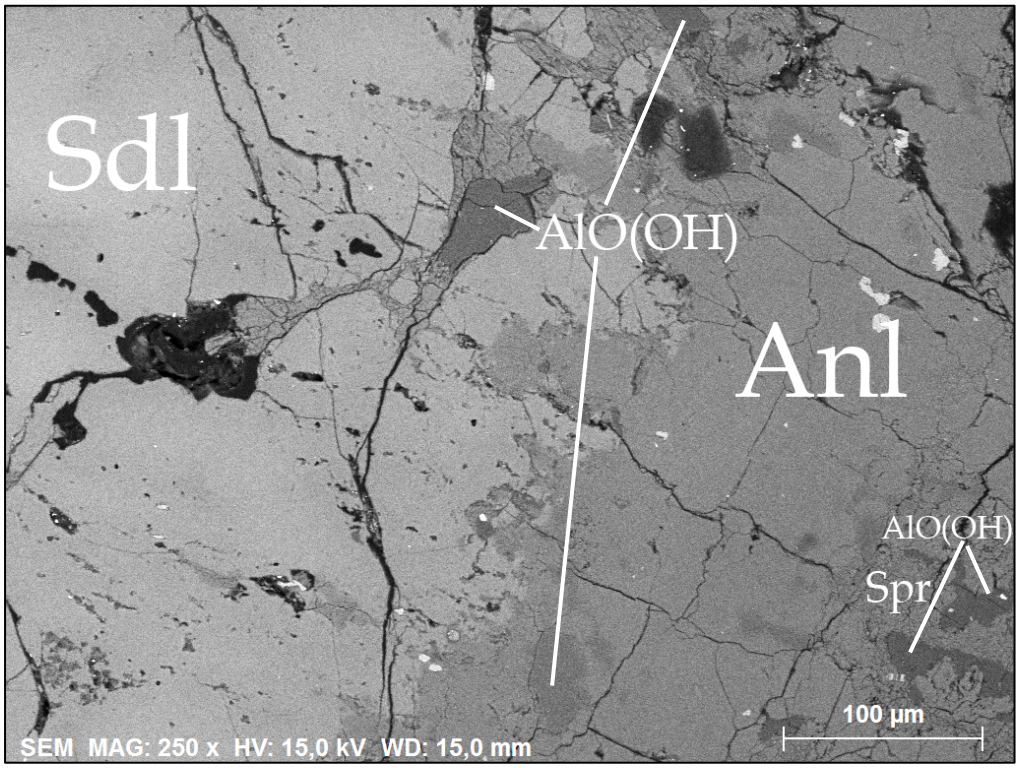

Figure 22: Secondary sodalite being replaced by later crystallization of analcime in sample EPX8. Al-hydroxides are widely present filling fractures or enclosed in analcime. AlO(OH)=Al-hydroxides, Anl=analcime, Sdl=secondary sodalite, Spr=spreustein.

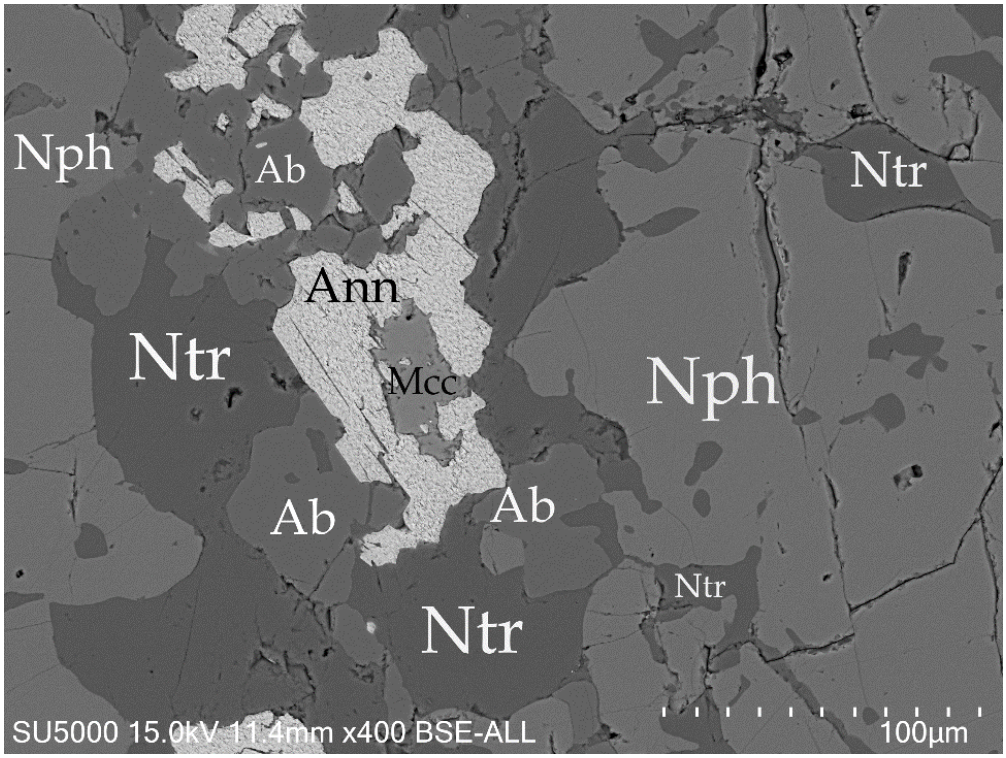

Figure 23: Grey nepheline and albite being replaced by natrolite. Microcline and annite are found as interstitial phases within nepheline, this is frequently observed in relation to sodalite replacement of nepheline. Sodalite could well be present here, but the two minerals have the same colours in SEM-BSE imaging and is therefore indistinguishable without running EDS. Ab=albite, Ann=annite, Nph=nepheline, Ntr=natrolite.

These findings do correlate well with observations from the miasktic to agpaitic pegmatites in mariupolite of the Oktiabrski Massif in SE Ukraine (Dumanska-Slowik et al., 2015). They presented reactions (3) and (4) to support the findings, reaction (4) is also in agreement with findings of Groome (2017) from the Bjønnes Syenite in the LPC. Reaction (4) has been modified from the original to accommodate the K^+ in the new ideal formula for nepheline, this is done for all reactions involving nepheline. Reaction (4) do explain how microcline and sodalite crystallize from nepheline when in contact with components from reaction (1) or (2) already in the system. This reaction does explain the sodalite and microcline inclusions seen within grey nepheline. Reactions (3) and (4) show that the composition of the fluids needed to form sodalite from nepheline and albite are identical. It also has the same composition as the proposed saline brine separating from the melt due to the immiscibility suggested by Sunde et al., (2019) initiating the hydrothermal stages of pegmatite formation.

Reaction (3)

$$6\mathrm{Na}[\mathrm{AlSi_3O_8}]\ (\mathrm{Ab}) + 2\mathrm{NaCl} \rightarrow \mathrm{Na_8}[\mathrm{Al_6Si_6}]\mathrm{Cl_2}(\mathrm{Sdl}) + 12\mathrm{SiO_2}\ (\mathrm{aq})$$

Reaction (4)

$$2(\mathrm{Na_3KAl_4Si_4O_{16}})(\mathrm{Nph}) + 4\mathrm{SiO_2} + 2\mathrm{NaCl} \rightarrow \mathrm{Na_8Si_6Al_6O_{24}Cl_2}\ (\mathrm{Sdl}) + 2\mathrm{KAlSi_3O_8}\ (\mathrm{Mcc})$$

Reaction (4) looks to be somewhat reliant on reaction (3) as some excess silica is needed for the reaction to occur. Drüppel et al., (2005) suggested two possible explanations for what could happen to the excess SiO_2 from reaction (3). Either it is transported out of the system to higher crustal levels via fluids or SiO_2 is incorporated into another silicate mineral. This can be explained by a reaction proposed by Finch (1991), reaction (5) where silica is consumed in a reaction with nepheline to form analcime and microcline (Fig. 6a). Nepheline forming analcime or natrolite depending on the relationship between Si^{4+} vs Al^{3+} activity in the fluids.

Reaction (5)

$$\mathrm{Na_3KAl_4Si_4O_{16}}(\mathrm{Nph}) + 5\ \mathrm{SiO_2}(\mathrm{aq}) + 3\ \mathrm{H_2O} \rightarrow 3\ \mathrm{NaAlSi_2O_6}\ \cdot\ \mathrm{H_2O}\ (\mathrm{Anl}) + \mathrm{KAlSi_3O_8}(\mathrm{Mcc})$$

The excess silica formed during the breakdown of albite to form sodalite is a potential source for the analcime observed interstitial with the aggregates of secondary rounded sodalite in some samples (Fig. 13c). This do also explain why these rounded aggregates is not always present, as it is highly dependent on the presence of albite. Since these pegmatites are silica undersaturated the produced SiO_2 is not in equilibrium with the existing mineral paragenesis. The question is whether reaction (3), (4) and (5) all occur simultaneously, the rounded aggregated of sodalite with analcime can based on their textural relationship be said to have crystallized at the same time. Microcline rimmed by analcime is also found in grey nepheline close to secondary sodalite, this reaction could also be explained by reactions (3)-(5) occurring simultaneously. If no albite is present, no excess silica would be realised and sodalite would form as euhedral to subhedral crystals, later replaced by analcime during the main zeolitization due to the increase in H_2O content of the fluid making sodalite unstable (Giehl et al., 2014).

In reaction (3), six albite gives one sodalite and 12 excess SiO_2 which incorporates into the fluids. This results in a large volume decrease -184 cm^3/mol sodalite. Reaction (4) requires two nephelines to form one sodalite and 2 microclines, this reaction results in a slightly higher volume increase than reaction (3) at 194 cm^3/mol. The vast amount of nepheline compared to albite in the system, indicates that a volume increase may occur. Albite is only rarely found within nepheline and never in large quantities, which can be explained by reaction (3) where it is fully consumed early in the hydrothermal stages. An increase in unit cell volume from 547$Å^3$ (Bueger et al., 1954) for nepheline to 701$Å^3$ (Hassan and Grundy, 1984) in sodalite is in agreement with the calculated values from reaction (4). A volume increase as such could result in fracturing of the sodalite, frequently observed. These fractures do commonly hosts later forming zeolites and *spreustein* (Finch, 1991), (Fig. 12b)

4.4 The transition from brown Fe-bearing nepheline to grey nepheline

Brown nepheline transitions into a grey variety in the presence of secondary minerals such as sodalite, cancrinite and zeolites forming when nepheline reacts with the hydrothermal fluid. None of the main alteration products of nepheline are known to incorporate any Fe^{3+} into its structure, which do indicate that the released Fe^{3+} from the breakdown of brown nepheline must go into some other phase. An interesting observation is the abundant inclusions of annite, microcline and sodalite found within grey nepheline, where microcline is a byproduct of reaction (4) and found to incorporate a small amount of Fe^{3+} (Table 9). The presence of microcline together with analcime found in nepheline is explained by reaction (5). It is interesting to note that the observed grey variant of nepheline forms close, but not necessarily directly in contact with the secondary minerals. This could mean that the transition itself, causing the incorporation of K^+ and release of Fe^{3+} and Si^{4+} occurs in response to the interaction with the fluids, where grey nepheline may represent the starting point of reactions (4) and (5). Small pods of sodalite and microcline are found within grey nepheline in BSE imaging, but are not visible in hand samples. Hansteen & Burke (1990), analysed fluids inclusions from alkaline granites in the Oslo rift, these consisted of Cl^-, Na^+ and K^+. The K^+ component from the fluid could be responsible for the increase in K^+ found in the grey nepheline as well as forming microcline. The observed decrease in silica when transitioning from brown to grey

nepheline may be explained by the formation of microcline and sodalite both incorporating a lot of silica into their structures.

4.5 Cancrinite

Edgar (1964) and later Sirbescu & Jenkins (1999) recognized that alteration resulting in cancrinite can be formed in the presence of calcite and a mixed H_2O-CO_2 fluid (6). Another possibility is that nepheline reacts with a fluid with dissolved complex anions including $2Ca^{2+}$ (Cl^-, CO_3^{2-}, SO_4^{2-}) (7), both reactions are modified to fit the K^+ in the nepheline structure. These two reactions are always in the presence of fluids (Dumanska-Slovik et al., 2016).

Reaction (6)

$$2(Na_3KAl_4Si_4O_{16})\ (Nph) + 2\ CaCO_3(Cal) + 4SiO_2 + nH_2O$$
$$\rightarrow\ Na_6Ca_2Al_6Si_6O_{24}(CO_3)_2\ \cdot nH_2O\ (Ccn) + 2KAlSi_3O_8\ (Mcc)$$

Reaction (7)

$$2(Na_3KAl_4Si_4O_{16})(Nph) + 2Ca(\ CO_3^-, SO_4^{2-}) + 4SiO_2 +\ nH_2O$$
$$\rightarrow\ Na_6Ca_2Al_6Si_6O_{24}(CO_3, SO_4^{2-})_2\ nH_2O\ (Ccn) +\ 2KAlSi_3O_8\ (Mcc)$$

According to Sirbescu & Jenkins, (1999) secondary cancrinite form as a product of hydrothermal alteration of nepheline forming pods or veinlets in the host mineral associated with calcite. Cancrinite in the analysed samples do not only form smaller veins and pods within the host minerals, but also forms larger crystals fully pseudomorphing the host. Cancrinite is commonly present with both nepheline and secondary sodalite in the samples. The formation of sodalite and cancrinite from nepheline occurred at the same time under the same conditions. Cancrinite formed over sodalite due to either a temporary prevalence of $CaCO_3$ over NaCl or due to progressive increase $CaCO_3$ as sodalite precipitation proceeded depleting the fluid in Cl^- (Dumanska-Slowik et al., 2016).

In the Sagåsen pegmatite Sunde et al. (2019) found that the fluids circulating in the LPC pegmatites are heterogeneous. They described the three segments of the Sagåsen pegmatite, all exhibiting different degrees of alteration and mineral assemblages. This could indicate that the circulating fluids react with the minerals it

encounters, and that the composition changed accordingly. This do favour the theory in which a local prevalence of $CaCO_3$ over NaCl can occur due to the presence of primary calcite. Crystallization of cancrinite will then be favoured over sodalite until the calcite is fully consumed. This could explain the lack of larger primary calcite in the samples as well as the abundance of larger cancrinite crystals present, though primary calcite has not been reported as abundant in the LPC (Larsen et al., 2010). Paleozoic sediments are known in the area (Fig. 2) and may also be a possible source of $CaCO_3$ in the system. Another possible way of forming cancrinite is when secondary sodalite is in the paragenesis with cancrinite, this alteration can be induced by H_2O-, Ca^{2+}- and CO_3^{2-}, but also Na^+- and Cl^- bearing fluids (Dumanska-Slovik et al., 2016). The excess Cl^- released during this reaction has not been found incorporated into the secondary cancrinite (Table 4), but it could readily be dissolved in the fluids and transported out of the system or incorporated into other phases such later forming eudialyte.

White cancrinite has been found in samples where primary yellow cancrinite has been altered to zeolites. The white equivalent has a low Ca^{2+} and CO_3^{2-} content and interpreted to be a reaction zone. Natrolite forming *spreustein* from cancrinite have a pink colour and contain a higher content of Ca^{2+} than natrolite forming *spreustein* from sodalite. Pink *spreustein* forming at the expense of nepheline is too often found in close proximity to white cancrinite, this was also observed by Moyd (1949) in samples from South-Eastern Ontario. The overall Ca-deficiency as well and the Na excess in the analysed cancrinite from the LPC do reflect the composition of its growth.

4.6 Microcline and annite

According to Dumanska-Slovik et al., (2015), the reactions forming sodalite and cancrinite from nepheline results in a release of K^+ into the fluid. This K^+ component together with the lower content of silica in both sodalite and cancrinite compared to nepheline results in a simultaneous precipitation of annite and microcline. This does explain the presence of microcline within nepheline as well as the abundant interstitial annite found within nepheline, sodalite, cancrinite and microcline. These reactions are though rather unlikely to occur, through reactions (4), (5), (6), (7), (11) and (12) it is evident that microcline do crystallize as a byproduct of both reactions

forming sodalite and cancrinite from nepheline. The low amount of Fe^{3+} released from nepheline, is far from enough to crystallize the Fe^{2+} rich annite crystals. Another argument is the oxidation states of the two, nepheline has Fe^{3+}, whilst annite incorporates Fe^{2+}, meaning there would also have to be a change in oxidation state of the system. An alternative and more likely explanation is therefore that annite forms when the fluid reacts with microcline and magnetite, forming annite in between the two phases. Magnetite crystals are also abundantly observed having annite coronas in close proximity to microcline (Fig. 24). This is widely observed all over the Oslo Rift (Andersen, 1984) and are in agreement with the findings of Groome, (2017) shown in reaction (8).

Reaction (8):

$$Fe^{2+}(Fe^{3+})_2O_4(Mt) + KAlSi_3O_8(Mcc) + H_2O \rightarrow K(Fe^{2+})_3AlSi_3O_{10}(OH)_2\ (Ann) + \frac{1}{2}O_2$$

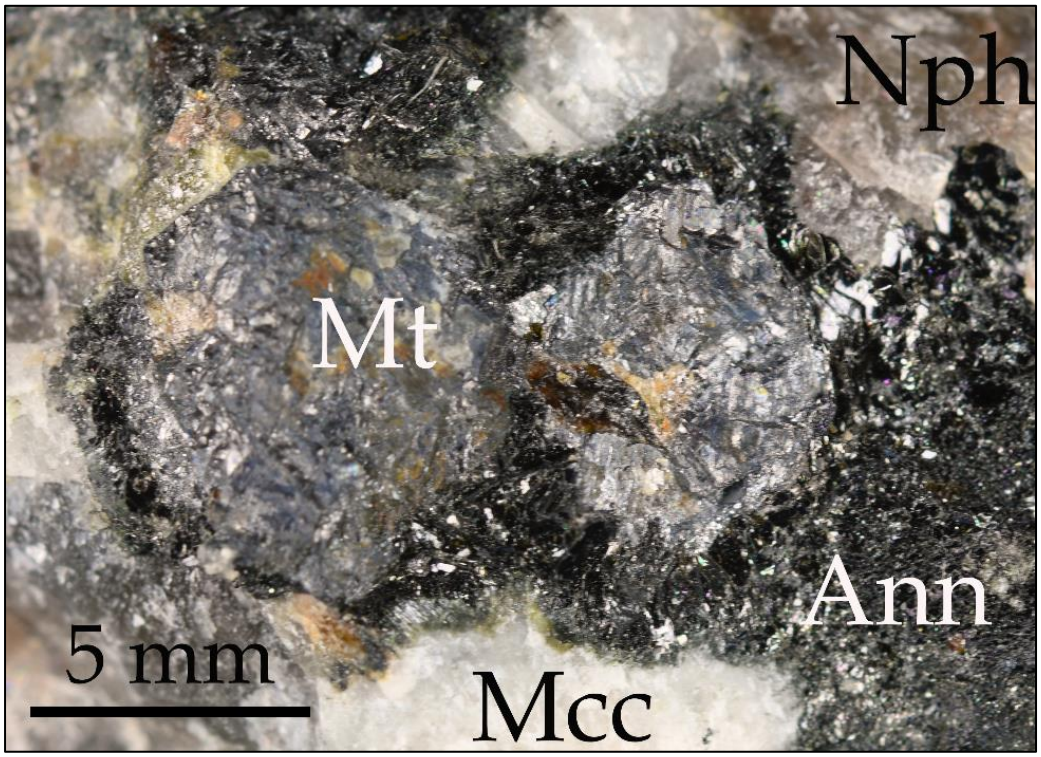

Figure 24: A sample from the Saga 1 quarry which show magnetite crystals with annite coronas observed in contact with microcline within a larger nepheline crystal. Ann=annite, Mcc=microcline, Mt=magnetite, Nph=nepheline.

4.7 Zeolitization

Zeolitization is a widely observed phenomenon in the LPC as well as in many other alkaline intrusive complexes around the world (Schilling et al. 2011 and references therein; Marks & Markl, 2017). It is evident from textural relationships that analcime is the first zeolite to form in the LPC. Analcime can form at higher temperature relative to natrolite, analcime macrocrysts are observed at temperatures up to 500°C (Henderson et al., 2014). This is also evident from Figure 25 which show that under stable pressure, analcime is favored at higher temperature, but with a decrease in temperature, an increase in *a*SiO_2 natrolite becomes the main zeolite.

This agrees with what observed in the samples, analcime is found to form as the earliest zeolite when nepheline (+albite) reacts with a saline brine to form secondary sodalite with an intestinal analcime phase. Natrolite is always found as rims or pseudomorphs after sodalite and nepheline. These minerals often have abundant analcime veins which must have crystallized before they were rimmed by *spreustein.* Dumanska-Slowik et al., (2015) suggested that the natrolite and analcime veins within nepheline, cancrinite and sodalite could have crystallized directly from a Si-undersaturated hydrothermal fluids enriched in Na^+ and Al^{3+}. This is rather unlikely to have occurred in the LPC, as this cannot explain the vast amounts of zeolitization observed as fully pseudomorphed nepheline and sodalite complexly altered to *spreustein.*

Thomsonite-Ca is the main observed Ca-zeolite in the samples and are commonly found with small inclusions of calcite within analcime in close proximity to cancrinite. Thomsonite-Ca is also found as an intimate intergrowth with calcite found to be an alteration product of cancrinite due to the process behind the zeolitization, see reaction (9).

Reaction (9)

$$2\ Na_6Ca_2(AlSiO_4)_6(CO_3, SO_4)_2 \cdot\ H_2O\ (Ccn) + 4H_2O \rightarrow NaCa_2(Al_5Si_5O_{24}) \cdot 6H_2O\ (Thm - Ca) + 2\ CaCO_3\ (Cal) + 10SiO_2 + 11Na^+ + 7Al^{3+}$$

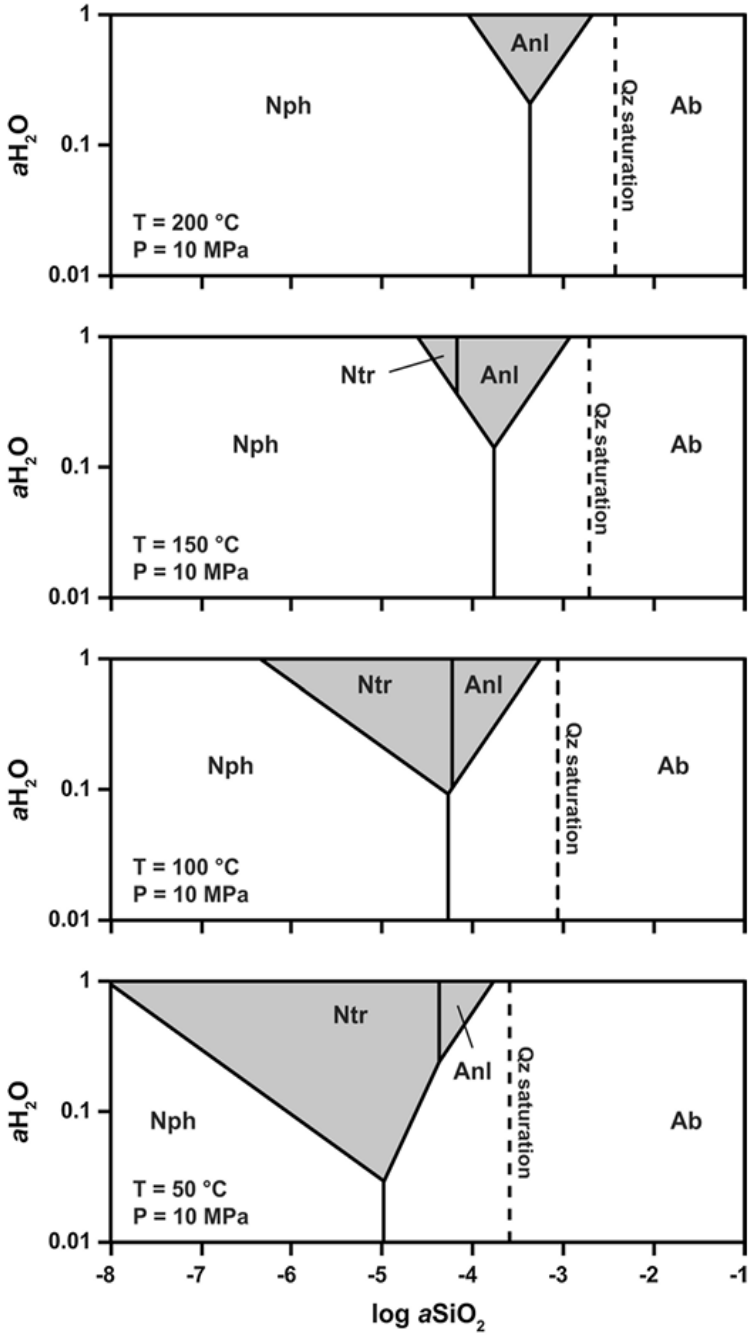

Figure 25: Show the stability field of analcime and natrolite in the presence of nepheline and albite, at stable pressure and decreasing temperature. From (Weisenberger et al., 2014)

Chakrabarty et al., (2016) has suggested the following reactions to explain the formation of analcime and natrolite from albite, nepheline or both. Weisenberger (2014) has suggested reaction (15) to explain the reaction forming natrolite from sodalite.

Reaction (10)

$$NaAlSi_3O_8\ (ab) + H_2O \rightarrow NaAlSi_2 \cdot H_2O(anl) + SiO_2(aq)$$

Reaction (11)

$$Na_3KAl_6Si_6O_{16}(Nph) + 5SiO_2(aq) + 3H_2O \rightarrow 3\ NaAlSi_2 \cdot H_2O(anl) + KAlSi_3O_8\ (Mcc)$$

Reaction (12)

$$2\ Na_3KAl_6Si_6O_{16}(Nph) + 7SiO_2(aq) + 6H_2O \rightarrow 3\ Na_2Al_2Si_3 \cdot 2H_2O(ntr) + 2KAlSi_3O_8\ (Mcc)$$

Reaction (13)

$$2NaAlSi_3O_8\ (ab) + 2H_2O \rightarrow Na_2Al_2Si_3 \cdot 2H_2O(ntr) + 3SiO_2(aq)$$

Reaction (14)

$$2NaAlSi_2 \cdot H_2O(anl) \rightarrow Na_2Al_2Si_3 \cdot 2H_2O(ntr) + SiO_2(aq)$$

Reaction (15)

$$Na_8Al_6Si_6O_{24}Cl_2(sdl) + 3SiO_2(aq) + 6H_2O \rightarrow 3Na_2Al_2Si_3O_{10} \cdot 2H_2O\ (ntr) + 2NaCl$$

It is evident from the reactions that the common denominator for zeolitization is the presence of silica and H_2O. Large amounts of silica are release by the formation of sodalite from albite in reaction (3) as well as the breakdown of eudialyte in reaction (1) together with the increasing H_2O content of the system as it evolved. The NaCl rich brine would likely be fully depleted in Cl^- and become very H_2O rich before zeolitization occurred. This is in agreement with the observed zeolitization happening at the expense of all the primary as well as the secondary phases formed in the pegmatites.

4.7.1 Substitutions in natrolite

The substitution observed inn red natrolite $Fe^{3+} \rightarrow Al^{3+}$ can reasonably be explained by the closeness of the effective ionic radii, Fe^{3+}=0.49Å and Al^{3+}=0.39Å (Shannon, 1976), but the substitution does induce a small distortion of the coordination tetrahedron (Vinokurov et al., 2002). The framework in natrolite consists of Al and Si tetrahedral, a coupled substitution between $(Al^{3+}+Fe^{3+}) \rightarrow Si^{4+}$ has been observed

(Fig. 26a) and explains the incorporation of Fe^{3+} into the framework. According to the ideal formula of natrolite Al^{3+} and Na^{+} content is supposed to be equal, in the red natrolite the EMPA infers a Na-deficiency. According to Dyer & Faghihian, (1998) sodium is displaced to fit the incoming replacement ions, in this case mainly Ca^{2+} and some K^{+}. This is in agreement with the results from the red natrolite (Table 6). The substitution $K^{+} \rightarrow Na^{+}$ means incorporating the larger K^{+} into a smaller Na^{+} vacant position and has not caused any implications in term of water mobility in natrolite, though this would prevent water molecule access in the framework of analcime (Dyer & Faghihian, 1998). This substitution has no implication on the charge balance of the structure. The substitution incorporating $Ca^{2+} \rightarrow Na^{+}$ is not as simple, to preserve the charge balance in the structure a coupled substitution must take place ($Si^{4+}+Na^{+} \rightarrow Al^{3+}+Ca^{2+}$) or a $2Na^{+} \rightarrow Ca^{2+}$ substitution, (Fig. 26b) show a correlation close to 1 for the coupled substitution in the natrolite structure. No such substitutions are observed to occur in the analcime structure. The nature of the natrolite structure makes it possible for it to expand by relaxations in the chains of Si, Al tetrahedral which are the building blocks of the framework. As previously mentioned this flexibility is not seen in the analcime framework whose three-dimensional nature enables restricted water mobility by the presence of even small amounts of larger cations (Dyer & Faghihian, 1998).

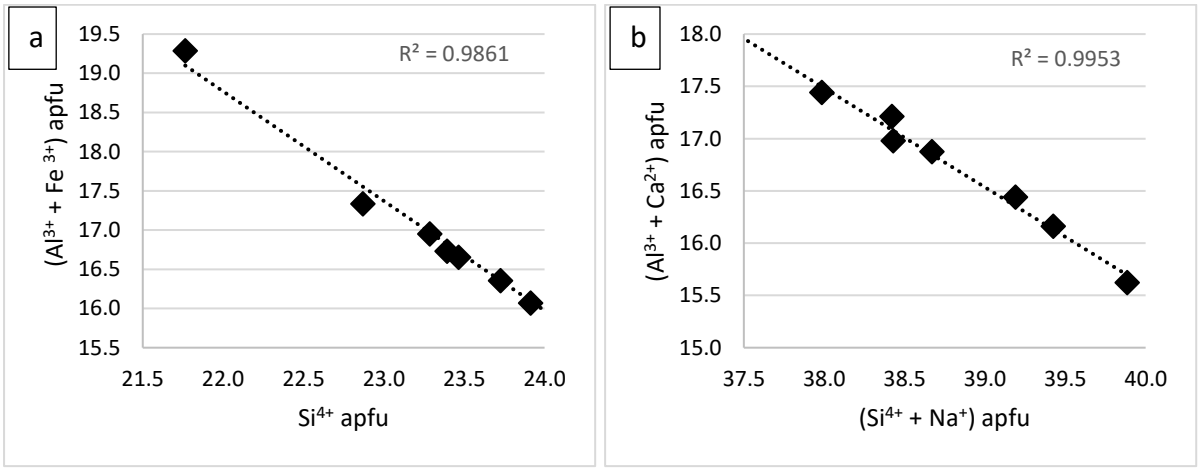

Figure 26: Graphical presentation of numbers from Table 7 showing the substitutional relationships found to occur in the analysed in natrolite.

4.7.2 The colour of natrolite and spreustein

Spreustein is found in a variety of colours in the LPC and seems to be strongly dependent on the mineral in which it formed from. As discussed, natrolite is found to

incorporate other elements through substitution. The most commonly observed incorporated ions are Fe^{3+} and Ca^{2+} in red *spreustein*, always found in close proximity to brown nepheline. Brown nepheline does not explain the Ca^{2+} content in natrolite, but as discussed earlier nepheline has been observed in contact with a red abrupt reaction rim with high content of Ca^{2+} and some Fe^{3+}. Another possible explanation is the Ca-deficiency of the cancrinite analysed from the LPC (Table 4). The low Ca^{2+} content, can possibly be explained by the incorporation of Ca^{2+} into the natrolite structure. *Spreustein* forming at the expense of cancrinite are usually pink in colour and do contain minor amounts of Fe^{3+} and some Ca^{2+}. Secondary cancrinite often with a lighter yellow colour, only forms natrolite with some incorporated Ca^{2+} as a product of zeolitization, no *spreustein* has been observed. Spreustein forming at the expense of sodalite has a tendency of being colourless to white and does only incorporate minor amounts of extra cations, these are the ones which are the closest to the ideal formula (Table 6). Analcime always has a white colour and is not found to incorporate any extra cations by substitution (Table 5).

4.8 The evolution of the system

The transition from the magmatic to the hydrothermal stages of pegmatite formation is a result of the crystallization of the mainly anhydrous mineral assemblage during the magmatic stages. As crystallization proceeded the residue melt got more and more enriched in fluids, at this point the melt and the fluids were still co-existing. As crystallization continuous the volatile component exceeded its saturation level and an immiscibility occurred between an aqueous NaCl brine and a Na-rich melt now primarily crystallize albite and aegirine (Sunde et al., 2019). Evidence for such a saline brine is found in fluid inclusions in the Eikern Ekerite complex, one of the youngest intrusions in the Oslo rift (Hansteen & Burke, 1990). They found that late hydrothermal fluids mainly contained Na, K and Cl at subsolidus temperatures.

Some samples were found where the main phases included sacchariodal albite and fibrous aegirine in relation to *spreustein*, as this is not the scope of this study, I have chosen not to go into that any further, an elaborated study on the topic can be found in Sunde et al., (2019). This saline brine reacted with the primary minerals to form secondary minerals. Nepheline and albite reacted with the brine to form secondary

sodalite and analcime. Cancrinite formed instead of sodalite from nepheline (+ sodalite) under the same subsolidus conditions due to temporary local prevalence of $CaCO_3$ over NaCl in the system. Mn-rich calcite is commonly found in the LPC, this can possibly explain the minor component of Mn found in all the analysed secondary cancrinite. As these reactions proceed the brine gets depleted in Cl^- and becomes progressively more H_2O rich, this puts an end to the crystallization of secondary sodalite and opens for the zeolite group minerals.

The zeolite group minerals are represented by analcime, natrolite and to some extent thomsonite-Ca in relation to the breakdown of cancrinite. Textural investigation reveals that analcime is mainly restricted to an interstitial phase in secondary sodalite formed from nepheline and albite as well as veins and pods in nepheline and cancrinite. Small analcime veins and macrocrysts are also present in *spreustein*. Natrolite is the main mineral forming *spreustein* as replacement of primary and secondary sodalite, nepheline and cancrinite, but in some rare cases also microcline and albite. The fluid responsible for the precipitation of the zeolite-group minerals can be the same deuteric fluid that caused the breakdown of eudialyte reported by Groome (2017) or originate from an external source. In the LPC it is likely that the fluids forming zeolites are the same deuteric fluid which caused eudialyte decomposition, as no larger calcite or zeolite veins are found between the surrounding larvikite and the pegmatites (Sunde et al., 2019). The Al-hydroxides böhmite and diaspore are widely found within analcime as a fully enclosed phase (Fig. 17), the textural relationship between these two phases can indicate a dissolution-precipitation relationship. Al-hydroxides associated with natrolite and *spreustein* has a euhedral to subhedral crystal shape and are found in voids within the porous *spreustein* rather than being fully enclosed as observed in analcime. The lack of larger veins of calcite or zeolites between the host larvikite and the pegmatites is not alone evidence to exclude the possibility that exterior fluids can have caused the final crystallization of Al-hydroxides. The following reaction (16) from Wilkin and Barnes (1998) show how an Al-phase can be released from analcime when flushed by an exterior source of H_2O. Reaction (17) is proposed as another possible reaction who could occur and produce the observed late mineral assemblage**.**

Reaction (16)

$$NaAlSi_2O_6 \cdot H_2O\ (anl) + 5H_2O \rightarrow Na^+ + Al(OH)_4^- + 2Si(OH)_4(aq)$$

Reaction (17)

$$NaAlSi_2O_6 \cdot H_2O\ (anl) + 4H_2O \rightarrow AlO(OH) + 2H_4SiO_4(aq) + Na^+(aq) + (OH^-)aq$$

If the source of this fluid is external meteoric waters, it will also explain the widely observed small pods and platy crystals of calcite with Al-hydroxides found in voids in *spreustein* (Fig. 27). In some areas calcite is also found with Na rich Al-hydroxides, also a product of reaction (16). That a network of micropores is present in the main minerals is evident from the literature and observations in the analysed samples. These enables the percolation of meteoric waters through the minerals as needed to form the latest Al-hydroxides and calcite observed in the samples. As suggested by Finch (1991) the hydrothermal alteration has been observed to occur not only at the grain boundaries, but following the permeable network of micropores in nepheline causing zeolitization. This is also found to occur in sodalite and microcline. Cancrinite has a zeolite-like structure with open cavities for H_2O. This could mean that even without the presence of a calcite or zeolite veins meteoric water could have percolated through the minerals itself and caused the final mineral assemblage observed. This does also explain why the Al-hydroxides are found in some samples but not in all, as it is highly dependent on the minerals assemblage and its ability to transport fluids through all the mineral structures present. Meteoric fluids flushed through the natrolite structure can cause an anisotropic “swelling” of the framework under high water pressure (Belitsky et al., 1992), this could cause an increase in volume of the mineral due to the extra H_2O molecules now filling more channels and the whole framework could be distorted. This is a possible explanation for the presence of the porous alteration product *spreustein and* can also explain why well-developed natrolite crystals do occur in voids without becoming *spreustein* as they have not come into contact with a later source of meteoric fluids. A complete overview of the evolution of the system is shown in Figure 28.

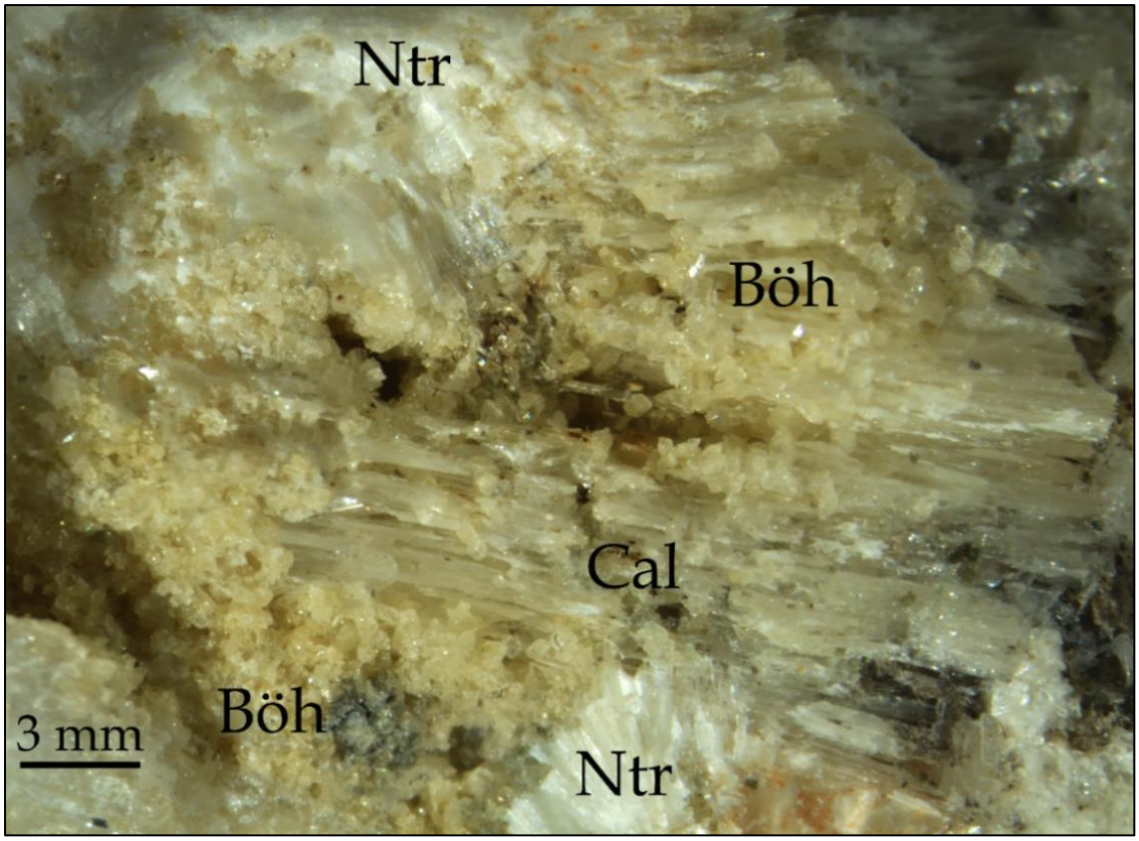

Figure 27: Late stage Al-hydroxides as böhmite with interstitial platy calcite in a void in white spreustein in a sample from the Saga 1 quarry. Böh=böhmite, Cal=calcite, Ntr=natrolite

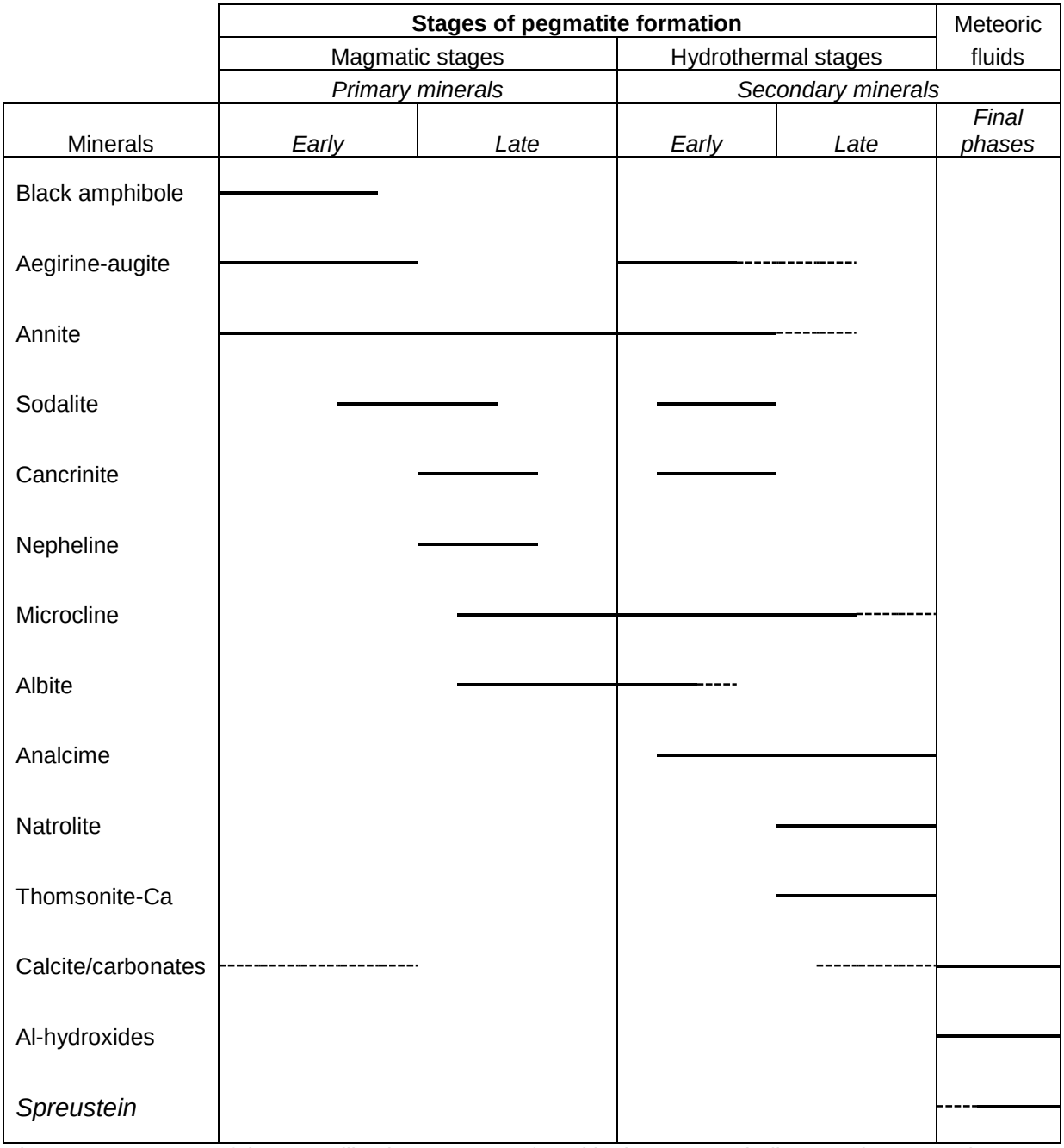

Figure 28: summary of the crystallization sequence found in the LPC nepheline syenite pegmatites. Dotted lines indicate that there is an uncertainty to the crystallization of the mineral in at that stage.

5. Conclusion

The mildly agpaitic Langesundsfjord nepheline syenite pegmatites are known for having a complex mineral assemblage. The primary minerals formed as part of the magmatic stages of pegmatite formation. The secondary minerals including the zeolitization formed in response to the evolving fluids formed from an immiscibility between a saline brine and a Na-rich melt initiating the hydrothermal stages. Secondary sodalite and cancrinite formed first when the saline brine reacted with nepheline, a temporary prevalence of cancrinite over sodalite occurred when calcite/carbonates was present. Simultaneous crystallization of rounded sodalite and cancrinite with analcime occurred in response to a concurrent reaction of the brine with albite, sodalite and local calcite.

As the saline brine became increasingly more water rich as the secondary minerals crystallized out, zeolites started to crystallize at the expense of primary and the newly formed secondary minerals. The immiscibility, crystallization of secondary feldspathoids and zeolitization all formed in a closed system. The latest phases in the LPC pegmatites are found to be Al-hydroxides, calcite and the porous alteration product *spreustein.* An anisotropic “swelling” of the natrolite formed from the main zeolitization occurred when it came in contact with meteoric water has been proposed as the process forming *spreustein*. Al-hydroxides are widely observed in voids in *spreustein* together with calcite or as a fully enclosed phase in analcime. Al-hydroxides are proposed to form in responses to a dissolution/precipitation relationship with analcime in contact with meteoric water. The small calcite inclusions in *spreustein* as well as platy calcite crystal together with sugar-like böhmite within vugs in *spreustein* are also indicative of an external source of water. The findings of this study support a simultaneous formation of *spreustein*, Al-hydroxides and calcite due to a reaction with a later source of external fluids in percolating through the open structures of the main minerals in the LPC pegmatites.

5.1 Further research

Until this project no one had looked at the alteration product *spreustein* replacing both primary and secondary feldspathoids in the Langesundsfjord area since Brøgger in 1890s. Further research in the area could include:

- Trying to connect the observed zeolitization and process behind the abundant alteration product *spreustein* to the widely observed saccharіodal albite and dense fibrous aegirine reported from the Sagåsen pegmatite. Are these processes related?

- A further isotope study of fluid inclusions in calcite or Al-hydroxides from the sampling localities would provide knowledge of the composition and possible source of the late meteoric fluids in the system.

- Incorporate the HFSE-and REE-minerals abundantly found in the LPC pegmatite into the study, where do they fit in to the mineral paragenesis?

- There are some interesting relationships between nepheline and cancrinite in the samples. What causes these different types of boundaries to occur?

Referances

Allan, T. (1813). II. Remarks on the transition rocks of Werner. *The Philosophical Magazine*, *42*(183), 15-25.

Andersen, T. (1984). Crystallization history of a Permian composite monzonite-alkali syenite pluton in the Sande cauldron, Oslo rift, southern Norway. *Lithos*, *17*, 153-170. https://doi.org/10.1016/0024-4937(84)90016-1

Andersen, T., Erambert, M., Larsen, A., & Selbekk, R. (2010). Petrology of Nepheline Syenite Pegmatites in the Oslo Rift, Norway: Zirconium Silicate Mineral Assemblages as Indicators of Alkalinity and Volatile Fugacity in Mildly Agpaitic Magma. *Journal Of Petrology*, *51*(11), 2303-2325. https://doi.org/10.1093/petrology/egq058

Andersen, T., & Seiersten, M. (1994). Deep cumulates in a shallow intrusion: origin and crystallization history of a pyroxenite (jacupirangite sl) body in the Larvik Pluton, Oslo Region, South Norway. *Neues Jahrbuch fur mineralogie monatshefte*, 255-255.

Armbruster, T., & Gunter, M.E. (2001). Crystal Structures of Natural Zeolites. *Reviews In Mineralogy And Geochemistry*, *45*(1), 1-67. https://doi.org/10.2138/rmg.2001.45.1

Barker, D. S. (1976). Phase relations in the system NaAlSiO4-SiO2-NaCl-H2O at 400°-800° C and 1 kilobar, and petrologic implications. *The Journal of Geology*, *84*(1), 97-106.

Barth, T., (1944). Studies on the Igneous Rock Complex of the Oslo Region. Systematic petrography of the plutonic rocks. *Skrifte Norske Vidensk-Akademie Oslo,* 9

Belitsky, I. A., Fursenko, B. A., Gabuda, S. P., Kholdeev, O. V., & Seryotkin, Y. V. (1992). Structural transformations in natrolite and edingtonite. *Physics and Chemistry of Minerals*, *18*(8), 497-505. https://doi.org/10.1007/bf00205264

Binsted N. (1981) The system Ab-Ne-NaCl-H_2O. *Prog. Exp. Petrol., N.E.R.C. Rept.* 5, 34-36

Brown, F. H. (1970). Zoning in some volcanic nephelines. *American Mineralogist: Journal of Earth and Planetary Materials*, *55*(9-10), 1670-1680.

Brøgger, W. C. (1886). *Ueber die Bildungs geschichte des Kristiania fjords: Ein Beitrag zum Verständniss der Fjord und See bildung in Skandinavien* (Vol. 30). Mallingske bogtrykkeri.

Brøgger W.C. (1890) Die Mineralien der Syenitpegmatitgänge der südnorwegischen Augit- und Nephelinsyenite. *Zeitschrift für Krystallographie, 16,* 1-235 & 1-663.

Buerger, M. J., Klein, G. E., & Donnay, G. (1954). Determination of the crystal structure of nepheline. *American Mineralogist: Journal of Earth and Planetary Materials*, *39*(9-10), 805-818.

Burnham, C.W., & Jahns, R.H. (1962). A method for determining the solubility of water in silicate melts. *American Journal of Science*, *260*(10), 721-745. https://doi.org/10.2475/ajs.260.10.721

Chakrabarty, A., Mitchell, R.H., Ren, M., Saha, P.K., Pal, S., Pruseth, K.L., & Sen, A.K. (2016). Magmatic, hydrothermal and subsolidus evolution of the agpaitic nepheline syenites of the Sushina Hill Complex, India: implications for the metamorphism of peralkaline syenites. *Mineralogical Magazine*, *80*(7), 1161-1193. https://doi.org/10.1180/minmag.2016.080.057

Chen, J., Ma, H., Liu, C., & Yuan, J. (2017). Synthesis of Analcime Crystals and Simultaneous Potassium Extraction from Natrolite Syenite. *Advances In Materials Science And Engineering*, *2017*, 1-9. https://doi.org/10.1155/2017/2617597

Clarke, F. W. (1886). ART. XXV.--The Minerals of Litchfield, Maine. *American Journal of Science (1880-1910)*, *31*(184), 262.

Corfu, F., & Dahlgren, S. (2008). Perovskite U–Pb ages and the Pb isotopic composition of alkaline volcanism initiating the Permo-Carboniferous Oslo Rift. *Earth And Planetary Science Letters*, *265*(1-2), 256-269. https://doi.org/10.1016/j.epsl.2007.10.019

Corfu, F., & Larsen, B. (2020). U-Pb systematics in volcanic and plutonic rocks of the Krokskogen area: Resolving a 40 million years long evolution in the Oslo Rift. *Lithos*, *376-377*, 105755. https://doi.org/10.1016/j.lithos.2020.105755

Dahlgren, S. (2010). The Larvik plutonic complex: The larvikite and nepheline syenite plutons and their pegmatites. In: Larsen, A. O. (ed.) *The Langensundsfjord: History, Geology, Pegmatites, Minerals* (pp. 26-37). Bode

Dahlgren, S., Corfu, F., & Heaman, L. M. (1996). U–Pb time constraints, and Hf and Pb source characteristics of the Larvik plutonic complex, Oslo Paleorift. Geodynamic and geochemical implications for the rift evolution. VM Goldschmidt Conference. In: Journal of Conference Abstracts 1, 120.

Demaiffe, D. & Michot, J., 1985. Isotope geochronology of the Proterozoic crustal segment of southern Norway: a review. In: A. Tobi & J. Touret (eds), *The Deep Proterozoic Crust in the North Atlantic Provinces*. (pp.411-433). D. Reidel Publ. Co.

Drüppel, K., Hoefs, J., & Okrusch, M. (2005). Fenitizing processes induced by ferrocarbonatite magmatism at Swartbooisdrif, NW Namibia. *Journal of Petrology*, *46*(2), 377-406. https://doi.org/10.1093/petrology/egh081

Dumańska-Słowik, M., Heflik, W., Pieczka, A., Sikorska, M., & Dąbrowa, Ł. (2015). The transformation of nepheline and albite into sodalite in pegmatitic mariupolite of the Oktiabrski Massif (SE Ukraine). *Spectrochimica Acta Part A: Molecular And Biomolecular Spectroscopy*, *150*, 837-845. https://doi.org/10.1016/j.saa.2015.06.039

Dumańska-Słowik, M., Pieczka, A., Heflik, W., & Sikorska, M. (2016). Cancrinite from nepheline syenite (mariupolite) of the Oktiabrski massif, SE Ukraine, and its growth history. *Spectrochimica Acta Part A: Molecular And Biomolecular Spectroscopy*, *157*, 211-219. https://doi.org/10.1016/j.saa.2016.01.007

Dunham, K. C. (1933). Crystal cavities in lavas from the Hawaiian Islands. *American Mineralogist: Journal of Earth and Planetary Materials*, *18*(9), 369-385.

Dyer, A., & Faghihian, H. (1998). Diffusion in heteroionic zeolites: part 1. *Microporous And Mesoporous Materials*, *21*(1-3), 27-38. https://doi.org/10.1016/s1387-1811(97)00035-8

Ebbing, J., Afework, Y., Olesen, O., & Nordgulen, Ø. (2005). Is there evidence for magmatic underplating beneath the Oslo Rift?. *Terra Nova*, *17*(2), 129-134. https://doi.org/10.1111/j.1365-3121.2004.00592

Edgar, A.D. (1964). Studies on cancrinites; Part 2, Stability fields and cell dimensions of calcium and potassium-rich cancrinites. *The Canadian Mineralogist*, *8*(1), 53-67.

Edgar, A.D. (1965) The mineralogical composition of some nepheline alteration products. *The American Mineralogist, 50(7-8), 978-989*

Falkum, T., 1985. Geotectonic evolution of southern Scandinavia in the light of a late-Proterozoic plate collision. In: A. Tobi & J. Touret (eds), *The Deep Proterozoic Crust in the North Atlantic Provinces*. (pp. 309-322). D. Reidel Pub. Co.

Finch, A.A. (1991). Conversion of nepheline to sodalite during subsolidus processes in alkaline rocks. *Mineralogical Magazine*, *55*(380), 459-463. https://doi.org/10.1180/minmag.1991.055.380.15

Finstad, K., (1972) En undersøkelse av utvalgte edelmetaller og sjeldne jordartselementer I noen norske, hovedsakelig basiske og ultrabasiske bergarter. *(unpubl. Cand. Real. Theisis)* University of Oslo.

Gaál, G., & Gorbatschev, R. (1987). An Outline of the precambrian evolution of the baltic shield. *Precambrian Research*, *35*, 15-52. https://doi.org/10.1016/0301-9268(87)90044-1

Giehl, C., Marks, M. A., & Nowak, M. (2014). An experimental study on the influence of fluorine and chlorine on phase relations in peralkaline phonolitic melts. *Contributions to Mineralogy and Petrology*, *167*(3), 1-21. https://doi.org/10.1007/s00410-014-0977-7

Gorbatschev, R. (1980). The Precambrian development of southern Sweden. *Geologiska Föreningen I Stockholm Förhandlingar*, *102*(2), 129-136. https://doi.org/10.1080/11035898009450890

Groome, N.T. (2017) A description of the Bjønnes nepheline syenite intrusion, part of the Larvik plutonic complex, Norway. Department of Geosciences, University of Oslo, Norway.

Hansteen, T. H., & Burke, E. A. (1990). Melt-mineral-fluid interaction in peralkaline silicic intrusions in the Oslo Rift, Southeast Norway. II. High temperature fluid inclusions in the Eikeren-Skrim. *Norges Geologiske Undersøkelse, 417,* 15-32.

Hassan, I., & Grundy, H. D. (1984). The crystal structures of sodalite-group minerals. *Acta Crystallographica Section B Structural Science*, *40*(1), 6-13. https://doi.org/10.1107/s0108768184001683

Henderson, C. M. B., Hamilton, D. L., & Waters, J. P. (2014). Phase equilibria in NaAlSiO4–KAlSiO4–SiO2–H2O at 100 MPa pressure: equilibrium leucite composition and the enigma of primary analcime in blairmorites revisited. *Mineralogical Magazine*, *78*(1), 171-202.

Jahns, R. H. (1953). The genesis of pegmatites: I. Occurrence and origin of giant crystals. *American Mineralogist: Journal of Earth and Planetary Materials*, *38*(7-8), 563-598.

Khomiakov, A. P. (1995). *Mineralogy of hyperagpaitic alkaline rocks*. Oxford University Press.

Kilinc, I.A., & Burnham, C.W. (1972). Partitioning of Chloride Between a Silicate Melt and Coexisting Aqueous Phase from 2 to 8 Kilobars. *Economic Geology*, *67*(2), 231-235. https://doi.org/10.2113/gsecongeo.67.2.231

Larsen, A.O., (1996). Rare earth minerals from the syenite pegmatites in the Oslo Region, Norway. In: Jones, A. P., Wall, F. & Williams, C. T. (eds) *Rare Earth Minerals. Chemistry, Origin and Ore Deposits* (pp. 151-166). Chapman & Hall

Larsen, A.O., Berge, A. B., Andersen, F., Larsen, K.E., & Burvald, I. (2010). The minerals of the pegmatites in the Larvik Plutonic complex. In: Larsen, A.O. (ed.) *The Langesundsfjord history, geology, pegmatites, minerals* (pp. 64-222). Bode

Larsen, B.T., Olaussen, S., Sundvoll, B., & Heeremans, M. (2008). The Permo-Carboniferous Oslo Rift through six stages and 65 million years. *Episodes*, *31*(1), 52-58. https://doi.org/10.18814/epiiugs/2008/v31i1/008

Le Maitre, R.W. (ed.) (2003). *Igneous rocks. A Classification and Glossary of Terms* (p. 236). Cambridge University Press.

London, D., & Kontak, D. J. (2012). Granitic pegmatites: scientific wonders and economic bonanzas. *Elements*, *8*(4), 257-261.

Marks, M. A. W., & Markl, G. (2017). A global review on agpaitic rocks. *Earth-Science Reviews*, *173*, 229-258. https://doi.org/10.1016/j.earscirev.2017.06.002

Miyawaki, R., Hatert, F., Pasero, M., and Mills, S. J. (2022). IMA Commission on New Minerals, Nomenclature and Classification (CNMNC) – *Newsletter 65, Eur. J. Mineral., 34,* 143–148, https://doi.org/10.5194/ejm-34-143-2022

Moyd, L. (1949). Petrology of the nepheline and corundum rocks of southeastern Ontario. *American Mineralogist: Journal of Earth and Planetary Materials*, *34*(9-10), 736-751.

Neumann, E.-R. (1976). Compositional relations among pyroxenes, amphiboles and other mafic phases in the Oslo Region plutonic rocks. *Lithos*, *9*(2), 85-109. https://doi.org/10.1016/0024-4937(76)90028-1

Neumann, E.-R. (1980). Petrogenesis of the Oslo Region Larvikites and Associated Rocks. *Journal Of Petrology*, *21*(3), 499-531. https://doi.org/10.1093/petrology/21.3.499

Neumann, E.-R., Dunworth, E., Sundvoll, B., & Tollefsrud, J. (2002). B1 basaltic lavas in Vestfold–Jeløya area, central Oslo rift: derivation from initial melts formed by progressive partial melting of an enriched mantle source. *Lithos*, *61*(1-2), 21-53. https://doi.org/10.1016/s0024-4937(02)00068-3

Neumann, E.-R., Olsen, K., Baldridge, W., & Sundvoll, B. (1992). The Oslo Rift: A review. *Tectonophysics*, *208*(1-3), 1-18. https://doi.org/10.1016/0040-1951(92)90333-2

Neumann, E.-R., Tilton, G., & Tuen, E. (1988). Sr, Nd and Pb isotope geochemistry of the Oslo rift igneous province, southeast Norway. *Geochimica Et Cosmochimica Acta*, *52*(8), 1997-2007. https://doi.org/10.1016/0016-7037(88)90180-9

Neumann, E.-R, Wilson, M., Heeremans, M., Spencer, E., Obst, K., Timmerman, M., & Kirstein, L. (2004). Carboniferous-Permian rifting and magmatism in southern Scandinavia, the North Sea and northern Germany: a review. *Geological Society, London, Special Publications*, *223*(1), 11-40. https://doi.org/10.1144/gsl.sp.2004.223.01.02

Nielsen, T.F.D. (1979). The occurrence and formation of Ti-Aegirines in peralkaline syenites. *Contributions To Mineralogy And Petrology*, *69*(3), 235-244. doi: https://doi.org/10.1007/bf00372325

Oftedahl, C. (1952) On «apoanalcite» and hydronephelite. *Norsk Geologisk Tidsskrift, 30,* 1-4.

Oftedahl C., & Petersen, J., (1978) Southern part of the Oslo rift. In: Dons, J., & Larsen, B. (eds.) The Oslo Paleorift. A Review and Guide to Excursions. *Norges Geologiske Undersøkelse, 337,* 163-182.

Olsen, M. T. (2018). Opprinnelsen og alderen til de yngste felsiske plutonene i Oslofeltet – En LAM-MC-ICPMS U-Pb og Lu-Hf-isotopstudie av zircon. Department of Geosciences, University of Oslo, Norway. [in Norwegian]

Onuma, K., & Yoshikawa, K. (1972). Nepheline solid solutions in the syste, Na2O-Fe2O3-Al2O3-SiO2. *The Journal of The Japanese Association Of Mineralogists, Petrologists And Economic Geologists*, *67*(12), 395-401. https://doi.org/10.2465/ganko1941.67.395

Onuma, K., Iwai, T., & Yagi, K. (1972). Nepheline-" iron nepheline" solid solutions. *Journal of the Faculty of Science, Hokkaido University. Series 4, Geology and mineralogy*, *15*(1-2), 179-190.

Paijkull, S.R. (1874). Ein neues Mineral von Brevig. *Berichte Deutsche Chemische Gesellschaft Berlin*, 7b, 1334-1335.

Pascal, C., Cloetingh, S., & Davies, G. (2004). Asymmetric lithosphere as the cause of rifting and magmatism in the Permo-Carboniferous Oslo Graben. *Geological Society, London, Special Publications*, *223*(1), 139-156. https://doi.org/10.1144/gsl.sp.2004.223.01.06

Passaglia, E., & Sheppard, R.A. (2001). The Crystal Chemistry of Zeolites. *Reviews In Mineralogy And Geochemistry*, *45*(1), 69-116. https://doi.org/10.2138/rmg.2001.45.2

Petersen, J. (1978). Structure of the larvikite-lardalite complex, Oslo-region, Norway, and its evolution. *Geologische Rundschau*, *67*(1), 330-342. https://doi.org/10.1007/bf01803271

Piilonen, P.C., McDonald, A.M., Poirier, G., Rowe, R., & Larsen, A.O. (2013). Mafic minerals of the alkaline pegmatites in the Larvik Plutonic Complex, Oslo Rift, Southern Norway. *The Canadian Mineralogist*, *51*(5), 735-770. https://doi.org/10.3749/canmin.51.5.735

Raade, G., (1973) Distribution of radioactive elements in the plutonic rocks of the Oslo region. *Unpubl. Cand. Real. Thesis,* University of Oslo.

Raade, G., (1978) Distribution of Th, U, K in the plutonic rocks of the Oslo Region, Norway. In Neumann, E., & Ramberg, I., (eds), *Petrology and geochemistry of Continental Rifts.* (pp. 185-192). D. Reidel Publ. Co.

Rämö, T., Andersen, T. & Whitehouse, M., 2022. Timing and Petrogenesis of the Permo-Carboniferous Larvik Plutonic Complex, Oslo Rift, Norway: New Insights from U-Pb, Lu-Hf and O Isotopes in Zircon. *Journal of petrology* (in review)

Rastsvetaeva, R.K., Pekov, I.V., Chukanov, N.V., Rozenberg, K.A., & Olysych, L.V. (2007). Crystal structures of low-symmetry cancrinite and cancrisilite varieties. *Crystallography Reports*, *52*(5), 811-818. https://doi.org/10.1134/s1063774507050100

Schilling, J., Marks, M. A., Wenzel, T., Vennemann, T., Horváth, L., Tarassoff, P. & Markl, G. (2011). The magmatic to hydrothermal evolution of the intrusive Mont

Saint-Hilaire complex: insights into the late-stage evolution of peralkaline rocks. *Journal of Petrology*, *52*(11), 2147-2185.

Sharp, Z.D., Helffrich, G.R., Bohlen, S.R., & Essene, E.J. (1989). The stability of sodalite in the system NaAlSiO4-NaCl. *Geochimica Et Cosmochimica Acta*, *53*(8), 1943-1954. https://doi.org/10.1016/0016-7037(89)90315-3

Shannon, R. D. (1976). Revised effective ionic radii and systematic studies of interatomic distances in halides and chalcogenides. *Acta crystallographica section A: crystal physics, diffraction, theoretical and general crystallography*, *32*(5), 751-767.

Sirbescu, M., & Jenkins, D. M. (1999). Experiments on the stability of cancrinite in the system Na2O-CaO-Al2O3-SiO2-CO2-H2O. *American Mineralogist*, *84*(11-12), 1850-1860. https://doi.org/10.2138/am-1999-11-1212

Sunde, Ø., Friis, H., & Andersen, T. (2019). Pegmatites of the Larvik Plutonic Complex, Oslo Rift, Norway: field relations and characterisation. *Norwegian Journal Of Geology*. https://doi.org/10.17850/njg99-1-05

Sundvoll B., (1978a) Rb/Sr-relationship in the Oslo igneous rocks. In: Neumann, E. & Ramberg, I. (eds.) *Petrology and Geochemistry of Continental Rifts* (pp. 181-184). D. Reidel Publ. Co.

Sundvoll, B., (1978b). Isotope- and trace-element chemistry. In: Dons, J., & Larsen, B. (eds.) The Oslo Paleorift. A Review and Guide to Excursions. *Norges Geologiske Undersøkelse, 337*, 35-40.

Starmer I., (1985) The Evolution of the South Norwegian Proterozoic as Revealed by the Major and Mega-Tectonics of the Kongsberg and Bamble Sectors. In: Tobi A. & Touret J. (eds) *The Deep Proterozoic Crust in the North Atlantic Provinces. NATO ASI Series (Series C: Mathematical and Physical Sciences), vol 158*. (pp. 259-290). Springer. https://doi.org/10.1007/978-94-009-5450-2_16

Swensson, E. (1990). Cataclastic rocks along the Nesodden Fault, Oslo Region, Norway: a reactivated Precambrian shear zone. *Tectonophysics*, *178*(1), 51-65. https://doi.org/10.1016/0040-1951(90)90459-l

Thomas, R., Webster, J. D., & Heinrich, W. (2000). Melt inclusions in pegmatite quartz: complete miscibility between silicate melts and hydrous fluids at low pressure. *Contributions to Mineralogy and Petrology*, *139*(4), 394-401.

Thugutt, S. J. (1932). Sur l'epinatrolite, mineral composant l'hydronephelinite. *Archive de mineralogie de la societé des sciences et des lettres de Varsovie*, *7*, 143-144.

Tilley, C. E., & Harwood, H. F. (1931). The dolerite-chalk contact of Scawt Hill, Co. Antrim. The production of basic alkali-rocks by the assimilation of limestone by basaltic magma1 (With Plates XVII and XVIII.). *Mineralogical magazine and journal of the Mineralogical Society*, *22*(132), 439-468.

Torsvik, T., Eide, E., Meert, J., Smethurst, M., & Walderhaug, H. (1998). The Oslo Rift: new palaeomagnetic and40Ar/39Ar age constraints. *Geophysical Journal International*, *135*(3), 1045-1059. https://doi.org/10.1046/j.1365-246x.1998.00687.x

Ussing, N. (1912). Geology of the country around Julianehaab, Greenland. *Meddelelser om Grønland Vol 38*. C.A. Reitzel.

Van Groos, A. K., & Wyllie, P. J. (1969). Melting relationships in the system NaAlSi3O8-NaCl-H2O at one kilobar pressure, with petrological applications. *The Journal of Geology*, *77*(5), 581-605.

Verschure, R., 1985. Geochronological framework for the late Proterozoic evolution of the Balatic Shield in South Scandinavia. In: A. Tobi & J. Touret (eds), *The Deep Proterozoic Crust in the North Atlantic Provinces*. (pp. 381-410). D. Reidel Pub. Co.

Vinokurov, V. M., Gaite, J. M., Bulka, G. R., Khasanova, N. M., Nizamutdinov, N. M., Galeev, A. A., & Rudowicz, C. (2002). Low-symmetry spin Hamiltonian and crystal field tensors analysis: Fe3+ in natrolite. *Journal of Magnetic Resonance*, *155*(1), 57-63. https://doi.org/10.1006/jmre.2002.2512

Walker, T. L., & Parsons, A. L. (1926). Minerals from the new nepheline syenite area, French River, Ontario. *Toronto IJ University Studies, Geological Series (Contributions to Canadian Mineralogy)*.

Warr, L., (2021). IMA–CNMNC approved mineral symbols. *Mineralogical Magazine*, 85(3), 291-320. doi:10.1180/mgm.2021.43

Weigand, P., (1975) Geochemistry of the Oslo basaltic rocks: *Skrifter Norske Vidensk-Akademie Oslo*. KIasse Ny Serie No. 34.

Weisenberger, T.B., Spürgin, S., & Lahaye, Y. (2014). Hydrothermal alteration and zeolitization of the Fohberg phonolite, Kaiserstuhl Volcanic Complex, Germany. *International Journal Of Earth Sciences*, *103*(8), 2273-2300. https://doi.org/10.1007/s00531-014-1046-1

Wilkin, R.T., & Barnes, H.L. (1998). Solubility and stability of zeolites in aqueous solution; I, Analcime, Na-, and K-clinoptilolite. *American Mineralogist*, *83*(7-8), 746-761. https://doi.org/10.2138/am-1998-7-807

Woolley, A.R., & Platt, R.G. (1988). The Peralkaline Nepheline Syenites of the Junguni Intrusion, Chilwa Province, Malawi. *Mineralogical Magazine*, *52*(367), 425-433. https://doi.org/10.1180/minmag.1988.052.367.01

Web pages

Mindat; Mindat.org - Mines, Minerals and More

Da Mommio, A. (2022). *Granitic Pegmatites*. Alexstrekeisen.it. Retrieved 20 April 2022, from http://www.alexstrekeisen.it/english/pluto/pegmatite.php.

Google Earth

Appendix I – Sample descriptions

Samples from Saga 1 quarry:

Sample Epx2

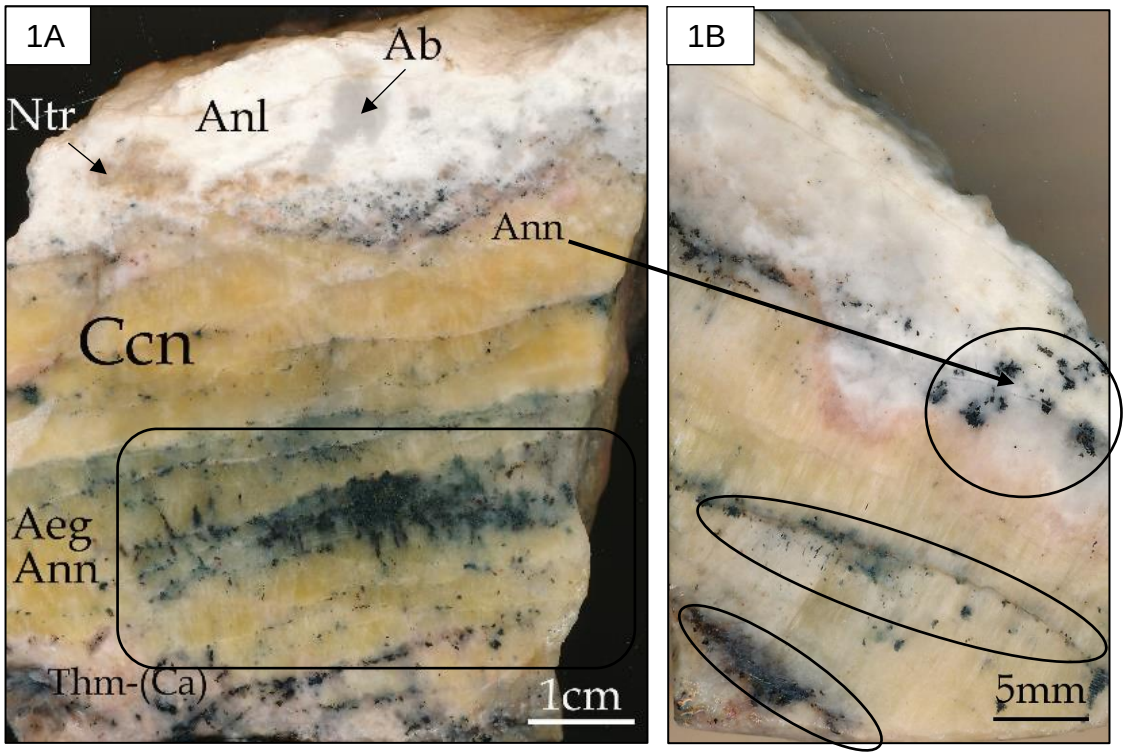

Sample Epx2 is part of the NHM rock collection and collected in the Saga 1 quarry. This sample exhibits a rather uncommon mineral assemblage amongst the collected samples. The main mineral is pale yellow cancrinite with abundant horizontal cracks hosting vast amounts of secondary small elongated black annite and green aegirine which exhibits a preferred orientation has highlighted in Figure 1A and 1B. Optical microscopy revealed a high abundance of smaller (<1-1mm) opaque minerals interstitial with both annite and aegirine, EDS and EMPA analysis confirm the presence of Fe-oxides in the sample which have caused the red staining visible in the left lower corner of Figure 1B. Extensive zeolitization has occurred in the top part where a white ~ 1cm thick rim of primarily analcime hosting natrolite and thomsonite-Ca with interstitial calcite. Another mineral found as an inclusion in analcime was the titanium manganese mineral pyrophanite. Analcime is replacing albite in this sample, some albite crystals are still visible rimmed by a white crust of analcime around the edges of the zeolite layer. Small clusters of annite are common inclusions in the zeolite layer and also abundantly seen around the boundary between the zeolite

layer and the main cancrinite. Pink larger clusters of thomsonite-Ca are scattered through the sample, seen as a layer between cancrinite and zeolite and as a larger aggregate widely intruded by annite and aegirine in contact with cancrinite as seen in the bottom part of Figure 1A.

Sample Epx5 & Epx6

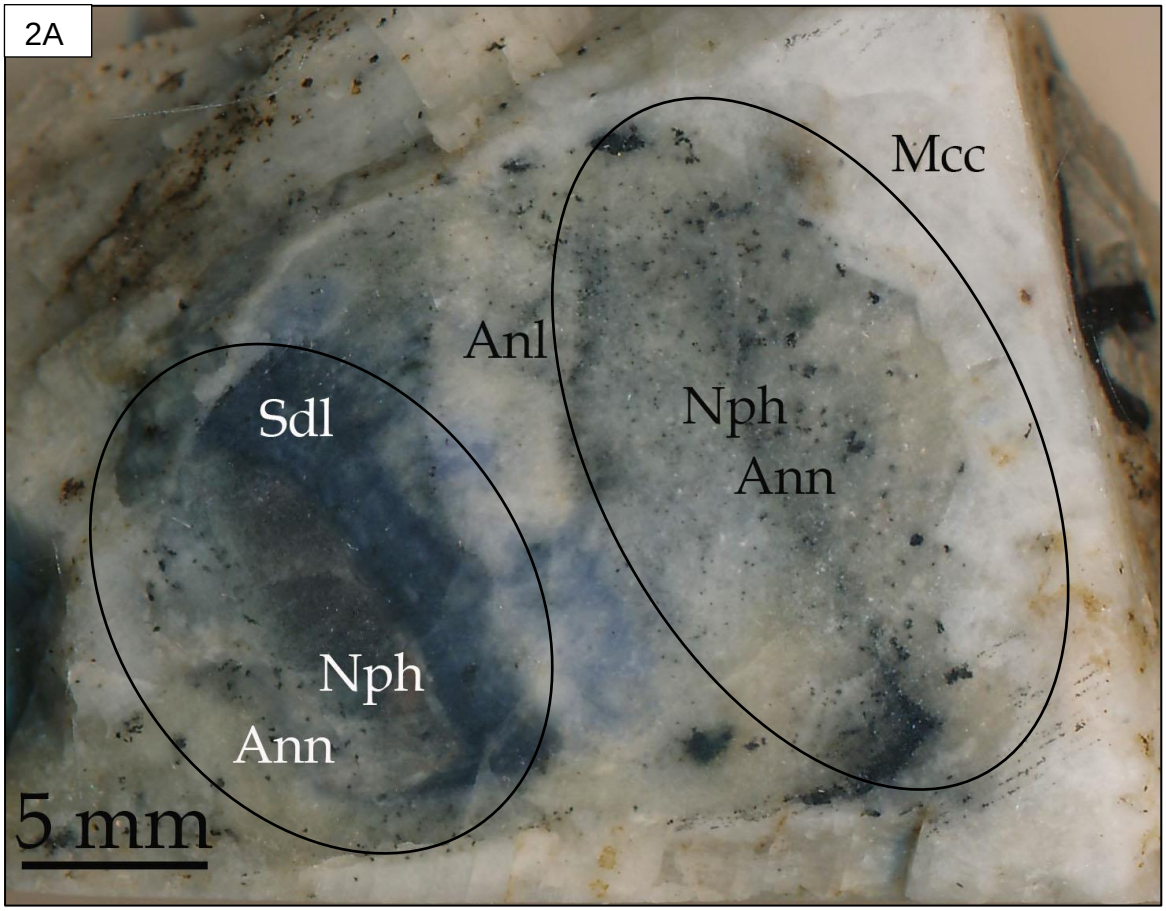

These two samples are from the same rock samples collected in the Saga1 quarry and was one of very few samples from this location found to contain blue sodalite. One of the most distinct features in this sample is the very sharp boundary between very deep blue secondary sodalite and brown nepheline that transitions into a light grey coloured variant away from the sodalite. The grey nepheline has abundant inclusions of secondary annite crystals as highlighted (Fig. 2A). Analcime with or without natrolite is often found as pods or filling cracks in larger brown nepheline crystals. The grey variety of nepheline hosts a lot of other mineral such as microcline, often rimmed by analcime or natrolite, and smaller albite crystals are commonly also present. A large annite crystal hosting inclusions of a Nb-mineral was

found at the boundary between brown and grey nepheline, other annite crystals are found with magnetite. The change from a deep blue to a light blue colour seen in sodalite correlates well with the observed amount of interstitial analcime in the mineral, the lighter the colour the more analcime is present. Blue sodalite is commonly hosting vast amounts of smaller annite and aegirine crystals. EMPA of brown nepheline gives about a 1 weight% Fe_2O_3 in the mineral, whilst its grey equivalent does not have Fe_2O_3 above detection limit. This transition is observed where an alteration product of nepheline is in close proximity, such as cancrinite, *spreustein* or blue sodalite also observed in sample SA1-13B, SA1-24, Epx 9, 10, 11 & 12. Nepheline has a seemingly sharp boundary to microcline in this sample, but smaller inclusions of microcline has been found around the transitional boundary of brown to grey nepheline.

Sample Epx8

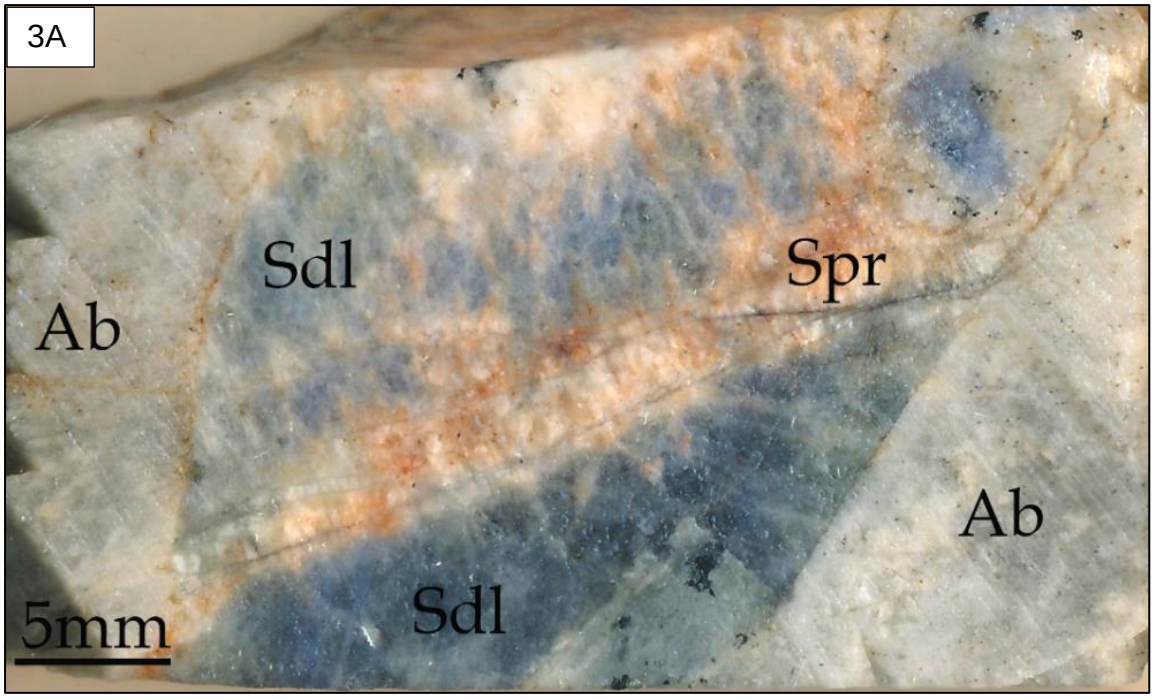

Sample Epx8 was collected in the Saga 1 quarry and is the only sample from this location in which blue sodalite is replaced by pink *spreustein* (Fig. 3A). In this case the nepheline host is fully pseudomorphed by its alteration product, blue sodalite with analcime. Small secondary annite (<1-1mm) are found interstitial inn all minerals of this sample. Zeolitization have occurred due to hydrothermal fluids percolating through the cracks which are still present in the rock. There is a strong correlation

between the presence of cracks and the presence of *spreustein* in this sample. *Spreustein* in this sample consists mainly of natrolite with some analcime and contains inclusions of annite, chamosite and very abundant Al-hydroxides.

Sample Epx9:

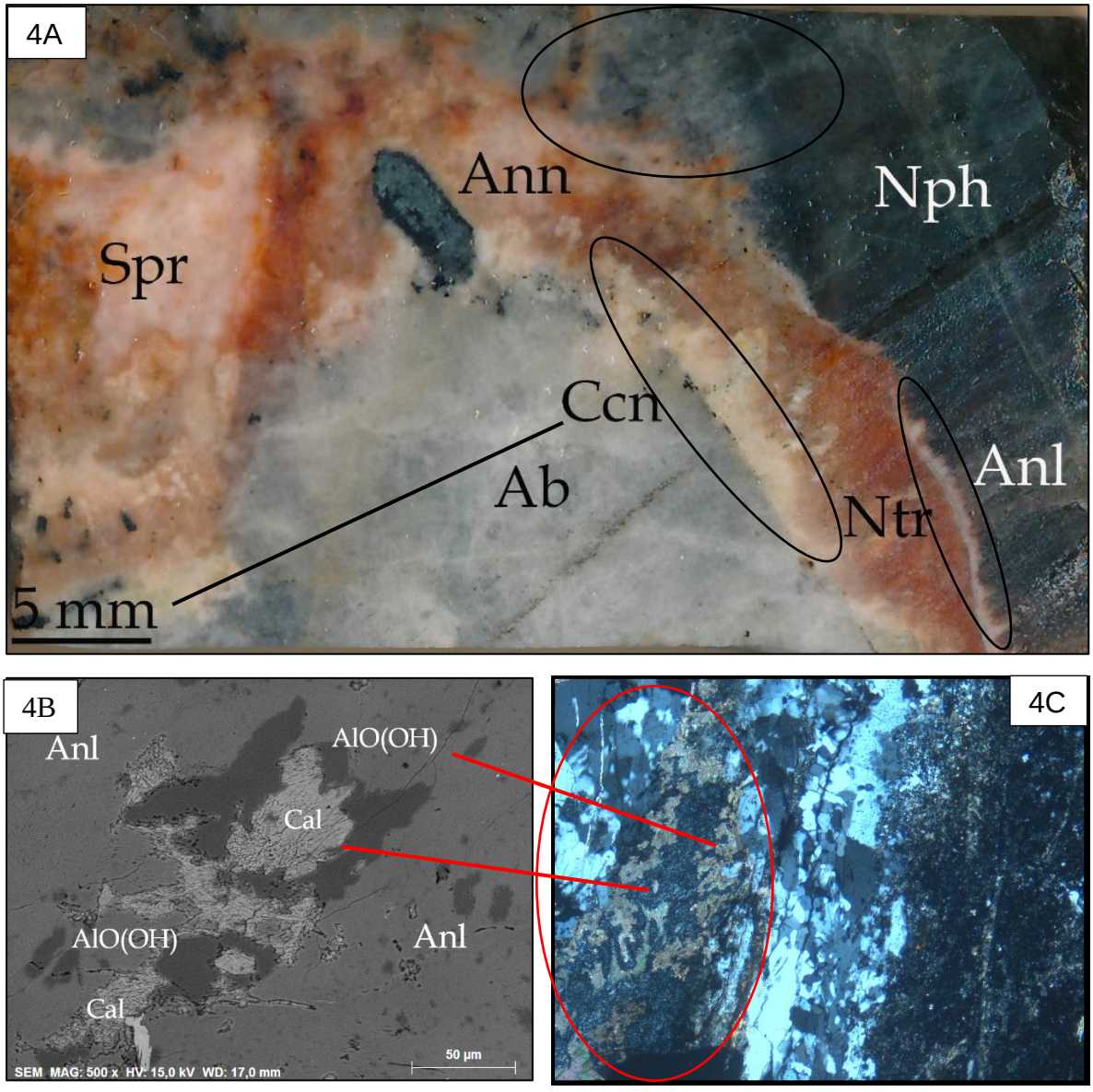

Sample Epx9 was collected in the Saga1 quarry and shows some extraordinary features. Brown nepheline transitions into its grey variant with interstitial annite highlighted in the top right corner of Figure 4A. Albite in this sample is unaltered and in contact with white coloured cancrinite highlighted in Figure 4A. Cancrinite has been observed to exhibit this colour in the presence of *spreustein* in multiple. Both EDS and EMPA confirms the presence of cancrinite in this sample. A very bright red

coloured *spreustein* is very prominent in this sample, containing mainly natrolite with some analcime. Very abundant Al-hydroxides interstitial with calcite is found within the red *spreustein*, observed in both EDS (Fig. 4B) and optical microscope (XPL) in Figure 4C with field of view of 2mm. Abundant secondary annite is found interstitial in in grey nepheline and *spreustein* and a larger Mg and Ti rich primary annite is present in contact with albite and *spreustein*. A thin white rim of pure analcime is present at the boundary between red *spreustein* and brown nepheline (Fig. 4A).

Sample SA1-3

Sample SA1-3 has undergone extensive hydrothermal alteration, the rock contains brown nepheline, albite, primary and secondary biotite/annite and very coarse grained fibrous *spreustein*. A red reaction rim is very prominent and located between *spreustein* and brown nepheline, the red square in Figure 5A shows where the thin section photos are taken, field of view is 2 mm in both Figures 5B (PPL) and 5C (XPL). The red reaction rims are also following cracks going through albite and within *spreustein*, but the colour is not as prominent, and it is not as abrupt as the one between nepheline and *spreustein*. EMPA of the red abrupt reaction rim reveals a Ca rich composition, red spreustein is also found to contain at least 1 weight% CaO, whilst white or light brown *spreustein* does not contain detectable CaO. The brown nepheline in contact with the red reaction rim is completely unaltered up to the sharp contact. Similar red layers, although much thinner have been observed in large crystals of brown nepheline in other samples from Saga 1. Unfortunately, *spreustein* in this sample was so porous quantitative analysis could not be made.

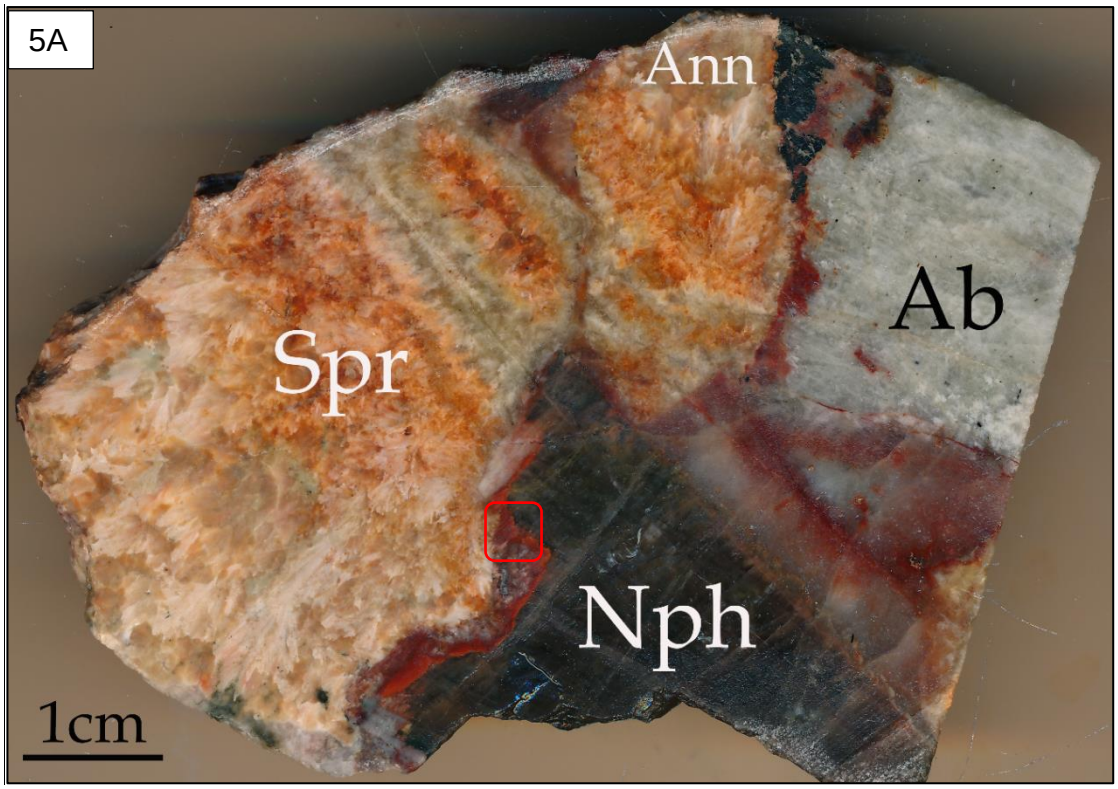

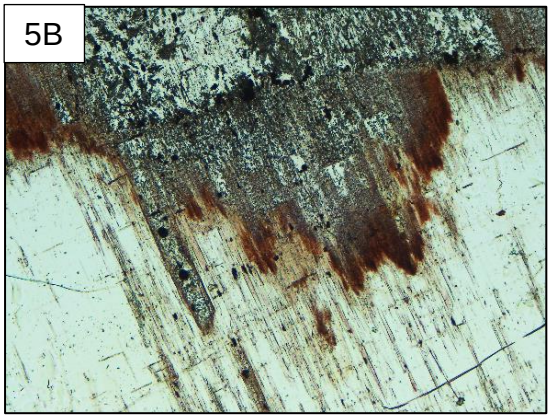

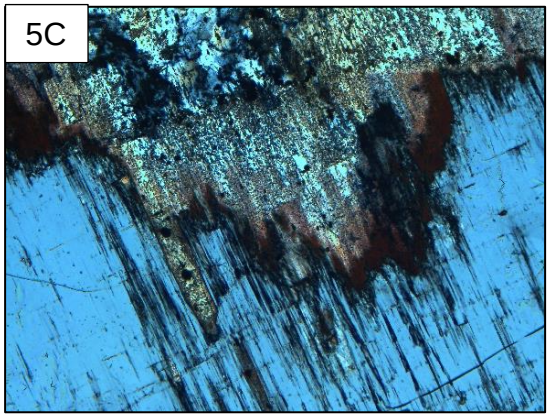

Sample SA1-13B

Sample SA1-13B was found in the Saga 1 quarry and originates from the same rock as samples Epx5 and Epx6. This sample contains microcline, albite, annite, brown and grey nepheline and a pale yellow secondary cancrinite. The red highlighted area (Fig. 6A) shows the location of the thin section photos, the photos have a field of view of 2mm. (Fig. 6B = PPL & Fig. 6C = XPL). An interesting observation in this sample is the narrow reaction rim that formed between brown nepheline and cancrinite (Fig. 6B & 6C), whilst the grey nepheline has a very transitional boundary into cancrinite. Brown nepheline in the top left corner of figure 6A does also transition into a grey variant with annite, the elongated drop like mineral is wöhlerite. The

seemingly large annite crystal is actually an aggregate of small (<1-2mm) annite crystals clustered together with some green aegirine.

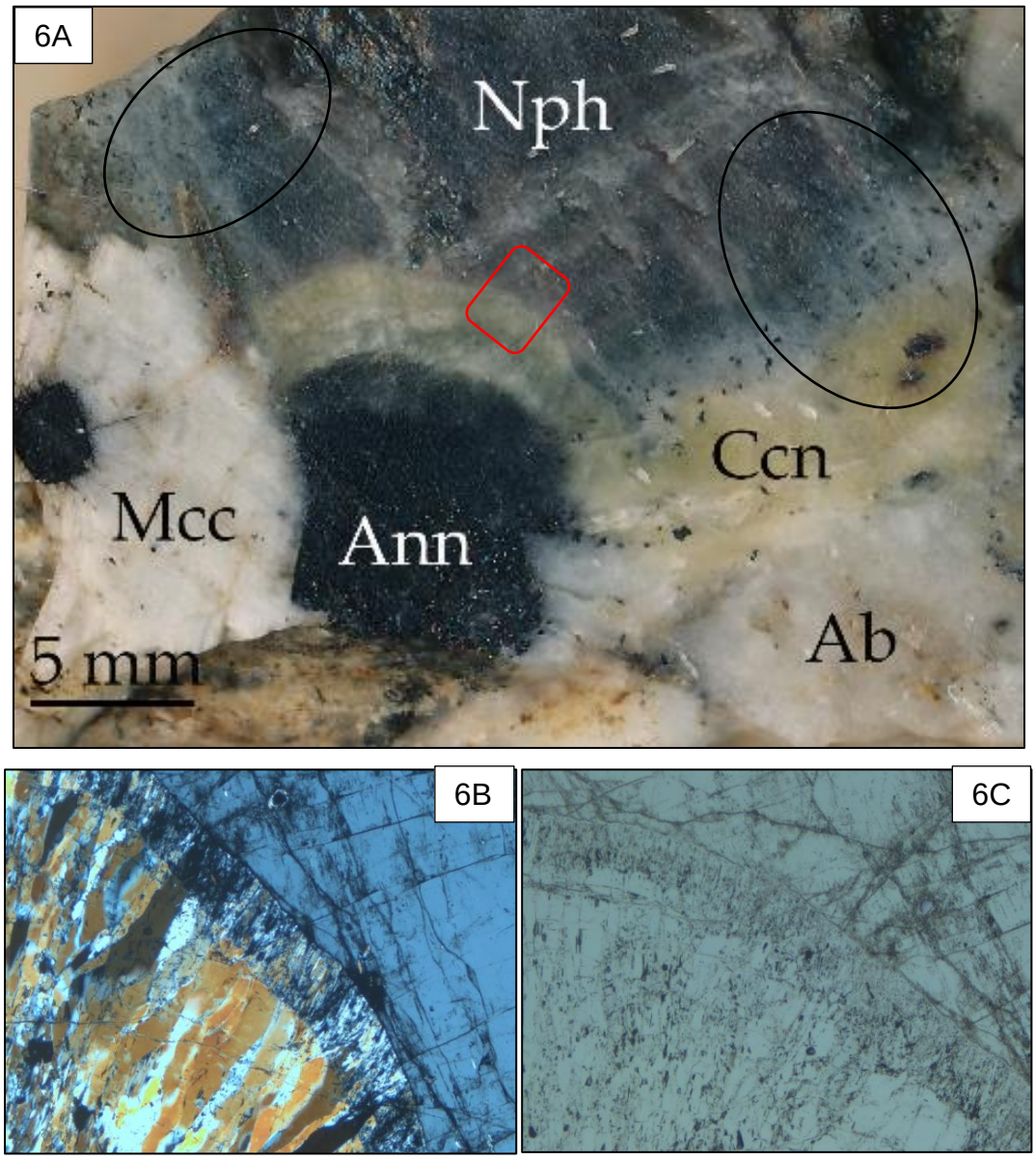

Sample SA1: 24

Sample SA1-24 was collected in the Saga 1 quarry and contains mainly *spreustein* and nepheline. This sample has Al-hydroxides as an interstitial phase in *spreustein*, but also zeolites and Al-hydroxides as well-developed crystals in vugs. In vugs in this sample we can find sugar-like crystals of brown böhmite, white flaky calcite, clusters of black annite, white natrolite and colourless to pink thomsonite-Ca crystals (Fig. 7B & 7C). A prominent feature in this sample is the colour changes of nepheline as we approach the area of zeolitization (Fig. 7A). A brown nepheline is turning more

reddish before transitioning into the grey variant of nepheline with interstitial annite as seen in multiple other samples. Optical microscopy reveals that the reddish coloured nepheline is being replaced by zeolites. XRD of the reddish nepheline also shows a large component of analcime compared to the brown nepheline in agreement with the findings from optical microscopy. At the boundary between nepheline and *spreustein* there is a transparent to translucent layer of natrolite which has not yet altered further into *spreustein*. This samples do contain abrupt bright red reaction rims cutting through the brown nepheline (Fig. 9).

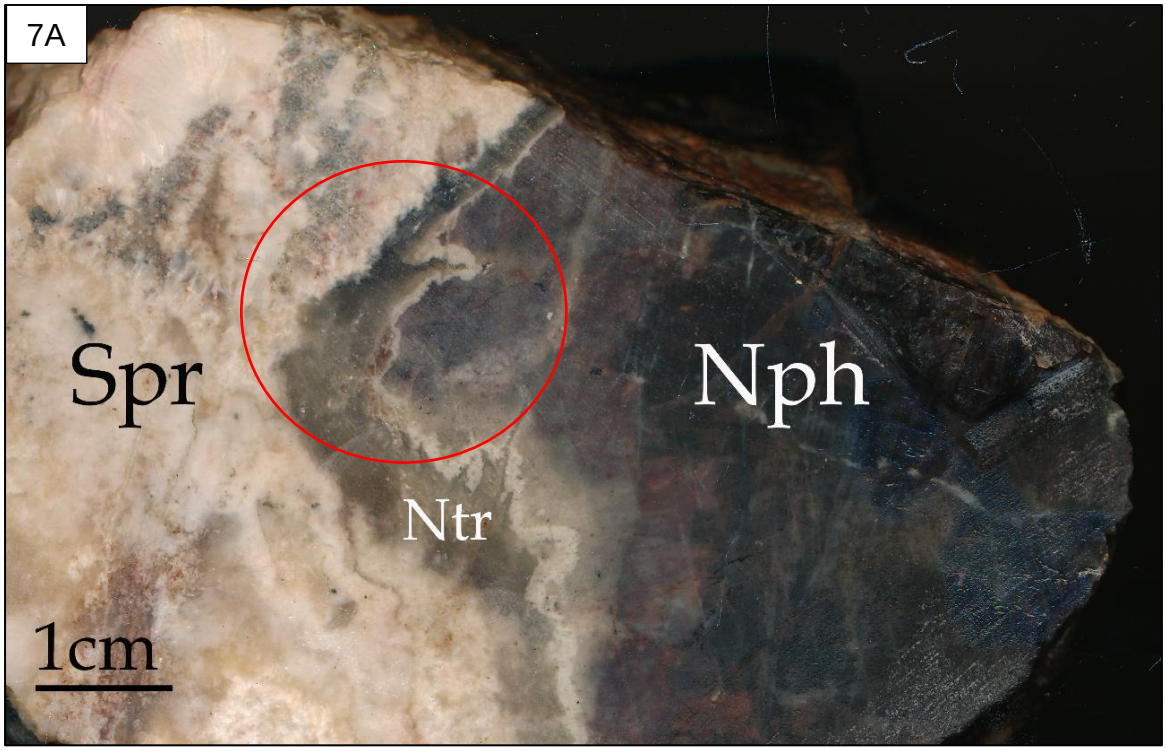

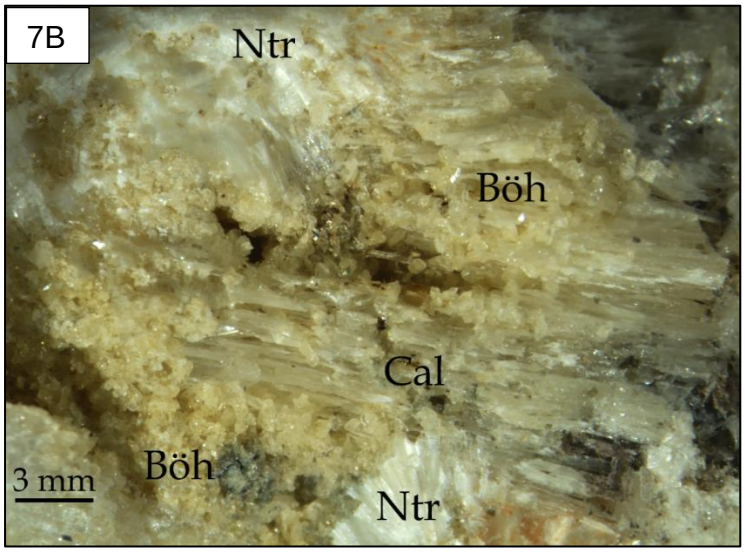

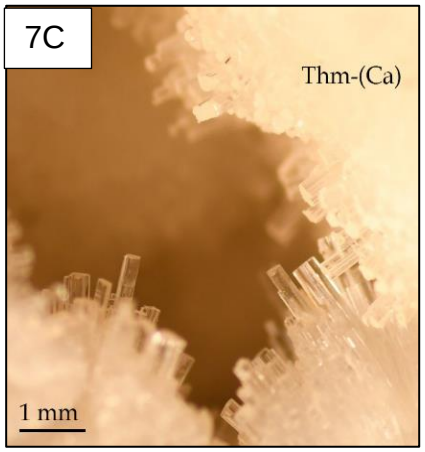

Samples from Tvedalen: The Vevja quarry

Sample TVE2

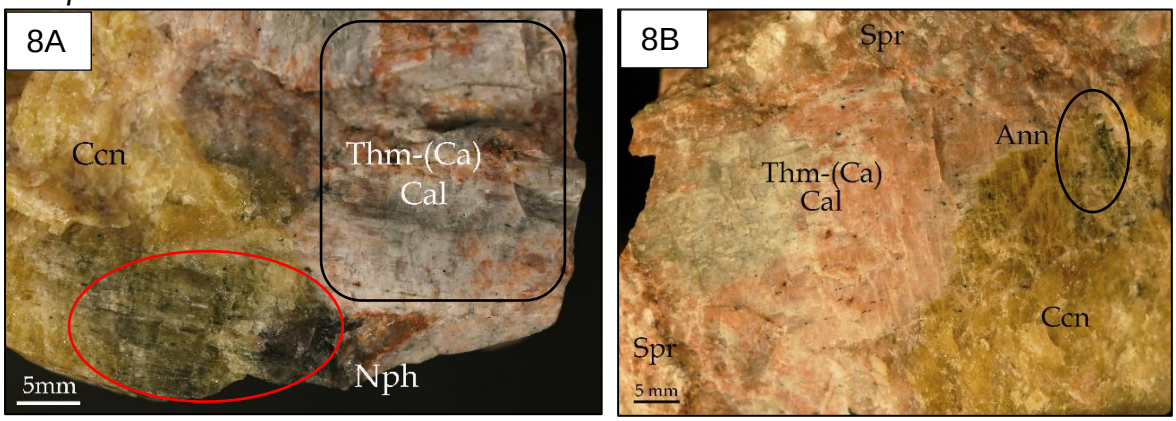

Sample TVE2 has the largest amount of cancrinite of all the collected samples. Such large sized cancrinite are known to be primary in the Tvedalen area (Larsen, 2010). Another interesting feature in this sample is the fibrous *spreustein* and the large volumes of a pink and grey aggregate comprising thomsonite-Ca as an intergrowth with calcite (Fig. 8A & 8B). The large aggregate looks massive with the naked eye but separates into very thin layers when knocked on by a hammer, small needle shaped minerals become very distinct when crushed in a mortar as preparation for PXRD analysis. The same pink aggregates are seen in sample Epx2 from Saga 1, where pink thomsonite-Ca and calcite are found together in the presence of large cancrinite. Cancrinite show a green/brownish colour where in contact with brown nepheline highlighted in red (Fig. 8A)

Sample Epx1:

Sample Epx1 was collected in the Vevja quarry and is part of the NHM rock collection. Most samples from Tvedalen contain cancrinite, often seen together with secondary blue sodalite. Blue sodalite is an alteration product of nepheline which has been observed having a light grey colour with intergrowths of annite when in close proximity of *spreustein*, cancrinite and sodalite in this sample being no exception. The boundary between blue sodalite and brown nepheline is, as seen in other samples, very sharp. Cracks in the rock are filled with hydrous minerals such as annite, aegirine and zeolites forming *spreustein* (Fig. 9A). Cancrinite has a very transitional boundary with grey nepheline in this sample (Fig. 9A) and could be replacing it, the presence of a lot of other secondary minerals within the nepheline

supports this theory. Red iron staining is also very abundant, magnetite is often found as intergrowths with larger annite or aegirine in the samples. Blue sodalite contains vast amounts of analcime, annite and aegirine, same is found in grey nepheline whilst albite in this sample is found to be unaltered.

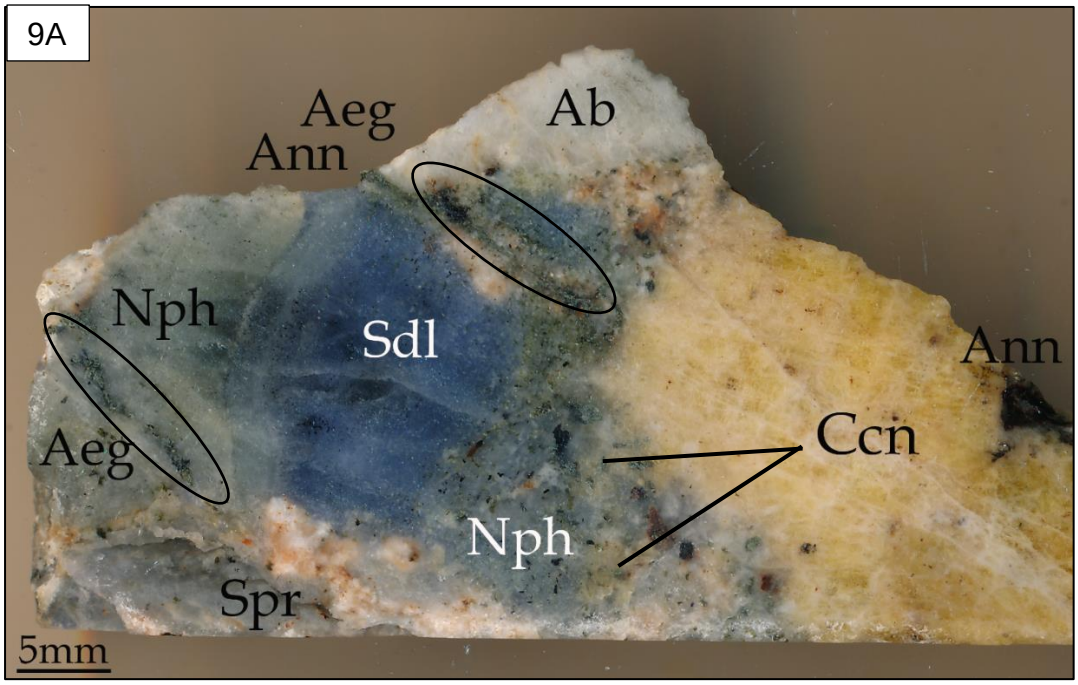

Sample Epx 3

Sample Epx3 was from the Vevja quarry and is part of the NHM rock collection. This sample contains cancrinite, blue sodalite, primary and secondary annite, microcline and pink *spreustein*. A very interesting feature in this rock is that primary cancrinite is replaced by zeolites and further altered into pink *spreustein*.

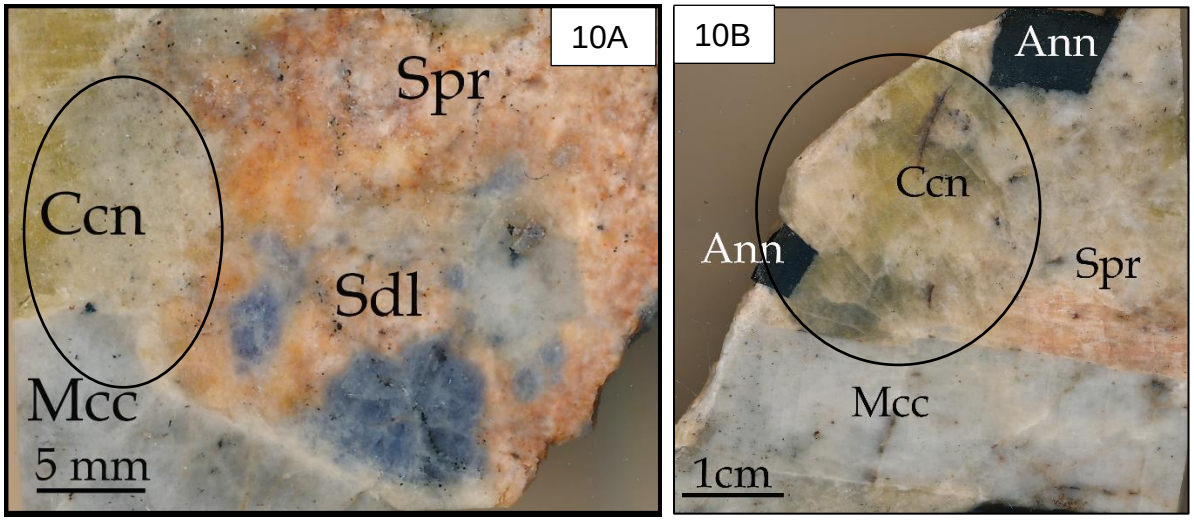

Another fascinating part is the colour change seen in cancrinite when it is being altered into pink *spreustein*, the bright yellow colour transitions into a white colour with abundant interstitial annite crystals (Fig. 10A & 10B). Cancrinite is often observed with blue sodalite, in this sample both cancrinite and blue sodalite are being replaced by zeolites and turned into *spreustein. Spreustein* in this sample contains abundant inclusions of Al-hydroxides, annite and chamosite.

Sample Epx11 & Epx12

Sample Epx11 and Epx12 were found in the Vevja quarry and are part of the NHM rock collection. This is another great sample exhibiting a transitional change from brown nepheline into grey nepheline with interstitial annite and an abrupt boundary between grey nepheline and blue sodalite as seen in Epx5 and Epx6 (Fig. 11A). Blue sodalite in this sample has vast amounts of aegirine and annite inclusions, seen to follow cracks in the mineral. Blue sodalite do contain vast amounts of analcime, the lighter the blue colour the more analcime is present. There is a sharp boundary is present between albite and sodalite and albite and *spreustein* in the top right corner. *Spreustein* are replacing blue sodalite in the lower right corner of the sample.

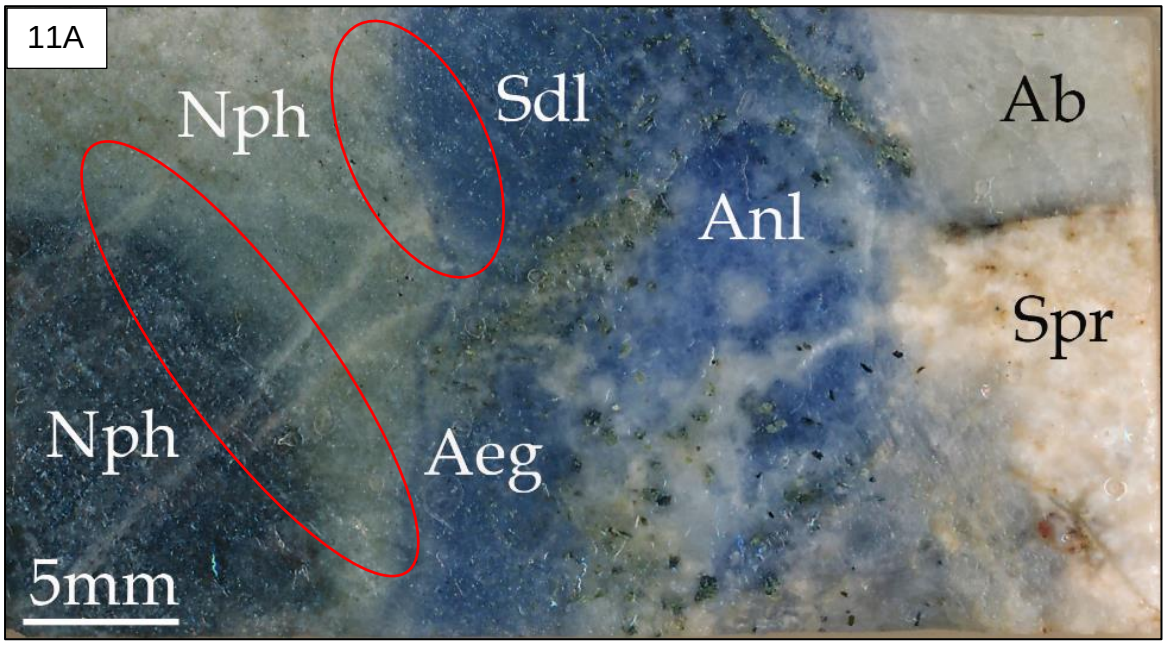

Samples from the Østskogen quarry

Sample Epx10

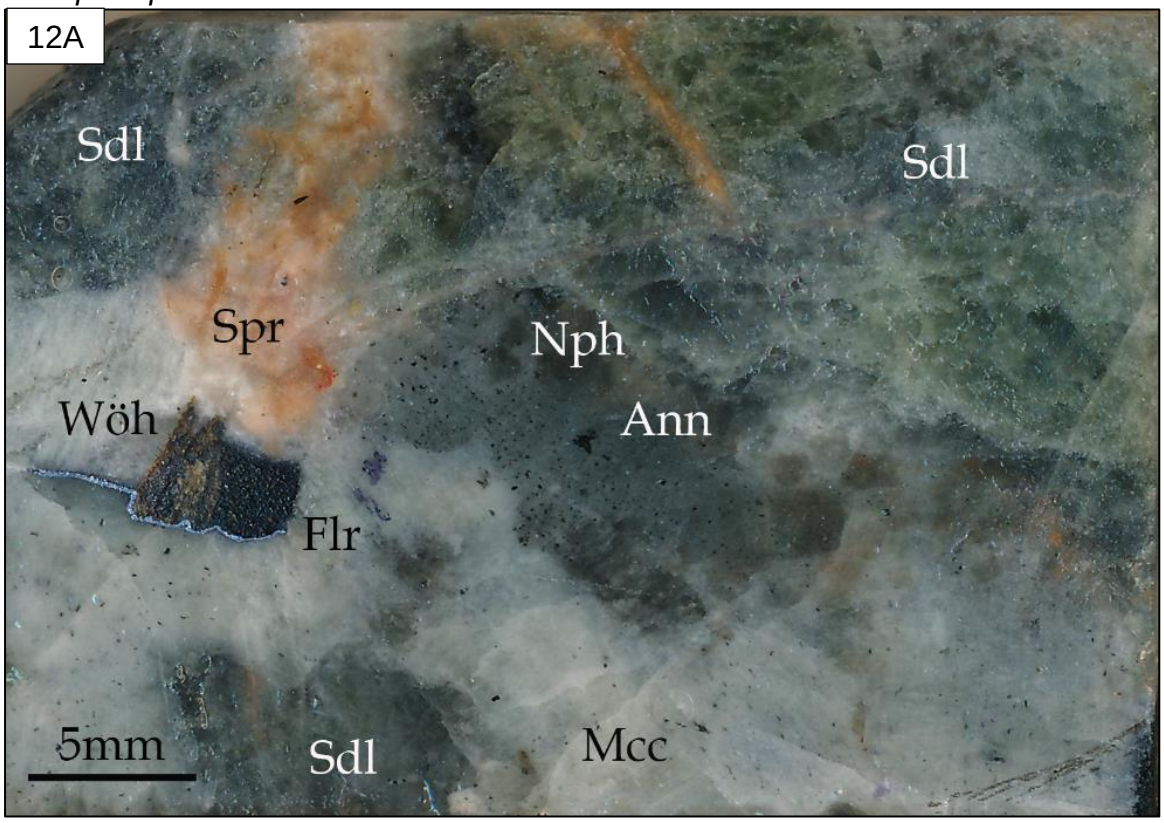

Sample Epx10 was collected in the Østskogen quarry and is the only sample from this location which was chosen for thin section making. This sample is a bit different from the other as it does contain fluorite, wöhlerite, thorite and zircon as well as sodalite, nepheline, microcline and pink *spreustein* (Fig. 12A). There is only greenish primary sodalite in this sample, no secondary blue sodalite. Microcline in this sample is rich in small annite crystals. Primary sodalite in this sample are vastly altered into pink *spreustein* with abundant inclusions of analcime, Al-hydroxides, chamosite and annite. Spots of brown nepheline are visible but are being replaced by its grey equivalent with annite located in-between microcline and sodalite.

Appendix II – rocks of the LPC

Table 1: The plutonic rocks in the LPC

Larvikites	Larvikite, both the light and dark variety are hypersolvus monzonitic rocks, which means they crystalized above the solvus temperature and therefore only contain one type of alkali feldspar. Larvikite is characterized by its prominent blue or silver schillerizing feldspars and are abundant in the Larvik area. There are large variations in both texture and mineral composition, larvikites can be different from pluton to pluton and each pluton is too internally magmatically layered (Dahlgren, 2010). Larvikites are course to very coarse grained, with feldspars (2-4 cm) which are rhomb shaped in cross-section. Main mineral are ternary feldspar, quartz (eastern end of the LPC) or nepheline (western end of the LPC). The mafic minerals include olivine, clinopyroxene (augite), biotite and amphibole whilst Fe-Ti-oxides, apatite, zircon and baddeleyite are typically minor or accessory minerals The syenite pegmatites related to the larvikite plutons are miaskitic in composition (Brøgger 1890, Neumann, 1980, Dahlgren et al., 1996).
Nepheline syenites	***Lardalite*** was first discovered by Brøgger (1897) in Lardal in Lågendalen and he described it as a large nepheline syenite pluton of a peculiar type. Lardalites always contain nepheline, up to 30% as phenocrysts or as an interstitial phase. Large feldspars (5-6 cm) but does rarely show blue schiller. Another textural characteristic feature of Lardalite is the poikilitic micas with sizes up to 10 cm across. Other mafic minerals include olivine, clinopyroxene and the minor phases include Fe-Ti oxides, apatite, zircon and baddeleyite (Dahlgern, 2010). ***Foyaite*** is a younger type of nepheline syenite found in the same area as Lardalite. It is white to grey coloured with characteristic platy K-feldspar crystals 1-1.5 cm long and 1mm thick, these feldspars form an open network with interstitial nepheline. Other mafic minerals include clinopyroxene (aegirine-augite with Na-enrichment towards the rims), biotite and titanite. Accessory minerals are Fe-Ti oxides, apatite and zircon (Dahlgren, 2010). ***The Langesundsfjord nepheline syenite*** are texturally and mineralogy different from one place to another and can appear as equigranular, porphyritic, gneissic or foyaitic (Dahlgren, 2010). Brøgger (1890) described their gneissic appearance as *fluidal structure* and commented on their intimate co-occurrence with deformed larvikite suggesting that partly crystallized nepheline syenite magma intruded into party crystallised larvikite magmas and deformed together. The Langesundsfjord nepheline syenites are fine to medium grained, rarely coarse grained or porphyritic. Major minerals include alkali feldspar and nepheline, with occasional sodalite and mafic mineral such as clinopyroxene, biotite, amphibole and rarely olivine. Minor mineral phases include apatite, Fe-Ti oxides, titanate, and fluorite. The nepheline syenite pegmatites related to this pluton are agpaitic in composition and compose most of the rare minerals found in the LPC (Dahlgren, 2010)
Tønsbergite	Tønsbergite is a reddish hypersolvus monzonite, found in the eastern parts of the LPC. Its distinct red colour is a result of red staining from hematite indicating that Tønsbergite is in fact a hydrothermally altered larvikite (Dahlgren, 2010).

Appendix III – EMPA data points

Not used – values too high, low or inconsistent.

Analysis no	Na2O	SiO2	Cl	K2O	CaO	FeO	Al2O3	MgO	MnO	SO3	Total	X	Y	Z
1 / 1 .	25.5057	36.5657	7.4016	0.0244	0.009	0.0488	30.858	0.0101	-0.0289	0.0336	100.457	-16402	-27864	-19
2 / 1 .	24.9438	37.3842	6.9744	0.0337	0.003	-0.0081	30.6277	-0.0172	-0.0111	0.0052	99.9719	-16356	-27864	-19
3 / 1 .	25.531	37.0868	7.3374	0.0457	0.0529	0.0428	30.6836	0.0404	-0.0313	0.0208	100.8413	-16332	-27995	-19
4 / 1 .	13.461	54.1607	0.0185	0.0808	0.0303	-0.0186	22.5277	0.0041	-0.0045	0.0108	90.294	-16309	-27736	-19
5 / 1 .	20.7551	37.4156	0.0061	0.0221	3.2053	0.0246	28.3334	-0.0288	0.0941	0.1667	90.023	-16309	-28061	-19
6 / 1 .	20.5665	37.0308	0.0042	0.0031	3.4042	0.0462	27.5445	0.0093	0.1514	0.1491	88.9093	-16392	-28003	-19
7 / 1 .	21.1477	38.0191	0.0167	0.0241	3.1141	0.0329	26.4562	-0.0163	0.0576	0.2084	89.0768	-16289	-27931	-19
8 / 1 .	14.0745	43.7439		0.2559	2.0563	0.0263	27.6674		0.0036		87.828	-11682	-23041	-9
9 / 1 .	12.2638	40.6984		0.2897	4.2285	0.0034	28.3386		-0.0186		85.8225	-10585	-21899	-6
10 / 1 .	0.3015	0.0856		0.0083	0.0909	0.0293	79.8627		-0.0036		80.3784	-7167	-22306	18
11 / 1 .	0.2509	0.1181		0.0304	0.089	0.1179	79.7726		0.0465		80.4255	-6406	-21288	18
12 / 1 .	25.5483	37.0343	7.2934	0.0116	0.0074	0.0917	31.0505	-0.007	-0.0044	0.0686	101.1059	-16023	-27840	-15
13 / 1 .	25.3016	36.8989	7.4097	0.0142	-0.0103	-0.016	31.2598	0.0211	-0.024	0.0457	100.9509	-15978	-28194	-15
14 / 1 .	25.5634	36.9365	7.2359	0.0078	-0.0044	0.0678	30.7364	0.0141	0.0327	0.0838	100.6784	-16012	-28348	-15
15 / 1 .	25.2981	36.9622	7.3534	0.0175	-0.0532	0.0478	31.1049	0.0141	0.0065	0.0533	100.8579	-16120	-28868	-15
16 / 1 .	25.4141	36.9871	7.2134	0.0259	-0.0044	0.0399	31.0201	0.0254	0.0218	0.0736	100.8213	-16079	-28873	-15
17 / 1 .	25.2994	36.7445	7.2234	0.0207	-0.0059	0.0618	30.8819	-0.0056	0.0065	0.0025	100.2408	-16048	-29303	-19
18 / 1 .	25.8323	37.2581	7.2443	0.0349	0.0369	0.0219	31.0188	0.0127	0.0196	0.0203	101.4999	-16122	-31382	-15
19 / 1 .	25.4346	36.9911	7.491	0.0103	-0.0148	0.014	31.1606	-0.0084	0.0131	0.0101	101.1249	-15906	-31560	-15
20 / 1 .	25.4534	36.9364	7.3862	0.031	-0.0399	0.0219	31.1503	0.0113	-0.0327	0.1167	101.1071	-16067	-31809	-18
21 / 1 .	25.2349	36.8588	7.3049	0.0388	0.0222	0.0758	30.3937	0.0028	0.0196	0.0076	99.9591	-15959	-31986	-18
22 / 1 .	25.2075	36.7985	7.2171	0.02	-0.0133	0.0239	30.801	0.0619	0	0.066	100.1958	-16189	-32003	-18
23 / 1 .	25.6012	37.0211	7.3378	0.0453	0.0015	0.0558	31.2526	0.0028	-0.0065	0.0152	101.3333	-16446	-32027	-18

24 / 1 .	25.3263	37.0208	7.2432	0.064	0.0192	0.0718	30.7661	0.007	-0.0393	-0.0152	100.5184	-16213	-32166	-19
25 / 1 .	25.463	36.8434	7.309	0.0226	-0.0148	0.0538	30.9812	-0.0141	-0.0218	0.0355	100.7085	-15976	-32252	-19
26 / 1 .	25.2556	36.9043	7.1796	0.0317	0.0192	0.0179	30.8266	-0.0338	0.0371	0.0203	100.2923	-15754	-32224	-15
27 / 1 .	25.8265	36.9028	7.265	0.0162	0.0266	0	31.0642	0.0056	0	-0.0076	101.1068	-15336	-32224	-15
28 / 1 .	25.3904	36.6885	7.2662	0.0084	0.0473	-0.008	31.0959	0.007	-0.0087	0.0102	100.514	-16196	-32380	-19
29 / 1 .	25.47	36.6721	7.2608	0.0168	-0.0044	0.0219	31.2624	-0.0155	0.0458	0.0584	100.8082	-16335	-32431	-19
30 / 1 .	25.365	36.997	7.4682	0.0078	-0.0015	0.0179	31.0585	0.0324	0.0196	0.0025	100.9689	-16460	-32482	-19
31 / 1 .	25.4379	36.6508	7.4183	0.0136	0.0665	0.0319	31.1154	-0.0085	-0.0109	0.0304	100.7648	-15972	-32373	-19
32 / 1 .	25.2725	37.2768	7.3274	0.0239	0.0074	0.0578	30.937	0.0239	0.0393	-0.0203	100.966	-15476	-32330	-15
33 / 1 .	25.2777	36.625	7.2687	0.0246	0.0015	0.0897	30.8707	0.0113	0.0305	0.0203	100.2199	-16186	-32557	-19
34 / 1 .	25.4335	36.7712	7.2465	0.0246	0.0458	0.0319	30.9745	0.0211	0.0153	0.0406	100.6051	-16006	-32559	-19
35 / 1 .	25.3728	36.966	7.3278	0.0045	0.0163	0.01	30.7801	-0.0169	0.0502	0.0076	100.5352	-15539	-32561	-19
36 / 1 .	25.5548	37.0038	7.253	0.0356	-0.0148	0.0399	31.1307	-0.0042	0.0044	-0.0152	101.022	-16354	-32571	-18
37 / 1 .	25.4066	36.7183	7.4471	0.0388	0.0089	0.0777	31.1318	0.0253	-0.0044	-0.0076	100.8544	-16733	-32571	-21
38 / 1 .	25.4915	37.0274	7.4109	0	-0.0015	0.0239	30.9961	-0.007	0.0218	0.0178	100.9894	-16218	-32769	-19
39 / 1 .	25.4522	36.8273	7.48	-0.0045	-0.0089	-0.006	30.9659	-0.0141	-0.0174	0	100.7255	-15891	-32755	-18
40 / 1 .	25.6669	37.239	7.4333	0.0239	0.0399	-0.012	31.2038	0	0.0153	0.0025	101.6247	-15691	-32755	-18
41 / 1 .	25.4889	36.6707	7.3481	0.0401	0.0133	-0.0179	31.2766	0.007	0.0218	0.0609	100.9274	-16577	-32804	-19
42 / 1 .	25.5099	36.8952	7.4106	0.0278	0.0118	0.0558	30.7186	-0.0042	-0.0044	0.0127	100.6424	-16256	-33103	-19
43 / 1 .	25.5101	37.036	7.4128	0.0194	0.0355	0.1037	30.7236	-0.0155	0	0.0025	100.8435	-16086	-33497	-19
44 / 1 .	25.399	36.9637	7.3083	0.0097	0.0517	0.0219	31.1193	0.0141	0.0218	0.0025	100.9121	-16027	-33606	-19
45 / 1 .	25.3088	36.7874	7.4904	0.02	0.0281	0.004	31.0754	0.0183	-0.0087	0.0076	100.7401	-15932	-33804	-19
46 / 1 .	24.9752	37.1837	7.1136	0.0155	0.0946	0.0299	30.9005	-0.0281	-0.0305	0.0152	100.3281	-15932	-33985	-19
47 / 1 .	25.3241	36.7068	7.3695	0.031	0.034	-0.014	31.0552	-0.0028	0.0087	-0.0102	100.5293	-15715	-33999	-19
48 / 1 .	25.5507	37.05	7.2553	0.0162	0.0281	0.012	30.9251	0.0465	-0.0022	-0.0279	100.8838	-15887	-34205	-19
49 / 1 .	25.3157	36.4091	7.2654	0.0181	0.003	-0.008	30.4279	0.0268	0.0153	0.0228	99.5041	-15474	-34483	-19
50 / 1 .	25.4336	36.5384	7.5047	0.0155	-0.0133	0.01	30.9316	-0.0324	0.0022	0.0279	100.4639	-15252	-35794	-19
51 / 1 .	25.2962	36.8985	7.3533	0.0168	-0.0355	-0.0319	30.8569	-0.0113	0.0327	0.0305	100.4848	-15167	-36209	-19
52 / 1 .	25.266	36.742	7.2711	0.0175	0.0059	0.0379	30.9354	0.0056	0.0065	0.0812	100.3691	-14856	-36912	-19
53 / 1 .	25.1863	36.6487	7.1556	0.0323	0.0251	0.1256	30.8169	-0.0113	-0.0153	0.0965	100.0871	-14861	-37298	-19

54 / 1 .	25.3874	37.3296	7.4938	0.0272	-0.0059	-0.002	31.2854	0.007	0.0567	-0.0152	101.587	-15010	-37347	-19
55 / 1 .	25.5007	37.2107	7.3868	0.0446	0.0015	0.012	30.9321	0.0225	-0.0065	0.0355	101.1464	-15157	-38087	-20
56 / 1 .	25.2712	36.7859	7.4772	0.0388	0	0.0339	30.5669	0.0282	0.0131	0.0482	100.2633	-14072	-38197	-19
57 / 1 .	17.8514	38.5112		1.0417	0.3032	0.0817	27.1225		0.0409		84.9527	-13442	-2903	-25
58 / 1 .	19.1308	38.5643		0.4617	0.3367	0.294	27.1552		0.1196		86.0622	-13405	-2980	-25
59 / 1 .	19.3863	39.136		0.3339	0.3721	0.1197	27.1029		0.101		86.5518	-13493	-3016	-25
60 / 1 .	18.8645	40.3274		0.5191	0.3245	0.0274	27.0282		0.1421		87.2331	-13619	-2820	-25
61 / 1 .	17.0506	40.6307		5.2433	0.0481	0.1229	31.5081		0.0299		94.6335	-13429	-3024	-25
62 / 1 .	15.9704	41.4739		7.4232	-0.0583	0.1467	32.8377		-0.0037		97.8518	-13472	-3055	-28
63 / 1 .	16.2019	41.8645		7.2609	-0.0051	0.2285	33.3878		0.0037		98.9473	-13541	-2875	-24
64 / 1 .	16.1279	41.4417		7.4482	-0.0431	0.1159	33.3422		-0.0037		98.4759	-13477	-2756	-24
65 / 1 .	14.6223	49.1484	-0.0069	0.7628	0.0059	0.0483	25.175	-0.0121	-0.0176	-0.0421	89.7627	-10179	5758	0
66 / 1 .	15.493	47.3303	0.023	2.6552	0.0059	0.2391	27.6108	0.0229	0.0066	-0.0078	93.3868	-10167	5794	0
67 / 1 .	15.7747	43.033	0.0143	6.6144	-0.003	0.014	32.2492	0.0188	0.0088	0.0283	97.7556	-10177	5809	0
68 / 1 .	16.6862	45.0699	-0.0008	5.5916	-0.0104	0.539	31.9707	0.0162	0.0153	-0.0594	99.889	-10158	5844	0
69 / 1 .	16.5913	45.0671	-0.0076	5.5615	-0.0252	0.581	31.2672	0.0135	-0.0131	0	99.0817	-10229	5866	0
70 / 1 .	16.5607	44.7878	0.0025	5.541	-0.0178	0.5371	31.1873	0.0054	-0.0088	-0.0207	98.6217	-10290	5959	0
71 / 1 .	4.6625	37.8329		0.0041	12.0636	0.0595	28.6359		-0.0072		83.2584	16466	-102	41
72 / 1 .	14.5803	45.615	-0.0061	0.0366	1.1163	-0.002	26.6832	0.0205	0.0268	-0.0133	88.0788	16554	-159	41
73 / 1 .											0	0	0	0
74 / 1 .	6.1351	39.0426		0.0086	10.5773	0.0448	28.5024		-0.0226		84.3109	16478	-164	41
75 / 1 .	4.0605	37.5873	-0.01	0.0163	13.149	0.006	28.9332	-0.0229	0.0242	-0.0229	83.7765	16466	-104	41
76 / 1 .	0.0588	0.1306	0.037	0.0034	50.0882	0.0256	0.0407	-0.06	0.7569	0.0247	51.1659	16651	-274	38

Analysis no	Na2O	SiO2	Cl	K2O	CaO	FeO	Al2O3	MgO	MnO	SO3	Total	X	Y	Z
1 / 2 .	12.0261	69.3279	0.0069	0.1362	-0.0537	0.2959	19.311	-0.0145	0.0111	-0.0107	101.115	-20811	-3634	-107
2 / 2 .	12.0759	69.333	0.0104	0.1069	0.0269	0.2878	19.1262	0.0172	-0.0155	-0.016	100.9842	-20962	-3653	-107
3 / 2 .	11.8498	69.0546	0.0165	0.1323	0.0045	0.2412	18.8404	0.0119	0.0022	-0.0027	100.1533	-20962	-3863	-107

4 / 2 .	11.9122	69.3542	0.0139	0.0919	0.0343	0.308	18.9963	-0.0053	0.0044	0.0266	100.7419	-20846	-3863	-107
5 / 2 .	12.0422	69.11	0.0217	0.1036	-0.0149	0.3323	18.8363	-0.0423	-0.0465	-0.0027	100.446	-20725	-3863	-107
6 / 2 .	12.0036	69.141	0.0009	0.1206	-0.0134	0.2351	18.7744	0.0066	-0.0133	0.0213	100.3035	-20962	-3942	-107
7 / 2 .	11.8466	68.7909	-0.0078	0.1154	0.0045	0.2453	19.0297	0	-0.0266	0.0346	100.0669	-20780	-3970	-107
8 / 2 .	11.8679	68.7467	0.0069	0.1303	0.0344	0.1865	18.8833	-0.0066	0.0355	-0.0027	99.8915	-20808	-4083	-107
9 / 2 .	11.7058	68.7846	-0.0052	0.1284	0.006	0.308	18.887	-0.0409	-0.0177	-0.016	99.8197	-20967	-4044	-104
10 / 2 .	21.5324	38.5246	0.0026	0.0301	2.7067	-0.0302	27.3871	-0.0071	0.0418	0.0104	90.2357	-21018	-4074	-107
11 / 2 .	21.6743	38.3637	0.0111	0.034	2.592	0.0806	26.9458	0.0043	0.022	0.0182	89.7459	-20796	-4138	-107
12 / 2 .	21.0212	38.3611	0.0068	0.0244	2.6041	-0.0081	27.0855	-0.0213	0.0286	0.0052	89.1369	-20796	-4192	-107
13 / 2 .	21.4058	38.0095	0.0153	0.0692	2.826	0.0503	28.0967	0.0114	0.0132	-0.0182	90.4975	-21062	-4180	-107
14 / 2 .	21.9094	37.9555	-0.0111	0.0103	2.7628	0	27.8892	-0.0214	0	0.0235	90.5506	-21062	-4349	-104
15 / 2 .	21.9434	37.9312	0.0256	0.034	2.4266	0.0322	28.0064	-0.0214	-0.0198	0.0261	90.4254	-20776	-4328	-104
16 / 2 .	16.1268	0.0074	0.027	0.0669	0.2356	0.022	45.9574	0.0042	0.0633	0.0386	62.5493	-20471	-6053	-88
17 / 2 .	16.1851	0.2274	0.0211	0.0344	0.1845	0.014	45.908	-0.0042	0.0328	0.0335	62.6408	-19703	-6010	-90
18 / 2 .	15.9187	0.0828	0.0245	0.0351	0.2138	0.018	47.2447	-0.0195	-0.0437	0.0077	63.5452	-19695	-6050	-90
19 / 2 .	14.6998	45.5453	0.0086	0.0731	1.0185	0.1151	27.3361	-0.0217	0.0331	-0.0079	88.8296	-17446	-5581	-95
20 / 2 .	14.8339	44.995	0.0189	0.0815	0.8949	0.1171	28.1434	0.0027	0.0817	0.029	89.1981	-17395	-5581	-95
21 / 2 .	14.871	45.6748	0.0103	0.0576	0.8224	0.1434	27.5423	-0.0244	0.0331	0.0211	89.1759	-17337	-5581	-96
22 / 2 .	14.4435	44.5235	0.0077	0.0491	1.0386	0.2261	28.4132	0.023	0.0331	0.0105	88.7684	-17268	-5575	-96
23 / 2 .	13.6849	42.0679	-0.0043	0.0575	1.0846	0.0182	31.6081	-0.0174	0.0066	0.0237	88.5516	-17201	-5610	-96
24 / 2 .	13.716	42.0438	0.0163	0.062	1.1259	0.0827	31.6196	0.004	-0.011	0	88.6704	-17193	-5631	-96
25 / 2 .	15.1432	45.8278	0.0077	0.0725	0.591	0.0788	27.4658	0.0027	0.0375	0.0105	89.2376	-17105	-5542	-96
26 / 2 .	14.8628	46.1543	0.006	0.1184	0.7175	0.0101	26.3994	-0.0081	0.0265	0.0185	88.3134	-17076	-5495	-96
27 / 2 .	12.5647	48.4196	0.0129	0.4361	3.0971	0.1172	24.2634	0.0094	0.0663	0.0131	88.9998	-17030	-5581	-96
28 / 2 .	13.1944	51.76	0.0026	0.1589	0.3631	0.0809	25.8245	-0.012	-0.0265	-0.0079	91.3845	-17016	-5650	-94
29 / 2 .	14.9173	51.3286	0.0173	0.1869	0.0982	-0.0222	24.2754	-0.0027	0.0155	0.045	90.8841	-16861	-5675	-94
30 / 2 .	13.5922	49.7098	0.0207	0.223	0.4999	0.0505	25.4287	0.0322	0.0597	0.0476	89.6643	-16823	-5650	-94
31 / 2 .	16.5868	45.1869	0.0119	5.5371	-0.0164	0.6356	31.6039	0.0095	-0.0044	0.0026	99.5742	-16796	-5695	-93
32 / 2 .	16.6427	43.4629	0.0245	6.5692	-0.003	0.1428	32.888	0.0108	-0.0264	0.0259	99.7667	-16740	-5852	-90
33 / 2 .	16.8284	45.4059	0.0025	5.3455	-0.0447	0.6517	31.3486	-0.0014	-0.0176	0.0285	99.6111	-12440	-6556	-84

34 / 2 .	16.8083	45.4216	0.0153	5.4106	-0.0268	0.5853	31.9855	-0.0136	0.0242	0.0078	100.2585	-14532	-6405	-87
35 / 2 .	17.0934	44.9743	0.0034	5.5413	0.0015	0.5651	31.797	0.0191	0.0286	0.0052	100.0289	13714	5729	-40
36 / 2 .	16.5907	44.7327	0.0195	5.5828	-0.0402	0.5551	31.8377	0.0204	-0.0088	0.0026	99.3415	13694	5639	-40
37 / 2 .	16.7919	45.5144	-0.0085	5.6406	-0.0224	0.6656	31.4101	0.0014	-0.0352	0.0156	100.0396	14059	4121	-41
38 / 2 .	16.6428	45.3167	-0.0051	5.1021	-0.0581	0.7624	31.2412	-0.0109	-0.022	0.026	99.0911	15189	4117	-44
39 / 2 .	16.4455	45.4259	0.0119	5.3528	-0.0164	0.7543	31.3851	-0.0149	-0.0088	-0.0026	99.3756	15189	4682	-44
40 / 2 .	16.7304	45.6065	0.0068	5.1809	-0.006	0.7805	31.5411	0.0299	-0.0154	-0.0156	99.8761	15196	5805	-44
41 / 2 .	16.6675	45.5676	0.0008	5.3675	-0.0447	0.7523	31.4514	0.0449	0.0242	0.0078	99.884	15680	6005	-44
42 / 2 .	16.7834	44.9922	-0.011	5.3563	-0.0194	0.7159	31.5479	0.0109	0.0154	0.013	99.435	15680	5031	-44
43 / 2 .	16.6851	44.4086	-0.0017	5.4718	-0.0253	0.6817	31.7892	0.0598	-0.0176	-0.013	99.0962	15635	4221	-44
44 / 2 .	16.394	42.255	0.0144	7.2055	-0.0134	0.1568	33.3761	0.0081	0.033	-0.0052	99.4429	16303	4270	-46
45 / 2 .	16.0955	41.516	0.0186	7.3774	0.0134	0.0362	33.5262	-0.0108	0.0374	0.0181	98.6388	16689	4669	-49
46 / 2 .	16.3832	42.4622	0.0186	7.2679	-0.0433	0.1367	33.6618	0.0149	0.0198	-0.0387	99.965	16922	4933	-50
47 / 2 .	16.4318	42.2631	0.0093	7.0676	-0.0463	0.0663	33.6516	0.0068	0.022	0.0284	99.547	16710	5277	-50
48 / 2 .	16.6777	42.4712	-0.0076	7.339	-0.0523	0.0744	33.9429	0.0365	0	-0.0026	100.5417	16893	6002	-47
49 / 2 .	16.3471	41.9652	-0.0008	7.556	-0.0463	-0.004	33.8765	-0.0121	0.011	0.0077	99.7634	19015	5988	-52
50 / 2 .	16.3695	41.8798	0.0017	7.5744	-0.012	0.0965	34.2755	0.0094	0.0022	0.0206	100.2296	18868	5575	-52
51 / 2 .	16.4596	41.7712	0.0068	7.4903	-0.0314	0.0543	33.6047	-0.0203	-0.0044	0.0232	99.41	19765	4849	-56
52 / 2 .	16.5876	42.2204	0.0279	7.2391	-0.0433	0.0764	33.938	-0.0297	0.0176	0.0052	100.1121	20245	4778	-56
53 / 2 .	25.8439	36.6762	7.2101	0.0383	-0.003	0.048	30.6451	-0.0043	-0.0241	0.0994	100.5609	21240	5300	-60
54 / 2 .	25.967	37.1065	7.1805	0.026	0.0223	0.1121	30.7859	0.0199	-0.0285	-0.0025	101.22	21250	5388	-60
55 / 2 .	14.3178	53.4197	0.0121	0.1098	0.0462	0.0303	23.3885	0.0242	-0.0133	0.0291	91.3778	21362	5334	-60
56 / 2 .	14.3835	53.6753	0.0052	0.1299	-0.0149	0.0566	23.727	-0.0323	0.0022	0.053	92.0328	21419	5210	-60
57 / 2 .	0.2903	64.6684	-0.0042	16.9617	-0.035	0.0322	17.9747	0	0.0066	0.0179	99.9518	21313	5229	-60
58 / 2 .	0.8511	65.6106	0.0243	16.1194	-0.0715	0.0665	18.0966	0.0099	-0.0397	-0.0307	100.7783	21368	5384	-61
59 / 2 .	26.0548	37.0773	7.2623	0.0253	0.0237	0.04	31.0335	-0.0099	0.0241	0.0255	101.5665	3563	-3751	-8
60 / 2 .	25.7098	37.0018	7.3534	0.0357	-0.0208	0.01	30.9691	0.0085	0.0307	0.0153	101.1342	3944	-3857	-11
61 / 2 .	25.9058	36.9395	7.2334	0.0266	-0.0208	0.028	31.1358	0.0043	-0.0263	-0.0051	101.2734	4016	-3713	-11
62 / 2 .	26.0272	37.5408	7.2241	0.2018	0.0045	0.0861	30.3951	-0.0071	0	0.0433	101.5229	4138	-3581	-12
63 / 2 .	26.0102	37.2841	7.134	0.0526	-0.0163	0.0621	30.5996	0.0114	0.0153	0.0382	101.2074	4138	-3449	-12

64 / 2 .	25.9173	36.8447	7.523	0.0325	0.0994	0.044	30.6426	0.0128	-0.0109	0.0407	101.1569	4009	-3333	-12
65 / 2 .	25.8214	37.3934	7.5413	0.0136	-0.0045	0.05	30.5853	-0.0198	-0.0285	0.0102	101.4153	4065	-3011	-12
66 / 2 .	16.4281	42.7695	0.0194	7.1575	-0.009	0.1327	33.5275	-0.0257	-0.0132	-0.0207	100.0348	4296	-2756	-11
67 / 2 .	16.6547	42.4905	-0.0042	7.1685	0.0358	0.0844	33.5879	0.0135	0.033	-0.0103	100.0684	4185	-2626	-11
68 / 2 .	16.5046	44.4366	0.028	6.0269	-0.0507	0.3218	32.144	-0.0068	0.0066	0.0052	99.4737	4355	-2451	-11
69 / 2 .	16.6721	42.9837	0.0093	6.8847	0.0075	0.2111	33.48	-0.0027	-0.0066	0.0568	100.3052	4333	-2342	-11
70 / 2 .	16.3425	44.4469	0.0254	5.8247	-0.0298	0.4626	31.946	-0.0149	0.0154	0.0207	99.0843	4383	-2042	-11
71 / 2 .	16.6168	43.3714	0.0093	6.5648	-0.0299	0.2393	32.6703	0.0203	0.0286	-0.0491	99.5208	4387	-1851	-11
72 / 2 .	16.6501	44.8204	-0.0017	5.6924	-0.0015	0.5431	31.8155	-0.0177	0.0506	-0.0207	99.572	4367	-1774	-11
73 / 2 .	16.6861	44.7595	0.0212	5.6022	0.0149	0.5672	32.0345	-0.0068	-0.022	0.0207	99.7064	4308	-1437	-14
74 / 2 .	16.5956	45.1255	0.0059	5.6529	-0.0254	0.5412	31.7077	-0.0027	-0.0308	-0.0337	99.6288	4308	-1241	-14
75 / 2 .	16.2915	44.2274	-0.0085	5.9571	-0.0269	0.4143	32.3391	-0.0081	-0.0132	-0.0052	99.2295	4308	-1130	-15
76 / 2 .	16.7897	44.2996	0.0212	5.6438	-0.0194	0.5551	32.1923	-0.019	-0.0088	-0.0052	99.5015	4207	-938	-11
77 / 2 .	16.5848	43.4993	0.0144	6.4536	-0.0343	0.1428	33.1305	-0.0257	0.0044	0.0207	99.8504	4289	-851	-14
78 / 2 .	16.4181	45.2077	0.0229	5.6171	-0.0358	0.5231	31.9046	0.0244	0.0088	0.0026	99.7293	4362	-660	-18
79 / 2 .	16.6817	44.5308	-0.0034	5.6122	-0.0104	0.543	31.6271	-0.0095	0.022	-0.0026	99.0168	4382	-462	-18
80 / 2 .	16.5889	43.7329	0.0008	6.4267	0.0314	0.0603	32.8175	0.0122	0.0132	0.0129	99.6969	4487	-255	-15
81 / 2 .	16.3844	44.7792	-0.0189	5.6304	0.056	0.7711	31.3454	0.0207	-0.0535	-0.0263	98.9873	2832	-1288	160
82 / 2 .	16.5293	44.7072	0.0017	5.6131	-0.0409	0.8449	31.2212	0.0277	0.0022	0.0158	98.9632	3033	-1364	159
83 / 2 .	16.4751	44.8812	0.0242	5.4393	-0.0318	0.7406	31.1567	0.0083	0.0022	0.0053	98.7329	3053	-1498	160
84 / 2 .	16.7494	44.7227	-0.0086	5.5097	0.0015	0.7528	31.1859	-0.0277	-0.0067	0.0158	98.9378	3084	-1630	160
85 / 2 .	16.4909	44.1774	0.025	5.7414	-0.0425	0.7302	31.2601	-0.0042	0.0291	-0.029	98.4541	3084	-1742	157
86 / 2 .	16.7587	44.7037	-0.0026	5.6316	0.0152	0.718	31.1506	0.0028	-0.0067	0.0053	98.9858	3077	-1815	160
87 / 2 .	16.3455	44.0655	-0.0026	5.572	0.1046	0.7958	31.3675	0.0166	0	0.0079	98.2755	3077	-1837	160
88 / 2 .	12.9293	42.2751	0.0009	4.0594	2.7309	0.7717	29.5167	0.0246	-0.0022	0.0421	92.3506	3232	-1817	157
89 / 2 .	15.5521	43.7831	0.0138	5.123	0.8635	0.6977	31.0369	0.0386	0.0201	-0.0422	97.1288	3403	-1750	157
90 / 2 .	16.6862	44.8503	0.005	5.4653	0	0.7704	31.0895	0.0284	0.024	-0.0103	98.9191	3383	-1058	163
91 / 2 .	4.3162	37.6009	0.0249	0.0859	12.1222	1.2445	27.6928	0.0651	0.024	-0.0152	83.1764	2651	-1890	157
92 / 2 .	6.8228	39.9577	0.0084	0.1473	9.6089	0.551	27.6818	0.2539	0.0219	-0.0255	85.0537	2651	-1924	157
93 / 2 .	4.3924	37.0698	0.0158	0.0298	12.764	0.752	29.06	-0.0038	0.024	-0.0127	84.1078	2534	-1914	157

94 / 2 .	4.5294	36.9807	0.0017	0.0211	12.4449	0.9093	28.9724	-0.0025	0.0153	-0.0253	83.8748	2819	-2053	157
95 / 2 .	3.9911	36.98	0.0017	0.0038	13.3259	0.9993	29.7082	0	0	-0.0258	85.0101	3083	-2065	161
96 / 2 .	16.1755	43.5014	0.0095	5.6105	-0.0076	0.7493	30.5702	-0.0069	-0.0045	0.0342	96.6506	-7402	8175	201
97 / 2 .	16.4557	44.8824	0.0042	5.5657	0.0163	0.8005	31.1201	0.0149	-0.0022	0.0232	98.883	-7192	7833	206
98 / 2 .	16.6825	45.0094	0.0076	5.3877	0.0119	0.7844	31.1244	0.0366	0.0088	-0.0052	99.0532	-7315	7808	205
99 / 2 .	16.7667	45.2883	-0.0161	5.0204	0.0341	0.7768	31.3279	0.042	-0.0066	-0.0284	99.2563	-7158	7688	206

Analysis no	Na2O	SiO2	CaO	FeO	Al2O3	MnO	SO3	MgO	TiO2	Cl	K2O	Cr2O3	Total	X	Y	Z
1 / 3	21.203	37.167	3.391	0.022	27.243	0.076	0.137	-0.016	-0.019				89.240	-13300	-23478	-14
2 / 3	21.289	37.831	3.141	0.041	26.812	0.022	0.179	-0.014					89.319	-13300	-23511	-14
3 / 3	21.031	36.621	3.392	0.076	26.929	0.011	0.170	-0.005	0.004				88.234	-13137	-23542	-16
4 / 3	21.154	37.262	3.383	0.012	26.922	0.082	0.121	-0.004	-0.021				88.937	-13675	-23268	-14
5 / 3	21.106	37.369	3.370	0.069	26.689	0.056	0.163	0.004	0.005				88.833	-13724	-23311	-14
6 / 3	21.224	36.792	3.461	0.000	26.959	0.089	0.158	-0.021	0.012				88.694	-13910	-23268	-14
7 / 3.	21.160	37.409	3.243	0.043	27.232	0.013	0.169	-0.043	-0.007				89.269	-13989	-23250	-10
8 / 3	21.452	36.304	3.214	0.068	27.543	0.086	0.132	-0.021	-0.035				88.799	-13237	-34963	-91
9 / 3	21.444	36.335	3.132	0.048	26.816	0.105	0.106	0.001	-0.034				87.987	-13169	-34859	-92
10 /3	21.147	36.404	3.502	0.033	27.105	0.042	0.171	-0.021	-0.031				88.403	-13194	-34616	-88
11 / 3	21.019	35.717	3.490	0.035	27.398	0.054	0.229	-0.011	-0.001				87.940	-13119	-34275	-85
12 / 3	21.217	37.569	3.095	0.067	26.782	0.051	0.116	-0.022	0.005				88.904	-15481	-18113	34
13 / 3	21.362	37.524	3.265	0.016	27.271	0.031	0.187	-0.008	0.007				89.662	-15624	-18234	34
14 / 3	19.809	37.168	4.815	0.057	27.392	-0.007	0.021	-0.001	-0.003				89.263	12839	-7711	37
15 / 3	20.420	36.507	4.945	0.012	27.474	0.018	-0.013	0.000	-0.022				89.376	15363	-5129	19
16 / 3	19.771	34.492	6.168	0.022	28.675	0.074	0.046	-0.032	-0.017				89.249	15253	-5009	21
17 / 3	20.959	37.675	3.620	0.092	27.167	0.057	0.013	-0.010	0.000				89.583	15095	-4798	21
18 / 3	18.938	34.185	7.082	-0.040	28.971	0.035	0.005	-0.021	-0.007				89.217	15010	-4605	21
19 / 3	20.805	37.859	3.479	0.030	26.994	0.015	-0.044	0.001	0.021				89.204	15105	-4617	21
20 / 3	20.992	38.214	3.479	0.069	26.798	0.007	0.011	-0.028	-0.018				89.570	15001	-4384	21

21 / 3	20.530	36.480	4.305	0.012	27.944	0.025	-0.003	-0.034	0.002			89.298	14651	-3202	17
22 / 3	21.037	37.467	3.487	0.055	26.651	0.070	0.003	-0.004	-0.013			88.768	14684	-3247	17
23 / 3	20.713	37.666	3.537	0.037	26.753	0.036	0.000	-0.025	-0.001			88.741	14689	-3070	17
24 / 3	13.751	54.956	0.023	0.027	22.735	-0.029	-0.003	0.027		-0.007	0.066	91.585	15792	-1154	8
25 / 3	13.775	54.952	0.008	0.027	22.485	-0.023	0.000	-0.022		-0.008	0.068	91.314	16601	-397	2
26 / 3	13.628	54.003	0.002	-0.041	22.097	0.016	0.000	-0.010		-0.004	0.056	89.800	16411	-1336	4
27 / 3	13.786	54.741	0.027	-0.004	22.334	0.018	0.019	-0.019		0.005	0.032	90.963	18142	-1349	0
28 / 3	13.695	55.018	0.016	-0.024	22.469	0.029	-0.048	-0.009		-0.011	0.050	91.278	18326	-1174	0
29 / 3	13.789	54.366	0.020	0.012	22.616	-0.004	-0.008	0.018	0.001			90.821	12287	3930	0
30 / 3	15.753	47.813	0.047	-0.008	26.069	0.020	0.003	-0.011		0.000	0.017	89.723	12827	3971	-3
31 / 3	15.613	47.507	0.031	0.055	25.745	0.027	-0.013	-0.005		0.002	0.030	89.008	13191	4002	-6
32 / 3	15.450	47.833	0.040	-0.002	25.506	-0.024	0.021	-0.008		-0.004	0.028	88.879	13487	3939	-6
33 / 3	15.650	47.430	0.048	0.028	25.595	-0.009	0.008	0.008		0.003	0.038	88.807	13713	3956	-5
34 / 3	15.433	47.542	0.022	-0.028	25.495	-0.040	-0.016	0.033		0.001	0.048	88.572	13981	4028	-9
35 / 3	13.710	54.559	0.022	-0.022	22.786	0.022	-0.011	-0.026		0.006	0.058	91.164	14703	4016	-5
36 / 3	13.800	54.780	-0.025	-0.036	23.249	-0.013	0.013	-0.001		0.029	0.092	91.962	14710	3898	-5
37 / 3	13.845	54.495	0.006	0.032	22.446	-0.009	0.029	0.012		-0.005	0.077	90.942	15064	3982	-9
38 / 3	15.740	47.943	0.097	0.008	26.186	0.022	0.013	0.008		0.018	0.052	90.086	15930	3966	-11
39 / 3	15.694	47.709	0.039	0.020	26.331	0.013	0.005	0.005		0.003	0.028	89.848	16062	4123	-12
40 / 3	15.485	47.793	0.018	0.030	26.112	0.000	0.029	0.001		0.015	0.050	89.533	15755	3819	-9
41 / 3	13.910	54.926	0.022	0.028	22.676	0.004	0.008	0.012		0.000	0.058	91.644	17504	3833	-18
42 / 3	13.873	54.483	0.009	0.004	23.043	-0.027	0.019	-0.004		-0.005	0.077	91.508	17432	3856	-17
43 / 3	15.730	48.059	-0.030	-0.042	25.931	-0.011	0.032	-0.005		0.026	0.029	89.805	17675	3885	-20
44 / 3	15.725	47.398	-0.006	-0.004	25.980	-0.004	-0.016	0.012		-0.007	0.034	89.148	17678	4007	-20
45 / 3	14.858	46.544	0.620	-0.014	25.498	-0.007	-0.026	-0.027		0.009	0.108	87.637	-12679	-34771	-94
46 / 3	15.293	45.952	0.749	0.034	26.512	0.011	0.005	-0.011		-0.001	0.090	88.645	-12634	-34794	-94
47 / 3	14.262	43.573	0.493	0.066	29.424	0.004	0.018	0.000		-0.019	0.079	87.920	-12705	-34045	-88
48 / 3	15.422	46.492	0.142	0.030	25.763	0.020	-0.008	0.001		-0.006	0.056	87.926	-12434	-33684	-89
49 / 3	15.320	46.279	0.319	-0.014	26.076	-0.002	0.011	-0.010		-0.003	0.072	88.076	-12258	-33688	-88

50 / 3 .	14.835	52.378	0.019	0.042	23.570	0.035	-0.058	-0.005		0.851	0.061		91.792	-13734	-23275	-12
51 / 3 .	13.767	53.972	0.019	0.004	22.566	-0.020	0.037	0.019		0.004	0.053		90.442	-13692	-23483	-14
52 / 3 .	13.695	54.131	0.028	-0.006	22.412	0.046	-0.058	-0.011		0.006	0.094		90.413	-13282	-23446	-18
53 / 3 .	13.607	54.271	0.036	-0.002	22.505	0.026	-0.021	0.012		-0.022	0.063		90.520	-13161	-23495	-18
54 / 3 .	21.623	37.306	3.370	0.044	27.326	0.018	-0.026	-0.039	-0.044				89.686	-19040	6457	0
55 / 3 .	21.592	37.110	3.388	-0.004	27.292	0.046	0.005	-0.017	0.012				89.445	-19135	6478	0
56 / 3 .	21.067	37.413	3.163	0.000	26.929	0.044	0.052	-0.055	0.007				88.674	-19096	6274	-3
57 / 3 .	21.500	37.662	3.347	0.018	26.980	0.042	-0.008	-0.020	0.022				89.570	-19314	6248	0
58 / 3 .	15.488	46.738	0.542	-0.014	26.352	-0.004	0.003	-0.001		-0.003	0.111		89.234	-18940	6278	0
59 / 3 .	15.440	46.731	0.498	0.008	26.324	-0.033	0.021	-0.030		-0.011	0.086		89.107	-18898	6267	0
60 / 3 .	15.057	45.639	0.946	-0.022	26.751	0.026	-0.003	0.005		0.017	0.111		88.553	-18479	6480	-2
61 / 3 .	15.202	46.596	0.708	-0.018	26.462	-0.026	-0.011	0.022		0.012	0.103		89.105	-18451	6543	-2
62 / 3 .	11.659	67.687	0.018	0.266	18.752	-0.035	-0.019	0.037		0.008	0.128		98.555	-21772	2588	10
63 / 3 .	11.839	68.283	-0.009	0.324	18.803	-0.011	-0.019	0.003		-0.001	0.102		99.354	-20644	-4195	7
64 / 3 .	17.446	0.013	0.181	-0.002	37.303	0.041	0.015	0.030	0.007				55.036	-19473	-4932	0
65 / 3 .	14.805	45.056	1.066	0.082	27.337	0.046	0.000	-0.001	0.036				88.427	-16698	-4847	-8
66 / 3 .	14.962	45.192	0.986	0.022	26.846	0.015	-0.013	-0.039		0.000	0.089		88.111	-16637	-4537	-8
67 / 3 .	14.672	44.912	0.998	-0.002	27.172	0.020	-0.039	-0.011		0.011	0.029		87.813	-16758	-4382	-8
68 / 3 .	10.057	43.863	0.262	1.900	33.880	-0.011	0.021	0.017		0.027	0.529		90.557	-16440	-4964	-11
69 / 3 .	13.607	51.852	0.078	0.084	24.221	-0.022	-0.005	0.003		0.015	0.165		90.026	-16418	-5326	-11
70 / 3 .	16.413	45.126	-0.058	0.700	31.727	0.009	0.003	-0.032		0.007	5.316		99.298	-16248	-5194	-9
71 / 3 .	0.056	31.612	0.064	37.129	13.397	0.612		0.416	0.250		8.600	0.016	92.152	-15845	-1158	-12
72 / 3 .	0.079	32.664	-0.029	38.443	13.024	0.296		0.305	0.084		9.056	-0.080	93.953	-13513	-1357	-22
73 / 3 .	0.068	32.137	-0.004	37.445	13.025	0.667		0.245	0.150		8.866	-0.025	92.602	-10735	-525	-37
74 / 3 .	0.055	32.991	0.012	37.270	12.256	0.593		0.589	0.593		9.182	-0.035	93.540	-11549	-529	-31
75 / 3 .	-0.002	0.682	0.019	79.177	0.445	0.599		0.046	0.136		0.127	0.024	81.255	-4322	-905	-63
76 / 3 .	0.110	32.781	-0.031	37.009	12.501	0.720		0.790	0.246		8.717	-0.028	92.873	-4142	-515	-60
77 / 3 .	0.099	31.958	-0.007	37.667	13.324	0.629		0.201	0.211		8.672	-0.027	92.759	-10229	-823	-38
78 / 3 .	0.050	0.728	-0.014	80.540	0.518	0.645		-0.002	0.155		0.078	-0.034	82.713	-10307	-791	-37

79 / 3 .	0.085	35.717	-0.010	32.276	10.459	0.556		3.171	3.098		9.335	-0.028	94.698	-21970	488	13
80 / 3 .	0.103	35.718	-0.040	32.896	10.528	0.646		3.133	2.644		9.223	0.023	94.914	-21653	403	13
81 / 3 .	0.106	34.815	-0.024	32.404	10.401	0.626		2.942	2.546		9.348	0.002	93.189	-21263	301	9
82 / 3 .	0.110	30.531	2.905	35.754	12.103	0.717		0.464	0.310		8.552	-0.058	91.445	-13055	1457	-26
83 / 3 .	16.383	42.022	0.043	0.004	33.476	0.020	-0.013	-0.019		0.006	7.558		99.512	-12959	1422	-26
84 / 3 .	16.468	42.287	-0.040	0.078	34.230	-0.002	0.033	0.019		0.009	7.277		100.400	-12398	1397	-26
85 / 3 .	16.350	41.974	-0.006	0.062	34.085	0.011	0.005	0.023		-0.018	7.565		100.073	-11888	1375	-30
86 / 3 .	0.096	33.112	-0.023	37.485	12.027	0.961		0.723	0.280		9.057	-0.005	93.740	-11687	1187	-32
87 / 3 .	0.036	32.414	-0.033	38.060	12.199	0.902		0.524	0.219		8.902	0.002	93.257	-11704	1246	-32
88 / 3 .	21.837	38.937	0.810	0.032	27.037	0.079	-0.013	-0.033		0.031	0.126		88.889	-11501	1588	-35
89 / 3 .	14.178	43.569	0.766	0.012	29.240	0.053	0.016	0.008	-0.007				87.842	-10921	1509	-34
90 / 3 .	21.078	38.746	0.936	0.026	26.754	0.059	0.021	-0.022	-0.007				87.619	-11509	1676	-34

Analysis no	Na2O	SiO2	Cl	K2O	CaO	FeO	Al2O3	MgO	MnO	SO3	Total	X	Y	Z
1 / 4 .	0.508	64.501	0.009	16.460	-0.123	0.114	17.744	-0.022	0.007	0.003	99.345	19968	-4643	-143
2 / 4 .	0.359	64.389	0.013	16.424	-0.071	0.067	17.710	-0.036	-0.049	0.003	98.965	20069	-4653	-143
3 / 4 .	0.527	64.492	-0.011	16.378	-0.080	0.096	17.867	0.013	0.005	-0.008	99.376	19929	-4691	-143
4 / 4 .	16.210	42.265	-0.002	6.574	0.011	0.067	32.930	0.019	0.011	0.047	98.135	19819	-4707	-143
5 / 4 .	16.128	41.934	0.002	7.441	-0.018	0.057	33.495	0.003	0.016	0.000	99.075	19791	-4571	-143
6 / 4 .	16.319	41.213	0.015	7.574	0.039	0.047	33.311	0.001	-0.005	0.026	98.545	19896	-4543	-143
7 / 4 .	16.417	42.717	0.006	6.674	0.024	0.179	32.835	-0.008	-0.016	-0.016	98.853	20001	-4473	-143
8 / 4 .	13.827	52.832	-0.003	0.186	0.005	-0.037	23.157	-0.025	0.031	0.048	90.086	19853	-4604	-143
9 / 4 .	13.938	53.452	0.014	0.253	0.041	0.023	23.165	0.000	0.040	-0.011	90.926	19996	-4552	-143
10 / 4 .	13.818	53.221	0.012	0.185	0.012	-0.010	23.456	-0.019	0.047	0.016	90.767	19895	-4722	-143
11 / 4 .	16.340	42.557	0.016	6.644	0.002	0.080	33.426	-0.019	0.031	-0.013	99.096	19762	-4382	-143
12 / 4 .	25.475	37.443	7.334	0.073	0.039	0.294	31.243	-0.017	0.018	0.049	101.968	18428	7926	-119
13 / 4 .	25.884	37.509	7.306	0.082	0.003	0.241	30.874	0.006	0.013	0.088	102.005	18482	7926	-119

14 / 4 .	25.868	37.157	7.323	0.072	0.032	0.229	31.189	0.019	0.007	0.067	101.962	18583	7928	-119
15 / 4 .	25.504	36.977	7.425	0.021	0.029	0.274	31.177	0.003	0.002	0.018	101.428	18604	7976	-119
16 / 4 .	14.730	44.468	-0.002	0.627	1.356	0.027	27.956	0.001	0.034	0.027	89.225	18666	7994	-119
17 / 4 .	15.628	47.774	0.010	0.059	-0.009	0.002	25.849	0.008	-0.011	0.005	89.336	18717	7977	-119
18 / 4 .	15.216	45.447	-0.014	0.814	0.381	0.047	27.130	0.001	-0.005	0.011	89.047	18777	7999	-119
19 / 4 .	15.723	45.630	0.000	1.091	0.128	0.031	27.694	0.004	0.000	0.040	90.341	18820	8003	-119
20 / 4 .	14.929	45.115	0.024	0.505	0.334	0.049	27.774	0.019	0.022	-0.003	88.772	18864	8016	-119
21 / 4 .	15.222	45.803	-0.004	0.268	1.004	0.076	26.980	-0.004	-0.007	0.021	89.374	18917	8090	-119
22 / 4 .	14.056	43.968	0.001	0.351	1.369	0.485	28.750	0.019	-0.009	-0.032	88.998	18950	8082	-121
23 / 4 .	21.977	40.961	4.846	0.447	1.366	0.933	28.727	-0.027	-0.042	0.049	99.306	19024	8163	-121
24 / 4 .	25.610	37.172	7.348	0.100	0.009	0.260	31.133	0.003	-0.004	0.041	101.676	19101	8139	-121
25 / 4 .	25.644	36.899	7.497	0.027	0.012	0.152	31.246	-0.010	-0.007	0.008	101.485	19153	8139	-121
26 / 4 .	25.983	37.137	7.332	0.034	0.059	0.229	31.388	-0.026	0.007	0.059	102.227	19210	8114	-120
27 / 4 .	25.817	37.385	7.446	0.102	0.017	0.225	31.000	-0.001	0.009	0.003	102.003	19429	8182	-120
28 / 4 .	25.728	37.072	7.451	0.013	-0.002	0.193	31.076	0.024	0.082	0.077	101.716	19483	8232	-125
29 / 4 .	25.911	36.977	7.300	0.047	-0.060	0.158	30.926	-0.026	0.038	0.062	101.418	19605	8308	-125
30 / 4 .	25.718	37.704	7.324	0.119	-0.006	0.266	30.947	0.024	0.000	0.052	102.154	19864	8284	-125
31 / 4 .	25.546	38.004	7.547	0.282	0.054	0.359	30.180	0.014	-0.016	0.178	102.165	20063	8207	-125
32 / 4 .	25.500	36.871	7.397	0.064	0.008	0.197	30.867	-0.012	0.011	0.080	100.993	20288	8208	-128
33 / 4 .	25.663	36.764	7.456	0.032	0.009	0.091	30.536	-0.014	0.049	0.090	100.690	12748	-7086	-112
34 / 4 .	25.652	36.760	7.354	0.067	0.017	-0.002	30.739	0.030	-0.013	0.119	100.738	12663	-6997	-112
35 / 4 .	16.328	42.529	-0.001	7.070	0.035	0.063	33.399	-0.001	-0.029	0.008	99.432	12727	-6908	-112
36 / 4 .	25.793	36.568	7.231	0.047	0.008	0.014	30.704	-0.006	0.029	0.142	100.536	12584	-6955	-112
37 / 4 .	16.339	42.170	-0.008	7.087	-0.062	-0.002	33.228	-0.011	-0.020	0.011	98.834	12471	-6795	-112
38 / 4 .	13.852	52.744	0.005	0.337	0.012	-0.016	23.177	-0.004	-0.002	-0.019	90.127	12417	-6811	-112
39 / 4 .	13.749	52.537	0.012	0.311	-0.006	0.033	23.881	-0.015	0.052	-0.022	90.576	12303	-6856	-111
40 / 4 .	13.355	52.590	0.003	0.363	0.032	0.027	23.751	-0.011	0.009	0.043	90.172	12267	-6820	-111
41 / 4 .	13.916	52.859	0.000	0.265	0.020	0.000	23.591	-0.019	0.016	0.008	90.674	12382	-6641	-111
42 / 4 .	0.662	63.963	0.000	16.212	-0.079	0.045	17.890	-0.003	0.025	-0.010	98.797	12260	-6929	-111
43 / 4 .	0.427	64.583	0.026	16.437	-0.066	-0.029	17.676	0.000	-0.036	0.021	99.171	12198	-6815	-111

44 / 4 .	0.516	63.947	0.021	16.431	-0.068	0.018	17.851	-0.001	-0.005	-0.031	98.784	12305	-6737	-111
45 / 4 .	1.129	64.547	0.009	15.549	-0.020	0.029	17.719	0.009	0.029	-0.029	99.020	12255	-6705	-111
46 / 4 .	0.954	64.262	-0.003	15.825	-0.076	0.035	17.837	-0.005	-0.018	0.003	98.915	12119	-6603	-111
47 / 4 .	0.750	64.457	0.022	16.063	-0.093	0.055	17.556	0.004	0.005	0.036	98.947	12059	-6601	-111
48 / 4 .	0.602	64.172	0.000	16.474	-0.057	0.078	17.836	0.035	-0.047	0.041	99.239	12079	-6494	-111
49 / 4 .	0.570	64.147	-0.007	16.429	-0.039	0.063	18.042	-0.014	-0.009	0.010	99.261	12032	-6385	-109
50 / 4 .	16.207	41.952	0.007	7.220	0.021	0.039	33.666	0.015	-0.049	-0.013	99.127	13271	-3052	-105
51 / 4 .	16.305	41.965	0.000	7.207	0.015	0.116	33.356	-0.010	0.002	-0.037	98.967	13322	-3066	-105
52 / 4 .	14.088	52.824	0.006	0.192	0.009	0.023	23.518	-0.019	-0.022	0.086	90.746	13368	-3108	-105
53 / 4 .	13.818	53.618	0.018	0.115	0.014	-0.033	22.986	0.008	-0.031	0.027	90.604	13344	-3145	-105
54 / 4 .	13.971	52.622	0.013	0.153	0.011	-0.039	23.363	0.026	0.034	0.022	90.214	13383	-3145	-105
55 / 4 .	16.115	41.918	0.010	7.328	-0.027	0.063	34.100	0.007	-0.020	0.021	99.562	13335	-3208	-105
56 / 4 .	0.492	64.080	-0.001	16.700	-0.017	-0.010	17.832	-0.014	-0.013	-0.016	99.104	13429	-3171	-105
57 / 4 .	0.450	64.728	-0.007	16.361	-0.052	0.106	18.053	0.034	-0.005	-0.029	99.732	13489	-3162	-105
58 / 4 .	0.541	64.959	-0.003	16.572	-0.048	-0.016	17.676	0.013	-0.011	0.000	99.761	13519	-3134	-105
59 / 4 .	0.510	63.941	0.031	16.314	-0.057	0.086	17.596	-0.018	0.007	-0.016	98.484	13644	-3218	-108
60 / 4 .	25.442	36.531	7.408	0.005	-0.008	0.069	30.828	0.022	0.016	0.008	100.326	-18366	5961	0
61 / 4 .	25.646	36.987	7.353	0.024	-0.002	0.006	30.907	0.032	-0.002	-0.005	100.955	-18309	5948	0
62 / 4 .	25.763	37.067	7.420	-0.002	0.021	-0.008	30.778	0.000	0.049	-0.018	101.098	-18060	5948	0
63 / 4 .	24.982	36.954	6.876	0.030	0.229	0.002	30.294	0.013	0.011	-0.003	99.391	-17953	5946	0
64 / 4 .	25.523	37.476	7.306	0.028	-0.003	0.024	31.107	-0.013	0.018	0.039	101.520	-17881	5976	0
65 / 4 .	25.245	37.030	7.314	0.062	0.021	0.079	30.870	-0.004	-0.056	0.026	100.646	-17804	5974	0
66 / 4 .	25.562	37.012	7.431	0.013	-0.005	0.020	31.074	-0.003	0.009	0.023	101.144	-17735	5988	0
67 / 4 .	25.405	36.787	7.369	0.035	0.017	0.004	30.638	-0.032	-0.033	-0.008	100.254	-17671	5988	0
68 / 4 .	25.725	37.032	7.364	0.036	-0.054	-0.028	30.667	0.037	-0.058	0.021	100.882	-17562	5985	0
69 / 4 .	13.875	53.652	0.006	0.181	0.003	0.023	22.894	-0.026	-0.002	0.032	90.666	-18338	5849	0
70 / 4 .	13.836	54.132	0.010	0.149	-0.017	-0.019	22.939	-0.011	0.025	0.024	91.114	-18226	5854	0
71 / 4 .	13.522	54.313	0.005	0.119	0.003	0.051	22.728	0.012	0.018	0.024	90.795	-17972	5880	0
72 / 4 .	14.030	53.301	0.039	0.277	0.015	0.019	23.288	0.019	0.011	0.024	91.022	-17600	5822	0
73 / 4 .	16.431	50.349	1.553	0.127	-0.023	0.020	24.114	-0.004	0.076	-0.003	92.670	-17462	5903	0

74 / 4 .	13.514	53.861	0.007	0.132	0.029	0.027	22.414	0.022	0.038	0.008	90.051	-17205	5968	0
75 / 4 .	25.082	37.329	6.997	0.044	0.274	0.028	30.339	0.019	0.013	-0.003	100.125	-12764	6883	2
76 / 4 .	25.767	37.212	7.431	0.016	0.021	0.002	30.851	0.003	0.013	-0.018	101.316	-12660	6876	2
77 / 4 .	24.331	36.817	6.232	0.091	0.449	0.028	29.923	-0.013	-0.004	0.010	97.883	-12696	6824	2
78 / 4 .	25.505	37.200	6.986	0.018	0.156	0.045	30.808	-0.003	0.009	-0.013	100.727	-12804	6961	2
79 / 4 .	16.813	44.722	1.678	0.538	0.783	0.067	25.863	-0.007	0.031	0.037	90.534	-12550	6920	2
80 / 4 .	16.544	44.713	-0.015	5.556	0.017	0.475	31.314	0.006	-0.042	0.003	98.626	-12516	6952	2
81 / 4 .	16.476	44.859	0.003	5.499	-0.026	0.514	31.414	0.012	0.025	0.034	98.836	-12536	6863	2
82 / 4 .	16.690	45.018	-0.019	5.564	-0.012	0.512	31.046	0.003	0.045	0.016	98.893	-12472	6856	2
83 / 4 .	16.390	44.725	0.010	5.586	-0.020	0.487	30.881	0.014	0.005	0.008	98.105	-12500	6830	2
84 / 4 .	16.530	44.767	0.014	5.441	0.018	0.502	31.101	0.021	-0.025	0.013	98.406	-12443	6799	2
85 / 4 .	16.416	45.271	-0.009	5.549	-0.011	0.477	31.697	-0.018	-0.009	-0.005	99.411	-12366	6748	3
86 / 4 .	16.636	43.668	0.006	6.418	-0.033	0.501	32.257	-0.018	-0.018	-0.016	99.485	-6607	6970	2
87 / 4 .	16.374	42.594	0.007	6.596	-0.036	0.495	32.392	-0.012	0.040	0.008	98.505	-6667	6919	2
88 / 4 .	16.563	44.076	0.002	6.143	-0.065	0.489	32.019	-0.001	-0.029	0.032	99.323	-6682	6872	2
89 / 4 .	16.371	42.904	-0.009	6.764	-0.023	0.298	32.021	-0.017	-0.016	-0.018	98.357	-6859	6762	2
90 / 4 .	16.620	42.803	-0.003	7.041	-0.006	0.200	33.052	-0.007	-0.051	0.008	99.722	-7057	6611	2
91 / 4 .	16.525	44.832	0.017	5.788	0.003	0.544	31.108	0.028	0.029	0.011	98.884	-7157	6522	2
92 / 4 .	16.672	44.962	-0.009	5.660	0.033	0.770	31.799	0.007	-0.018	-0.024	99.903	-7183	6412	3
93 / 4 .	25.373	36.813	7.472	0.016	0.033	-0.002	30.775	-0.003	0.013	0.000	100.495	-20933	127	-21
94 / 4 .	25.466	36.748	7.509	0.018	0.021	0.026	30.972	-0.016	0.020	-0.010	100.780	-20959	108	-21
95 / 4 .	25.637	36.966	6.947	0.011	0.053	0.079	30.259	-0.010	0.004	-0.047	99.957	-20967	57	-21
96 / 4 .	25.598	36.727	7.539	0.029	-0.002	-0.022	31.097	-0.020	0.004	-0.041	100.993	-20973	39	-21
97 / 4 .	14.012	53.112	0.004	0.223	0.017	-0.004	23.369	-0.011	0.016	0.013	90.765	-21013	6	-21
98 / 4 .	14.056	52.260	0.312	0.215	-0.027	0.033	23.571	-0.023	-0.045	-0.016	90.446	-20906	-51	-21
99 / 4 .	25.471	36.533	7.354	0.018	-0.009	0.014	30.579	0.019	-0.004	0.057	100.045	-20955	-31	-21
100 / 4 .	25.614	36.597	7.359	0.022	0.033	0.043	30.863	0.024	-0.038	0.028	100.584	-20983	-24	-21
101 / 4 .	25.698	36.498	7.424	0.021	-0.003	0.035	30.703	-0.017	0.004	0.034	100.416	-21061	15	-21
102 / 4 .	14.073	52.098	0.014	0.252	0.095	0.021	23.425	-0.007	0.020	0.003	90.000	-21025	-62	-21
103 / 4 .	25.270	37.086	7.410	0.036	0.054	0.028	31.041	0.013	-0.036	-0.008	100.937	-21039	-116	-21

104 / 4 .	25.465	36.770	7.090	0.020	0.020	-0.002	31.254	-0.029	-0.007	0.016	100.634	-21058	-126	-21
105 / 4 .	16.579	44.993	-0.008	5.408	0.014	0.618	31.532	-0.076	-0.036	-0.021	99.142	-21119	-188	-21
106 / 4 .	16.380	44.626	-0.001	5.676	-0.006	0.495	31.544	0.017	0.025	0.000	98.762	-21223	-230	-21